

**Modeling and Detection of Stator Winding Insulation Degradation  
in VSI-fed Electric Machines Under High  $dv/dt$**

Ashutosh Patel

A Thesis  
In the Department  
of  
Electrical and Computer Engineering

Presented in Partial Fulfillment of the Requirements  
For the Degree of  
Master of Applied Science (Electrical and Computer Engineering) at  
Concordia University  
Montreal, Quebec, Canada

December 2020

© Ashutosh Patel, 2020

**CONCORDIA UNIVERSITY**  
**SCHOOL OF GRADUATE STUDIES**

This is to certify that the thesis prepared

By: Ashutosh Patel

Entitled: Modeling and Detection of Stator Winding Insulation Degradation in VSI-fed Electric Machines Under High dv/dt

and submitted in partial fulfillment of the requirements for the degree of

**Master of Applied Science (Electrical and Computer Engineering)**

complies with the regulations of this University and meets the accepted standards with respect to originality and quality.

Signed by the final examining committee:

\_\_\_\_\_ Chair

Dr. Pragasen Pillay

\_\_\_\_\_ External to Program

Dr. Chunjiang An

\_\_\_\_\_ Examiner

Dr. Pragasen Pillay

\_\_\_\_\_ Thesis Supervisor

Dr. Chunyan Lai

Approved by

\_\_\_\_\_

Dr. Yousef R. Shayan, Chair of Department

December 21, 2020

\_\_\_\_\_

Date of defense

Dr. Amir Asif, Dean,

Gina Cody School of Engineering and Computer Science

# ABSTRACT

## **Modeling and Detection of Stator Winding Insulation Degradation in VSI-fed Electric Machines Under High $dv/dt$**

**Ashutosh Patel, MAsc.**

**Concordia University, 2020**

Nowadays, in many advanced applications, for example electric vehicles and aircrafts, electric motors are being fed by voltage source inverters (VSIs). These inverters generally utilize fast-switching power electronics devices to provide the modulated pulse voltages for motor operation. Motor's winding insulation undergoes additional electrical stress due to high voltage slew rate ( $dv/dt$ ) resulted from the use of VSI, which may cause accelerated insulation degradation. To investigate and quantify this electrical stress, various modeling techniques have been proposed over the years with a goal to optimize the motor stator design for safer and more reliable operation. In this thesis, various winding insulation modeling techniques are investigated, in which a simple case study along with comparative analysis is performed to analyze the electrical stress for different  $dv/dt$  levels. Based on this investigation, finite element (FE) based approach is selected for detailed stator winding insulation modeling, parameter determination and analysis.

Degradation of winding insulation is inevitable due to various internal and external factors. Therefore, monitoring of the insulation condition becomes necessary to ensure a safe and reliable operation of the VSI-fed electric machines. Detecting degradation in insulation in an early stage can prevent major failure in the machine and the drive system. To this end, an online insulation monitoring technique is required. Based on the existing literature, the high frequency transient current could be a good indicator for online insulation monitoring. In this thesis, how winding insulation degradation affects the machine transient current is investigated. To do so, complex random wound stator winding is modeled at first using the FE based approach, in which detailed arrangement of each wire inside the stator slot and different insulation layers are considered. Thereafter, insulation degradations of various types and severity are emulated within the FE based model, including the turn to ground (TG) degradations and turn to turn (TT) degradations. With the emulated winding insulation degradations, the effectiveness of the detection techniques is investigated. In this work, a new insulation condition detection technique based on current

response and wavelet packet decomposition (WPD) is proposed, which has the capability to determine the overall state of health (SOH) of insulation and classify types of insulation degradation. Therefore, the stator winding insulation is modeled and the SOH indicator for insulation degradation detection is also developed through this thesis research.

# Table of Contents

List of Figures .....	vii
List of Tables .....	x
Chapter 1: Introduction .....	1
1.1. Overview and Motivations .....	1
1.2. Research Objective and Contributions .....	4
1.3. Dissertation Layout .....	5
Chapter 2: Machine Winding Modeling Techniques .....	6
2.1. Literature Review .....	6
2.1.1. Finite Element (FE) Based Modeling Technique .....	8
2.1.2. Equivalent RLC Based Modeling Technique .....	9
2.1.3. Multi-Conductor Transmission Line Model .....	11
2.1.4. Parameter Computation .....	13
2.2. Comprehensive Studies Through Simulations .....	16
2.2.1. Geometrical Configuration of Stator Winding .....	16
2.2.2. Parameter Computation .....	18
2.2.3. Winding Modeling .....	20
2.3. Summary .....	28
Chapter 3: Emulation of Insulation Degradation .....	30
3.1. Insulation System in Stator Winding .....	30
3.2. Insulation Degradation .....	31
3.2.1. Thermal Stress .....	32
3.2.2. Electrical Stress .....	33
3.2.3. Environmental Stress .....	33

3.2.4. Mechanical Stress .....	34
3.3. Emulation of Insulation Degradation .....	35
3.3.1. Emulation of Insulation Degradation Using FE based approach .....	36
3.3.2. Parameter Computation .....	39
3.3.3. Integration of External Circuit with Transient Solver .....	40
3.3.4. Emulation of Insulation Degradation .....	43
3.4. Influence of Insulation Degradation on Current Response .....	44
3.5. Summary .....	51
Chapter 4: Detection and Classification of Insulation Degradation .....	52
4.1. Condition Monitoring Techniques .....	52
4.1.1. Offline Monitoring Techniques .....	52
4.1.2. Online Monitoring Techniques.....	57
4.2. A Novel approach for Detection and Classification of Insulation Degradation .....	59
4.2.1. Methodology.....	59
4.3. Investigation of the Influence of Degradation on Transient Current Response.....	62
4.3.1. Turn to Ground (TG) degradation .....	62
4.3.2. Turn to Turn Degradation.....	68
4.4. Indicators for Determination of SOH and Classification from WPD. ....	72
4.5. Summary .....	76
Chapter 5: Conclusions and Future Work.....	77
5.1. Conclusions .....	77
5.2. Future Work .....	78
References.....	79

## List of Figures

Figure 1–1 Typical powertrain system .....	1
Figure 2–1 FE based model .....	8
Figure 2–2 RLC based model for 3 turns.....	11
Figure 2–3 Winding distributed over different regions .....	12
Figure 2–4 Cascaded chain matrices.....	12
Figure 2–5 Cross section of form wound coil.....	17
Figure 2–6 Maxwell capacitance matrix for form wound coil (nF).....	19
Figure 2–7 Capacitance matrix for form wound coil (nF).....	19
Figure 2–8 Inductance matrix for form wound coil.....	20
Figure 2–9 Illustration of termination technique .....	21
Figure 2–10 TT voltage stress for 1750 V pulse with 25ns rise time (FE Model) .....	21
Figure 2–11 TT Voltage stress for 1750 V pulse with 100ns rise time (FE Model) .....	22
Figure 2–12 Maximum TT stress for 1750 V pulse with different rise time (FE Model) .....	22
Figure 2–13 TG Voltage stress for 1750 V pulse with 25ns rise time (FE Model).....	23
Figure 2–14 TG Voltage stress for 1750 V pulse with 100ns rise time (FE Model).....	23
Figure 2–15 TT voltage stress for 1750 V pulse with 25ns rise time (RLC Model) .....	24
Figure 2–16 TT voltage stress for 1750 V pulse with 100ns rise time (RLC Model) .....	25
Figure 2–17 Maximum TT stress for 1750 V pulse with different rise time (RLC Model).....	25
Figure 2–18 TG Voltage stress for 1750 V pulse with 25ns rise time (RLC Model).....	26
Figure 2–19 TG Voltage stress for 1750 V pulse with 100ns rise time (RLC Model).....	26
Figure 2–20 Maximum TG stress for 1750 V pulse with different rise time (RLC Model).....	27
Figure 2–21 Comparison of maximum TT stress obtained from different model .....	27
Figure 3–1 Insulations in (a) random (b) form wound coil .....	30
Figure 3–2 Effect of temperature on dielectric strength of insulation [35] .....	33
Figure 3–3 Effect of humidity on dielectric properties [38] .....	34
Figure 3–4 Emulation of insulation degradation .....	36
Figure 3–5 Typical machine model .....	37
Figure 3–6 Stator connection diagram.....	37
Figure 3–7 Detailed phase A winding .....	37

Figure 3–8 Detailed slot model.....	37
Figure 3–9 Coil connections in phase A.....	38
Figure 3–10 Reduced winding.....	38
Figure 3–11 Strand level Maxwell capacitance matrix (pF).....	39
Figure 3–12 Turn level Maxwell capacitance matrix (pF).....	40
Figure 3–13 Connection of various parameters in external circuit.....	41
Figure 3–14 Complete circuit for one coil.....	41
Figure 3–15 Complete circuit for winding.....	42
Figure 3–16 TT degradation emulation.....	43
Figure 3–17 TG degradation emulation.....	43
Figure 3–18 Current response to applied voltage pulse.....	44
Figure 3–19 Current for T1G degradation.....	45
Figure 3–20 Current for T2G degradation.....	45
Figure 3–21 Current for T3G degradation.....	46
Figure 3–22 Current for T4G degradation.....	46
Figure 3–23 Current for T5G degradation.....	47
Figure 3–24 Current for T6G degradation.....	47
Figure 3–25 Current for T7G degradation.....	48
Figure 3–26 Current for T8G degradation.....	48
Figure 3–27 Current for TT12 degradation.....	49
Figure 3–28 Current for TT34 degradation.....	49
Figure 3–29 Current for TT56 degradation.....	50
Figure 3–30 Current for TT78 degradation.....	50
Figure 4–1 IR insulation test model.....	53
Figure 4–2 Insulation model with equivalent resistance and ideal capacitance.....	55
Figure 4–3 Winding with four coils.....	59
Figure 4–4 Steps for signal processing.....	60
Figure 4–5 Three level WPD.....	61
Figure 4–6 Transient current for T1G degradation.....	62
Figure 4–7 Transient current for T2G degradation.....	63
Figure 4–8 Transient current for T3G degradation.....	63

Figure 4–9 Transient current for T4G degradation.....	63
Figure 4–10 Transient current for T5G degradation.....	64
Figure 4–11 Transient current for T6G degradation.....	64
Figure 4–12 Transient current for T7G degradation.....	64
Figure 4–13 Transient current for T8G degradation.....	65
Figure 4–14 Amplitude spectrum of transient current for T1G degradation .....	65
Figure 4–15 Amplitude spectrum of transient current for T2G degradation .....	66
Figure 4–16 Amplitude spectrum of transient current for T3G degradation .....	66
Figure 4–17 Amplitude spectrum of transient current for T4G degradation .....	66
Figure 4–18 Amplitude spectrum of transient current for T5G degradation .....	67
Figure 4–19 Amplitude spectrum of transient current for T6G degradation .....	67
Figure 4–20 Amplitude spectrum of transient current for T7G degradation .....	67
Figure 4–21 Amplitude spectrum of transient current for T8G degradation .....	68
Figure 4–22 Transient current for TT12 degradation .....	69
Figure 4–23 Transient current for TT34 degradation .....	69
Figure 4–24 Transient current for TT56 degradation .....	69
Figure 4–25 Transient current for TT78 degradation .....	70
Figure 4–26 Amplitude spectrum of transient current for TT12 degradation .....	70
Figure 4–27 Amplitude spectrum of transient current for TT34 degradation .....	71
Figure 4–28 Amplitude spectrum of transient current for TT56 degradation .....	71
Figure 4–29 Amplitude spectrum of transient current for TT78 degradation .....	71
Figure 4–30 Five level WPD for degradation detection and classification .....	73
Figure 4–31 Norm form packet p0 for different degradations.....	74
Figure 4–32 Norm form packet p10 for different degradations.....	75

## List of Tables

Table 2-1 Main parameters for RLC based model.....	10
Table 2-2 Main winding parameters .....	17
Table 2-3 Comparison of maximum TT voltages.....	27
Table 3-1 Main parameters of insulations .....	38
Table 4-1 Norms from p10 for TG degradations .....	75
Table 4-2 Norms from p10 for TT degradations .....	75

# Chapter 1: Introduction

## 1.1. Overview and Motivations

Electric Vehicles (EVs) and hybrid electric vehicles (HEVs) have proven their candidacy as a potential mode of transportation for the coming future. In 2010, only 17000 EVs were on road globally. In past decade, EVs experienced rapid growth bringing the total no of EVs on road at 7.2 million in 2019 [1]. In Canada, the federal government has announced iZEV (Incentives for the Zero-Emission Vehicles) program to promote low carbon transportation and boost sales of light EVs and HEVs by making it more affordable [2]. Additionally, provincial governments also offer similar incentives [3]. Substantial amount of research is being done to electrify other modes of transportation and to make them more efficient and reliable.

In any electrified vehicle, powertrain is considered the heart of the whole system. Powertrain mainly consists of three things batteries, variable speed drive, and electric machine. Fig. 1-1 typical powertrain. Currently, permanent magnet synchronous machines (PMSMs) and induction machines (IMs) are being used widely in EVs due to their high power density and performance. Recent research shows that synchronous reluctance machine (SynRM) offers interesting characteristics along with advantages like low cost, rigid structure, high fault tolerance capability etc. which is suitable for EVs [4].

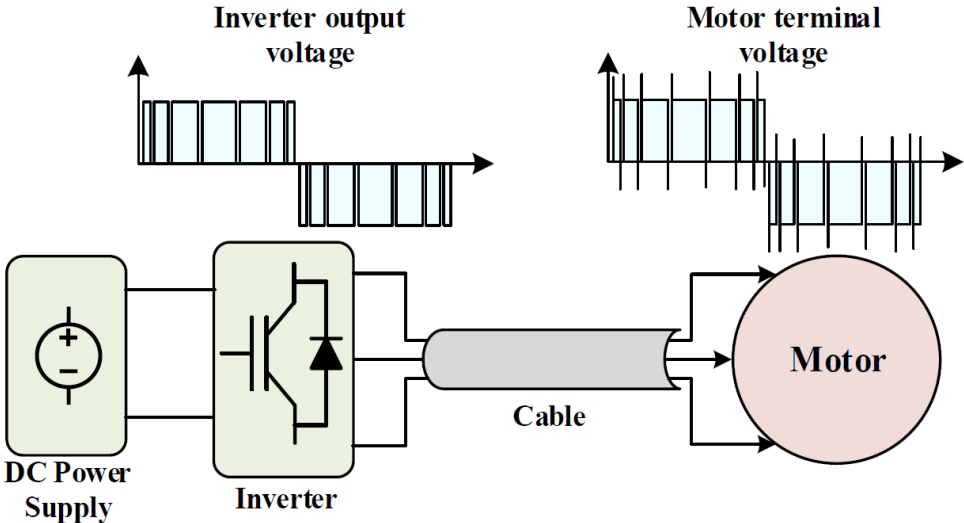


Figure 1–1 Typical powertrain system

Variable speed drives are very common and efficiently utilized to control these motors over a wide speed and torque envelope. These drives are built on fast power electronics devices, commonly controlled using the pulse width modulation (PWM) technique. These drives have been proven advantages in certain aspects, but the insulation of machine's stator winding undergoes very high electrical stress. In [5], it is shown that 70% of faults in the machine's stator are due to insulation failure and fast switching devices make it even worse. Fast switching of power electronics devices causes high  $dv/dt$  and reflected wave phenomenon due to cable, which can lead to voltage overshoots at machine's winding terminals and these overshoots can be about twice the DC bus voltage. Fig. 1-1 shows typical voltage output at inverted output and voltage at machine's terminals. Additional stress due to overvoltage can lead to accelerated insulation degradation and in some cases, pre-mature insulation failure. Partial Discharge (PD) activity is considered one of the main reasons for pre-mature insulation failure. So, for more reliable operation machines driven by these drives require different insulation, which is different from insulation in machines driven directly from grid power. The insulation material used is supposed to be PD resistant. However, PDs cannot be avoided due to factors like presence of micro voids in material, temperature level, and presence of moisture etc. With the application of even faster wide band gap (WBG) devices like gallium nitride (GaN) and silicon carbide (SiC), the occurrence of PD can take place even at lower voltages. Moreover, higher switching frequency offered by WBG devices will lead to more repetitive PD activity hence faster degradation of insulation.

The overvoltage at winding terminals is non-uniformly distributed inside coils and turns of winding and the degree of non-uniformity depends on voltage rise time, length of the connecting cable, parasitic parameters, and winding parameters. Overvoltage can appear at several locations inside the machine winding. If the aforementioned current and voltage distributions are predicted, electrical stress on insulation at various parts of machine winding can be obtained, which can be utilized to optimize the stator design for more safe and reliable operation and to assist filter design and converter design. So that most out of the system can be achieved.

Since degradation of insulation is a major cause of machine failure and it puts safety and reliability at risk, researchers have worked on various machine winding modeling techniques to investigate electrical stress on insulation and to understand voltage propagation inside the machine winding. In the past few decades, Various machine winding modeling approaches have been proposed and

investigated with a motive to understand voltage propagation and voltage distribution in machine winding. In the literature, motor winding modeling practices can be found as early as in the 1970s. In 1979, R. E. Adjaye represented machine winding by two port network [6]. In 1983, M.T. Wright applied multi conductor transmission line theory and scatter matrix theory to model winding and obtained interturn and intercoil voltages introduced due to steep-fronted switching surges. Thereafter, many models using lumped parameter equivalent RLC-circuits to represent motor windings have been proposed and investigated [7]–[13]. After that, transmission line theory based models were proposed [14]–[22]. Overtime various methods utilizing multiconductor transmission line (MTL) theory were proposed [23]–[27]. Recently, finite element (FE) based models are used which has a capability to obtain the most accurate electrical stress [28]–[30]. There are various modeling approaches have been presented over the years. However, it is not clear that which technique is advantageous or disadvantageous and at what aspect. Therefore, this thesis focuses on comparative analysis to understand how selected modeling techniques performers and to understand capability and limitations associated with them.

As a matter of fact, degradation in insulation cannot be avoided due to material decomposition, thermal stress, mechanical stress, and contamination from surroundings. Failure in insulation puts the safety and reliability of machine on risk. In industries, frequent inspection and maintenance of a machine is very common. However, in applications like EVs and aerospace where safety is very critical, continuous health monitoring becomes essential. Recently, immense amount of research being done in machine's health monitoring domain. Detecting degradation in insulation in an early stage can prevent major failure in machine and prevent major system failure. For monitoring of insulation condition, various techniques have been proposed which can be mainly categorized into two types. One is offline monitoring, in which a machine is required to be taken out of the service to perform tests. Another is online monitoring, in which a machine is kept on service to perform tests. Online monitoring is most desired method to avoid down time and comparatively less expensive compare to with offline monitoring. There are various online monitoring techniques were proposed over the years like partial discharge based monitoring, on-line surge test, leakage current monitoring, current sequence detection and transient current response-based monitoring. Transient current response-based monitoring technique caught the author's attention as it does not require additional sensors. However, none of these techniques were able to classify the type of degradation. Keeping online insulation condition monitoring technique in focus, this thesis

investigates condition monitoring techniques by utilizing finite element (FE) based technique to emulate insulation degradation to investigate condition monitoring technique.

## **1.2. Research Objective and Contributions**

Analysis of electrical stress is very important to understand how it affects the insulation and to optimize the stator's design for more reliable operation. While monitoring of insulation and detection of degradation at an early stage is also very crucial to avoid unpredicted downtime and ensure the safety of the machine and drive system in applications like electric mobility and aerospace. To achieve such research objectives, this thesis contributes to:

1. Comprehensive modeling of machine winding insulation and comparative analysis on various machine winding modeling techniques for electric stress determination in a form wound electric machine stator.
2. Modeling of a random wound machine stator and emulation of insulation degradation of various types and severity using FE based approach.
3. A new winding insulation degradation detection technique which can classify types of insulation degradation and provide state of health (SOH) of the insulation.

Contributions in form of publications are as follows.

### **Patent:**

- A. Patel, C. Lai, N. C. Kar, G. Schlager, M. Winter, A. Exl and K. L. Varaha Iyer "Degradation and Classification of Electric Motor Winding Insulation Degradation" U. S. Patent 63111366 (provisional application filed on November 9, 2020)

### **Conference paper:**

- A. Patel, C. Lai, K. L. Varaha Iyer, G. Schlager and N. C. Kar, "Investigations on Winding Modeling Techniques for Electrical Stress Analysis in VSI-Fed Traction Electric Machines," in the proceedings of *IEEE Transportation Electrification Conference (ITEC-India)*, Bengaluru, India, 2019.

### 1.3. Dissertation Layout

Chapter 2 presents a comprehensive review of some of the motor winding modeling techniques. Then to understand the capabilities and limitations associated with them, a comparative analysis on some of the approaches is performed. To do so, simple case study using form wound machine winding is presented, in which winding is modeled using different modeling techniques. Comparative analysis is performed by analyzing electrical stress obtained for different  $dv/dt$  voltage pulses. In addition, some points on how existing modeling techniques can be made more accurate are discussed.

Chapter 3 mainly presents the emulation of degradation of insulation using FE based approach. Initially, a random wound machine winding is modeled, where the detailed arrangement of each wire or strand inside the slot and different insulation layers are considered. Then, a detailed procedure and fundamentals behind emulation are presented. Turn to ground (TG) insulation degradations and turn to turn insulation degradations of different severity inside the winding are emulated. In the end, how these degradations of insulation affect the transient current response when the voltage pulse is applied to the winding is presented. Results obtained from emulation are analyzed and further used to investigate insulation degradation detection techniques.

Chapter 4 proposes a new insulation condition detection technique based on current response and wavelet packet decomposition (WPD). This method can determine the overall state of health (SOH) of insulation and type of degradation. Generally, there are mainly two types of degradations, one is degradation in turn or strand insulation and the other is degradation in groundwall insulation. Degradation classification capability is unique to this method. However, there are some limitations associated with this technique which are discussed.

Chapter 5 summarizes the work in this thesis and possible future work along with some suggestions are presented.

## Chapter 2: Machine Winding Modeling Techniques

To understand how each winding modeling technique performs and to understand the capability and limitations associated with them, it is essential to evaluate the modeling procedures and results. To this end, this chapter presents some of the machine winding modeling techniques in detail. Moreover, a simple case study using form wound machine winding is presented, in which the stator winding is modeled using different modeling techniques and comparative analysis is presented. Which also includes, electrical stress for different  $dv/dt$  pulses.

### 2.1. Literature Review

Three main approaches for modeling of machine winding are:

1. Finite Element (FE) based technique
2. Equivalent RLC based technique
3. Transmission line based modeling technique

In [28], Finite Element based modeling technique was introduced to model simple form wound and complex random wound machine winding with a motive to understand impacts of PWM excitation on insulation by analyzing electrical stress. This model has the capability to obtain currents and voltage at desired strands and turns of the winding. In [29], the effect of position of wires inside the slot on voltage stress and current distribution was investigated using FE based technique, and experimental results were also provided. Same model was used to investigate effect of factors like rotor position, rotor saliency, current level, voltage level, torque level and speed of rotation on electrical stress [30], experimental results presented assures the reliability of the modeling techniques. Finite Element based modeling technique is considered most accurate. This modeling technique provides freedom to easily investigate factors which can affect electrical stress, factors like effect of rotor position, rotor saliency, rotation speed and other factors in the drive system can be investigated with great ease.

The equivalent RLC based technique is the simplest and can be found in literature very often. In [31], form wound stator winding was represented by a lumped equivalent circuit to obtain voltage distribution at different turns in winding due to impulse voltage. In [7], a similar model was used to model coil with four turns and to obtain maximum voltage stress between various turns, effect

of different arrangements of turns with different parallel wires on electrical stress was investigated. In [8], the influence of the turn to turn capacitance on the whole winding was investigated using a similar model. In [9], a similar equivalent circuit based model was used to model winding with 56 turns, frequency response from simulation matched well with experimental results. In [10], equivalent RLC based model was used for electrical stress analysis and effect of wires on electrical stress was investigated. Experimental results matched with simulation results to a certain extent. However, these publications did not consider a change in parameters in overhang region. In [11], a similar model was extended to consider parameters change in overhang region and experimental results matched decently with simulation for form-wound machine. In [12], [13], a similar approach was used to obtain voltage distribution in transformer windings due to lightning impulse voltage. Application of equivalent RLC based modeling approach can be found in various other publications for similar applications. However, during modeling, some assumptions were made for modeling which are arguable. Moreover, it is not clear that how this modeling technique performs over other approaches.

Transmission line models (TLM) are also very common. Transmission line theory model can be represented as RLC circuit elements. Transmission line can be represented as lumped or distributed parameters circuit, which is series of T or  $\pi$  circuit sections. In [14], voltage distribution due to PWM pulse was investigated, first few turns were modeled as a distributed transmission line and the rest of the winding was represented by equivalent circuit. In [15], similar work was done for form wound machine using TLM and results were compared with simplified lattice diagram analysis and experimental results. In [16], the effect of rise time on electrical stress was investigated using TLM. However, the losses in the stator core were not considered. In [17], losses in the stator core were considered which resulted in even more accurate results. In [18], transmission line theory was utilized for electrical stress analysis and the influence of rotor on it was investigated. Moreover, in [19], the influence of end-winding or overhang region on electrical stress was investigated. In [20], TLM with frequency dependent inductances and resistances was presented and simulation results matched well with experimental results. Other application of TLM model can be found in [21]. TLM is very similar to equivalent RLC based model, however they are not as detailed as RLC models. For instance, each turn in winding may have multiple parallel strands or wires, in most TLM, this bunch of wires is considered as one conductor. While RLC models available in literature used both ways to model the winding. In [22], coils were represented

as a lossy multiconductor transmission line for voltage stress analysis, where losses in conductors and dielectric were considered, which resulted in more accurate results for that time period. Multiconductor transmission line (MTL) model can be considered as other variants of simple transmission line models, MTL model can represent the effect of wave propagation and electromagnetic coupling among the conductors more accurately than simple RLC based technique. In [23], a numerical method based MTL theory was utilized for voltage stress analysis in form wound stator. In [24], MTL theory was used to model form wound coils and electrical stress was obtained. In [25], MTL model was used to estimate voltage stress in a taper winding of a transformer. In [26], [27], non-uniform MTL model based on the cascaded connection of chain matrices was proposed and used to obtain voltage distribution in form wound machine, experimental results matched well with the simulation results. MTL based approach is used in various electrical stress estimation surge propagation studies. It is also important to note that in all these modeling techniques, the insulation is represented by different capacitances.

**2.1.1. Finite Element (FE) Based Modeling Technique**

This method utilizes FE tools to obtain electrical stress in the winding. The stator winding can be represented as a combination of resistances, inductances, and capacitances.

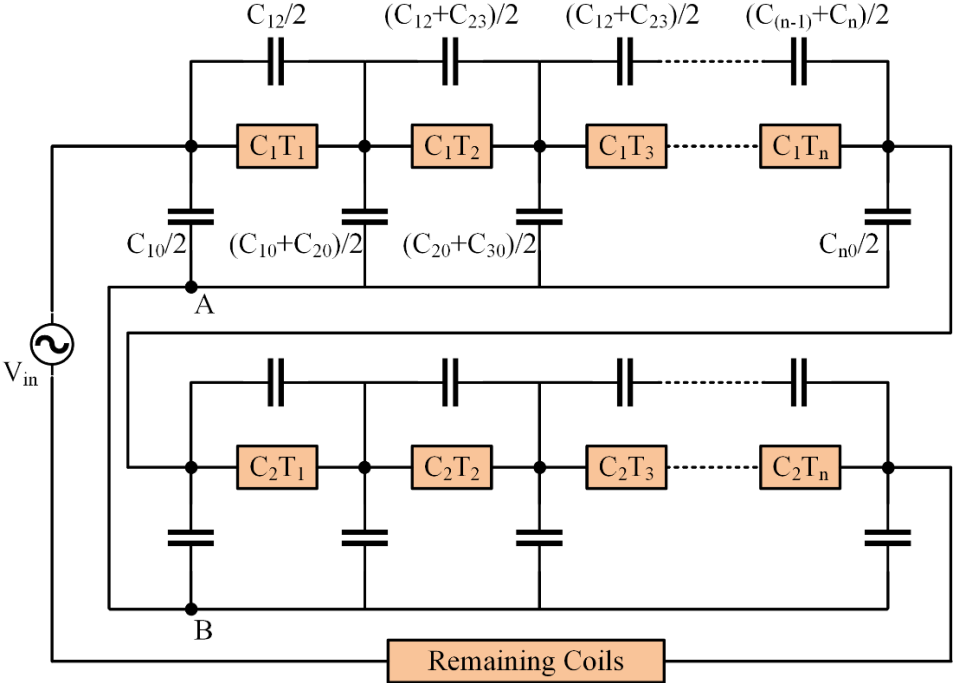


Figure 2–1 FE based model

A typical FEA tool uses a magnetic solver to calculate magnetic fields, inductances, currents, and voltages while an electrostatic solver can be used to obtain electric field and capacitance. However, currently there is no FEA tool that can combine electric and magnetic analysis. Therefore, in this modeling approach, the parasitic capacitances are calculated first using the electrostatics solver in FEA tool, then calculated capacitances are combined with other elements using external circuit within FEA tool. In Fig. 2-1, orange box marked by  $C_i T_i$  represents the  $j^{th}$  turn of the  $i^{th}$  coil, and  $C_{ij}$  is the inter-turn capacitance and  $C_{i0}$  is the turn to ground capacitance. Box  $C_i T_i$  contains resistance and inductance for respective turns. Here, in Fig. 2-1, just two coils are shown for illustration purpose. Generally, each turn consists multiple strands or wires connected in parallel. The circuit becomes more complex with more detailed strand level modeling however the fundamental concepts for modeling remain the same. In wave propagation studies, the stator is considered grounded which is represented by points A and B in the figure. Here  $V_{in}$  is the voltage excitation pulse applied to the winding, desired PWM pulse with desired  $dv/dt$  can be applied and electrical stress and current responses can be obtained.

### 2.1.2. Equivalent RLC Based Modeling Technique

In this modeling technique, each element of the equivalent circuit that represents a part of the coil must be much smaller than the wavelength corresponding to the frequency of transient voltage. The assumption made for this modeling approach is that voltages and currents do not vary over the whole turn. This assumption was supported by considering the wavelength of traveling wave due to the surge or switching pulse.

Due to the switching pulse, the maximum frequency component introduced in the system can be given by

$$f_{max} = \frac{1}{t_{rise}} \quad (2-1)$$

Here,  $f_{max}$  is the maximum frequency component and  $t_{rise}$  is the rise time of the applied switching pulse. The wavelength  $\lambda_{min}$  corresponding to that frequency can be given as following equation.

$$\lambda_{min} = \frac{v}{f_{max}} \quad (2-2)$$

Here,  $\lambda_{min}$  is the shortest resulting wavelength due to the travelling wave and  $v$  is the speed of travelling wave can be given by

$$v = \frac{1}{\sqrt{\mu\epsilon}} = \frac{c}{\sqrt{\epsilon_r}} \quad (2-3)$$

Where  $c$  is the speed of light and  $\epsilon_r$  is the relative permittivity of the medium surrounding the conductor which is insulation. The assumption is that the voltage and current distribution inside a part of the winding is considered constant for a length if it's less than one tenth of the wavelength. For example, if the rise time of the pulse is 10ns, the maximum frequency component in the applied pulse is 100 MHz, and wavelength related to this frequency would be 1.73 meters. So that, based on the assumption, the distribution of voltage and current can be considered constant over the length of winding up to 0.173 meters. The assumption can be argued since the coil is distributed over two regions, slot region and overhang region, and since the surrounding medium is different which results in different distribution of voltage and current over that region due to difference distribution of magnetic and electric field. However, this approach is used in various publications and considered fairly accurate.

In this approach, lumped circuit parameters are used, main circuit parameters are summarized in Table 2-1 and Fig. 2-2 shows a circuit for three turns. However, the model can be extended for multiple turns and coils. Moreover, a strand level model can be created by following same fundamentals.

Table 2-1 Main parameters for RLC based model

<b>Parameter</b>	<b>Description</b>
$L_p$	Turn inductance
$R_s$	Turn resistance
$R_p$	Resistance representing losses in core
$C_m$	Turn to ground capacitance
$C_t$	Turn to turn capacitance
$R_m$	Resistance representing turn-ground dielectric loss
$R_t$	Resistance representing turn-turn dielectric loss

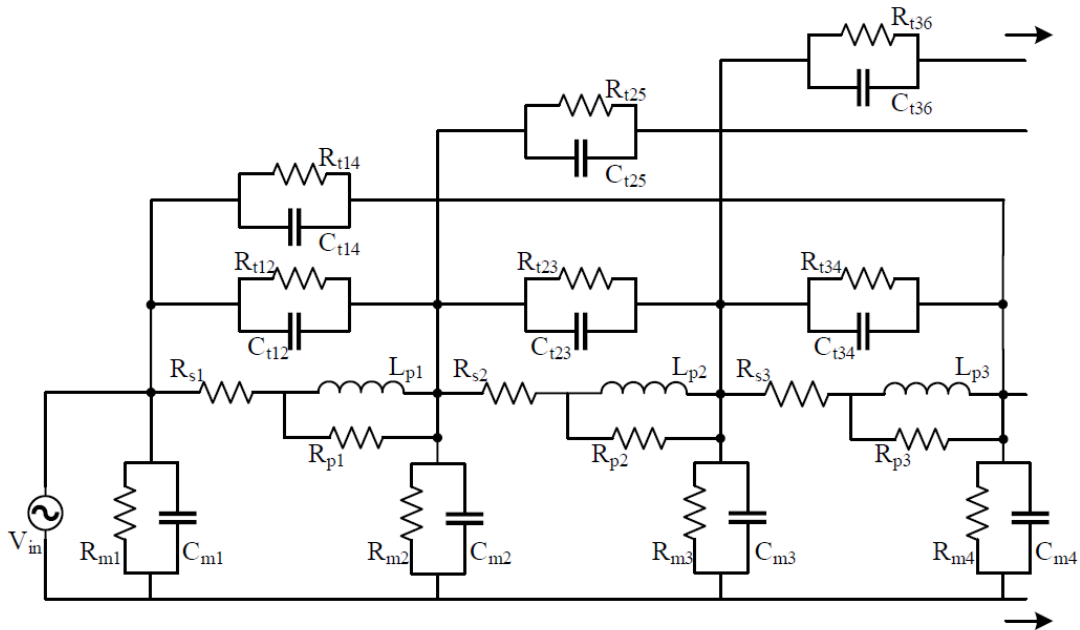


Figure 2–2 RLC based model for 3 turns

Parameters for this model are listed in the table.  $R_S$  and  $L_P$  are turn resistance and turn self-inductance respectively, mutual inductance among the turns is also considered. Resistance  $R_p$  is connected in parallel with inductance which represents the losses in stator core, this value is generally very high, and the influence of iron losses is negligible.  $C_t$  and  $C_m$  are turn to turn and turn to ground capacitances respectively which are due to the insulation system. Dielectric losses in the insulation are represented by resistances  $R_t$  and  $R_m$ , which represents turn to turn and turn to ground dielectric losses. In various literature, different level of details is considered. For instance, some of the parameters like  $R_m$ ,  $R_t$  and  $R_p$  have less influence on the modeling so they can be ignored. The parameters required for modeling can be calculated using FEA or analytical approach, then the circuit is simulated to obtain electrical stress.

### 2.1.3. Multi-Conductor Transmission Line Model

Using this modeling approach, the pulse propagation along the winding can be calculated by using transmission line theory and telegrapher's equation. Each coil or turn is distributed in two regions as shown in Fig. 2-3, slot region and overhang region. Electric and magnetic field distributions in slot region and overhang region of the coil are different depending on the arrangement of conductors and insulation system design resulting in different coil parameters for different regions.

Conductors in each region are coupled with each other and can be represented by MTL. Since the parameters for each region is different, the characteristic impedance for each region is different. By representing each region as MTL, voltage reflection between the regions due to impedance mismatch can be also considered. In the MTL model where the difference in parameters considered is called the non-uniform MTL model. In this section, non-uniform MTL model is explained as it is considered more accurate.

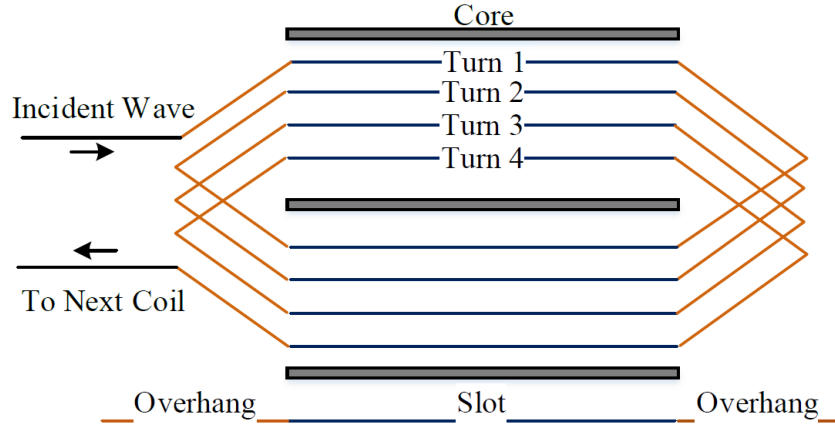


Figure 2-3 Winding distributed over different regions

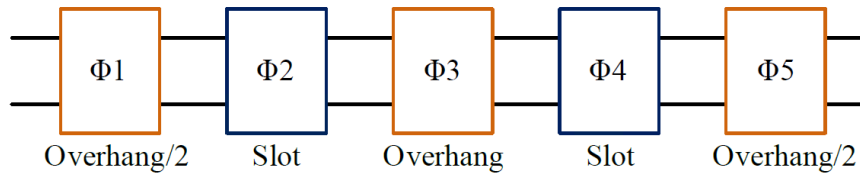


Figure 2-4 Cascaded chain matrices

As demonstrated in Fig. 2-4, to consider parameter variation in slot and overhang region, for each region the chain matrices for each region are calculated. Then computed matrices are cascaded in particular order to obtain the relationship between currents and voltages at both ends of turn. As discussed, the parameters for each region can be considered constant. For that segment of length  $\Delta x$  over which the parameters considered constant, the relation between current and voltage can be described as

$$\begin{bmatrix} V(x + \Delta x, s) \\ I(x + \Delta x, s) \end{bmatrix} = \phi(\Delta x, s) \begin{bmatrix} V(x, s) \\ I(x, s) \end{bmatrix} \quad (2-4)$$

The chain matrix (ABCD parameter matrix) can be given by

$$\phi(\Delta x, s) = \begin{bmatrix} \cosh(\psi\Delta x) & -Y_0^{-1} \sinh(\psi\Delta x) \\ -Y_0 \sinh(\psi\Delta x) & Y_0 \cosh(\psi\Delta x) Y_0^{-1} \end{bmatrix} \quad (2-5)$$

The propagation constant  $\psi$  can be given by:

$$\psi = M\sqrt{\lambda}M^{-1} \quad (2-6)$$

$M$  and  $\lambda$  are eigenvalue and eigenvector matrices of the product of impedance and admittance matrices. The characteristic admittance matrix  $Y_0 = Z(x, s)^{-1}\psi$ .

Parameters for slot and overhang region are calculated separately. The chain matrix for each segment is computed and cascaded as given in the following equation to obtain the relationship between currents and voltages at both ends of turn.

$$\begin{bmatrix} V_R \\ I_R \end{bmatrix} = [\phi_1][\phi_2][\phi_3][\phi_4][\phi_5] \begin{bmatrix} V_S \\ I_S \end{bmatrix} = \begin{bmatrix} \phi_{11} & \phi_{12} \\ \phi_{21} & \phi_{22} \end{bmatrix} \begin{bmatrix} V_S \\ I_S \end{bmatrix} \quad (2-7)$$

Then this chain matrix is transformed into other form to introduce a zig-zag connection. By solving the equation 2-7, the relation between input and output voltages and currents can be obtained.

#### 2.1.4. Parameter Computation

In each modeling techniques parameter like resistances, capacitances and inductances are required. Each literature had its choice of method for parameter computation. Parameter computation methods can be mainly categorized into two types, analytical computation and FEA based computation. In this section, resistance, inductance and capacitance calculation procedures are presented.

##### 2.1.4.1. Resistance Calculation

The resistance offered by the conductor is needed to calculate. Resistance calculation for each turn or strand considering skin effects can be calculated utilizing the complex penetration depth concept. Resistance calculation for both square conductor and round conductor is explained. The frequency  $f_h$  at which all the parameters are needed to be calculated is frequency related to the rise time of the applied pulse. In other words, it is the maximum frequency component in applied pulse. By applying Fast Fourier Transform (FFT) on the excitation pulse  $f_h$  can be obtained. Most accurate resistance can be calculated using FEA tools. However, it is not discussed in this section. Analytical method for rectangular and circular conductors is presented.

### Resistance calculation for rectangle conductor:

Per unit length resistance,  $Z_c$ , for rectangle conductor can be computed from the dc resistance  $R_{dc}$  and  $Z_{hf}$ , the impedance calculated at frequency  $f_h$ .

$$Z_c = \sqrt{(R_{dc}^2 + Z_{hf}^2)} \quad (2-8)$$

$$R_{dc} = \frac{\rho_c}{wh} \quad (2-9)$$

$$Z_{hf} = \frac{\rho_c}{2p(w+h)} \quad (2-10)$$

$$p = \sqrt{\frac{\rho_c}{j\omega\mu_c}} \quad (2-11)$$

Here,  $\rho_c$  is the resistivity and  $\mu_c$  is the permeability of the conductor material,  $w$  and  $h$  are the width and height of the cross section of conductor,  $p$  is complex penetration depth related to skin effect. Eddy current solver in FEA software can be used the resistance as well.

### Resistance calculation for circular conductor:

Per unit length resistance  $Z_c$  computed as [32]:

$$Z_c = R_{dc} \left( \frac{1}{4} + \frac{r_0}{2p} + \frac{3p}{32r_0} \right) \quad (2-12)$$

$$R_{dc} = \frac{\rho_c}{\pi r_0^2} \quad (2-13)$$

$$p = \sqrt{\frac{\rho_c}{\omega\mu_c}} \quad (2-14)$$

Here,  $\rho_c$  is the resistivity and  $\mu_c$  is the permeability of the conductor material,  $r_0$  is the radius of the wire,  $p$  is complex penetration depth related to skin effect.

#### 2.1.4.2. Capacitance Calculation

The capacitance matrix can be calculated analytically or by FEA. Most accurate capacitances can be obtained through FEA by using an electrostatics solver. Considering  $n$  conductors in the slot, initially one conductor is excited with 1V and all other conductors are excited with 0 V. FEA tool calculates energy stored in the electric field considering electric field distribution, and it can be expressed as:

$$U = \frac{1}{2} CV^2 \quad (2-15)$$

Where  $C$  is capacitance and  $V$  is the applied voltage across the dielectric. Capacitance can be expressed as following equation for each conductor  $i$ .

$$C = \frac{2U}{V^2} \quad (2-16)$$

Then the FEA tool internally repeats this procedure for all conductors internally and provides  $n \times n$  Maxwell's capacitance matrix for a system with  $n$  conductors. Capacitances with respect to ground and mutual capacitance can be obtained from Maxwell's capacitance matrix. Magnitude of capacitances barely changes with frequency so these capacitances can be considered constant.

#### 2.1.4.3. Inductance Calculation

The inductances can be obtained using a FEA tool. Typical magnetic field solvers available in most FEA tools can be used to obtain inductances. Considering  $n$  conductors in the slot,  $n$  field simulations are automatically performed to obtain a complete matrix containing self and mutual inductances. The diagonal elements in the inductance matrix are self-inductances which are numerically equal to the flux linkage in the respective conductor when current excitation is applied, and no current is flowing in other conductors. Off-diagonal elements represent mutual inductances which are numerically equal to flux linkage in one conductor when current excitation is applied to other conductor, and no current is flowing in the other loops. The energy stored on the magnetic field that couples two conductors is computed and given by:

$$W_{ij} = \frac{1}{2} LI^2 = \frac{1}{2} \int B_i \cdot H_i d\Omega \quad (2-17)$$

Where  $W_{ij}$  is the energy stored in a magnetic field linking two conductors  $i$  and  $j$ . Current excitation to conductor  $i$  is  $I$ .  $B_i$  is the magnetic flux density at conductor where current excitation is applied to the conductor.  $H_j$  is the magnetic field at another conductor  $j$  because of current excitation at conductor  $i$ . The inductance coupling between conductors  $i$  and  $j$  can be obtained as:

$$L_{ij} = \frac{2W_{ij}}{I^2} = \int B_i \cdot H_i d\Omega \quad (2-18)$$

The solver internally repeats this procedure for all conductors and provides  $n \times n$  inductance matrix.

## 2.2. Comprehensive Studies Through Simulations

This section presents results from various modeling techniques and the comparative analysis is presented. Form wound winding is modeled using three different approaches and the results are compared with results from [27], in which winding was modeled as non-uniform MTL and the approach was experimentally verified. Form wound winding was modeled using FE based technique and equivalent RLC based technique. Then step voltage of 1750 V with two different rise times of 25ns and 100ns, i.e.  $dv/dt$  is 70 kV/ $\mu$ s and 17.5 kV/ $\mu$ s, is applied and electrical stress across each turn or turn to turn stress and turn to ground stress is investigated.

### 2.2.1. Geometrical Configuration of Stator Winding

A form wound winding with 36 coils, 10 turns in each coil is modeled. Cross section of the coil is shown in Fig. 2-5, there are three different layers of insulation which are inter-turn insulation, main insulation, and ground wall insulation. Main parameters of a coil are provided in Table 2-2.

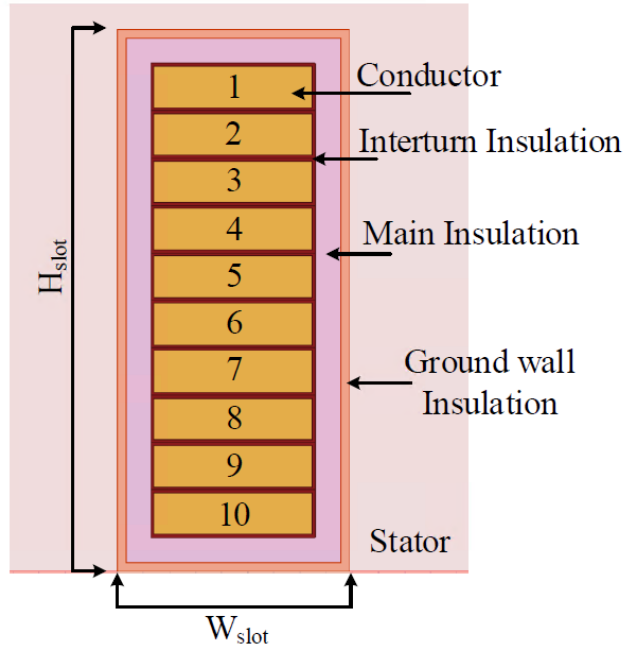


Figure 2–5 Cross section of form wound coil

Table 2-2 Main winding parameters

Parameter	Value
Turns per coil	10
Length of overhang region	0.2 m
Conductor width ( $w$ )	6.08 mm
Conductor height ( $h$ )	1.59 mm
Resistivity of stator bar conductor	$1.7 \times 10^{-8} \Omega\text{m}$
Thickness of inter-turn insulation	0.11 mm
Thickness of main insulation	0.96 mm
Thickness of ground wall insulation	0.33 mm
Relative permittivity of inter-turn insulation	2.5
Relative permittivity of main insulation	2
Relative permittivity of ground wall insulation	4
Slot width ( $W_{slot}$ )	8.9 mm
Slot height ( $H_{slot}$ )	20.7 mm
Slot length	0.38m
Number of coils	36

## 2.2.2. Parameter Computation

Parameters required for modeling are obtained using FE based method or analytical calculations. Capacitance and inductance are obtained using FE based method. While resistance for copper was calculated using analytical calculation. Coil along with insulation layers is modeled in FE software.

### 2.2.2.1. Capacitance Calculation

Then capacitance matrix is obtained by performing electrostatic analysis. Since there are 10 conductors in each slot,  $10 \times 10$  matrix is obtained. Most FEA based tools provide capacitances in form of a maxwell capacitance matrix. The Maxwell capacitance matrix provides the relation between the charge of  $i^{th}$  conductor to the voltage of all conductors in the system. One can easily identify the Maxwell capacitance matrix by its negative off-diagonal elements. For a system with N conductors, Maxwell capacitance matrix can be given by following equation.

$$\begin{pmatrix} Q_1 \\ Q_2 \\ \vdots \\ Q_N \end{pmatrix} = \begin{bmatrix} \sum_{i=1}^N C_{1i} & -C_{12} & \cdots & -C_{1N} \\ -C_{21} & \sum_{i=1}^N C_{2i} & \cdots & -C_{2N} \\ \vdots & \vdots & \ddots & \vdots \\ -C_{N1} & -C_{N2} & \cdots & \sum_{i=1}^N C_{Ni} \end{bmatrix} \begin{pmatrix} V_1 \\ V_2 \\ \vdots \\ V_N \end{pmatrix} \quad (2-19)$$

Here, diagonal terms  $C_{ii}$  represent self-capacitance of the conductors. Numerically, it is equal to the charge on a respective conductor when one volt is applied, while all the other conductors are set to zero volts. The off-diagonal terms  $C_{ij}$  are simply the negative of the mutual capacitance values. Obtained Maxwell capacitance matrix for a coil with 10 conductors and three different layers of insulation is provided in Fig 2-6.

Turn to ground or turn to stator capacitances  $C_{c,ii}$  can be obtained by adding all the elements from the same column to the diagonal element. The resulting capacitance matrix which contains turn to turn  $C_{c,ij}$  and turn to ground capacitance  $C_{c,ii}$  is presented in 2-7, diagonal elements are turn to ground capacitance and off-diagonal elements are negative values of mutual capacitances.

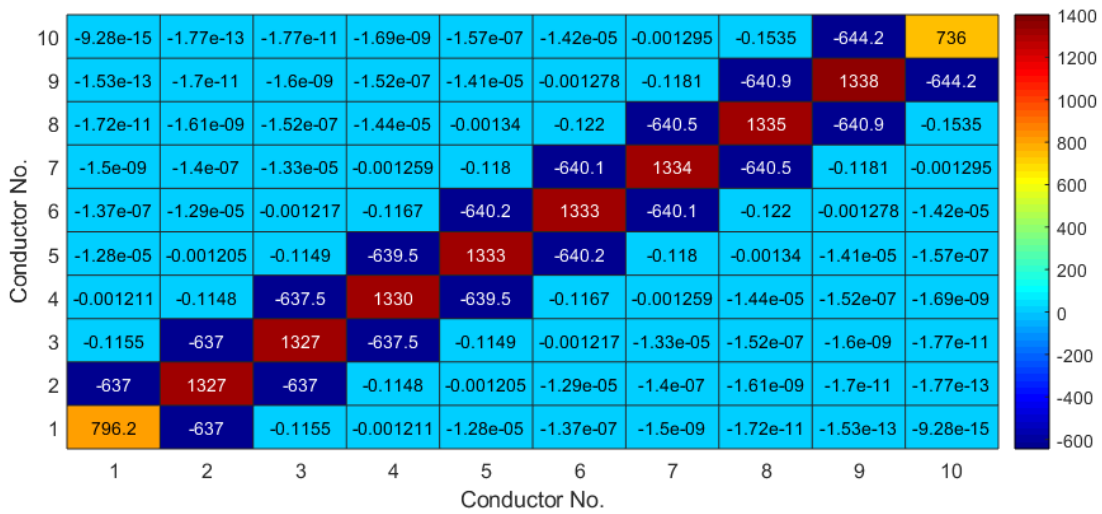


Figure 2–6 Maxwell capacitance matrix for form wound coil (nF)

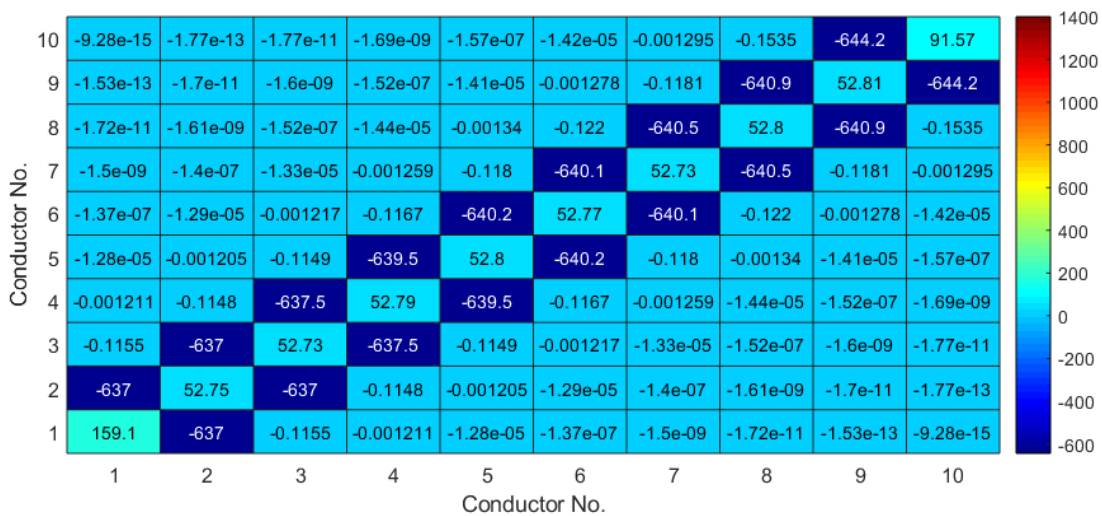


Figure 2–7 Capacitance matrix for form wound coil (nF)

### 2.2.2.2. Inductance calculation

Inductive coupling among the conductors is calculated using magnetostatic analysis. Similar to the capacitance matrix,  $10 \times 10$  inductance matrix is obtained. Diagonal elements of the matrices are self-inductances for respective turn while off diagonal elements are mutual inductances, the matrix is symmetrical along the diagonal. The inductance matrix is presented in Fig. 2-8.



Figure 2–8 Inductance matrix for form wound coil

### 2.2.2.3. Resistance Calculation

Since rise times of the applied voltage pulse are 25ns and 100ns, the resistance is required to be calculated at the frequency corresponding to this rise time. The resistance for a rectangular conductor is calculated using the analytical method. The frequency corresponding to 25ns is 40MHz, and resistance per turn is 0.12  $\Omega$ . While frequency corresponding to 10ns is 10MHz, and resistance per turn is 0.062  $\Omega$ .

### 2.2.3. Winding Modeling

Parameter computation required for this study is presented in the previous section. In this section, results for TT and TG stress is presented. Moreover, comparative analysis from this study is presented and discussed. For simplifying in winding modeling, termination technique is used which is discussed in the following sub-section.

#### 2.2.3.1. Resistive Termination

Termination techniques are commonly used for electrical stress and wave propagation analysis, which helps to reduce complexity and reduces computation cost. Generally, first few coils in the winding experience high electric stress and higher transient overvoltage compare to the rest of the winding. So transient study can be limited to the first few coils for simplification. The concept behind the termination technique is to represent some part of winding by equivalent resistance or a combination of resistance and inductance. In this study, the fist coil is modeled in detail and rest

of the winding is represented by its equivalent resistance. Fig 2-9 illustrates the termination technique.

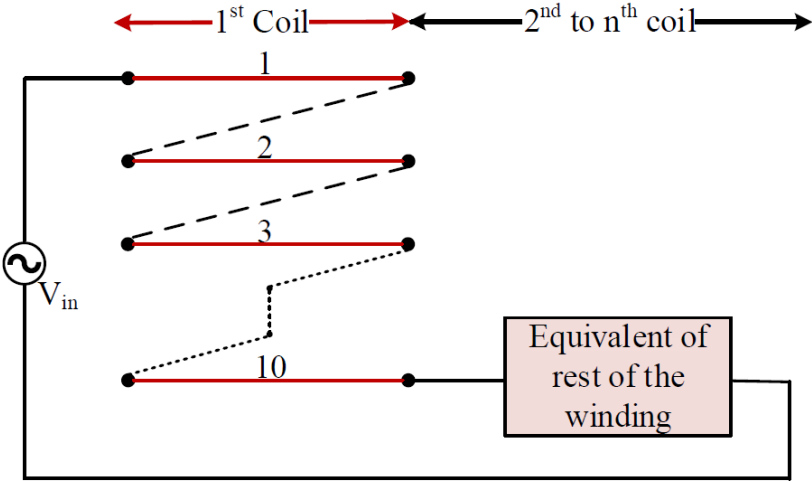


Figure 2–9 Illustration of termination technique

There are total 36 coils in the winding and each coil has 10 turns in it. The first coil or first 10 turns are modeled rigorously while rest of 35 coils are represented by equivalent resistance. To obtain equivalent resistance to be used as equivalent for rest of the winding, impedance corresponding to the switching frequency is obtained.

**2.2.3.2. Comparative Analysis and Discussion**

**FE Model:**

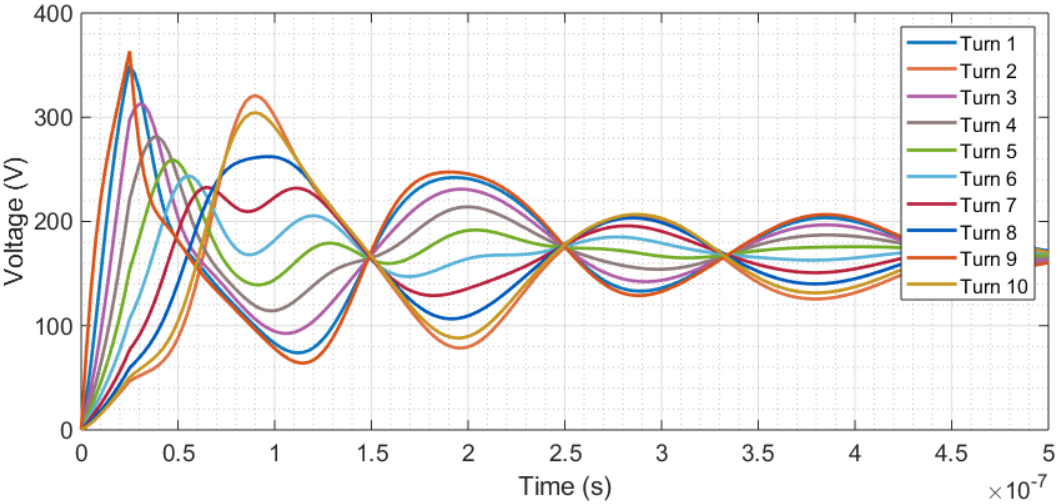


Figure 2–10 TT voltage stress for 1750 V pulse with 25ns rise time (FE Model)

Figs. 2-10 and 2-11 show voltage across each turn or turn to turn (TT) voltage for a pulse with two different rise times, 25ns and 100ns. For each case, voltage stress across each turn is not the same and ringing can be observed. Voltage ringing decays over time and the stress reaches steady, this is a realization of the fact that switching transitions impose additional electrical stress on winding. It can be observed that voltage stress is comparatively more on first few and last few turns. Voltage stress across turn 9 and turn 10 are lagging by those on turn 1 and turn 2 by about 180°, this is due to the phenomenon of wave propagation. Moreover, the influence of rise time can be observed since stress for the pulse with less rise time is high compare to the pulse with higher rise time.

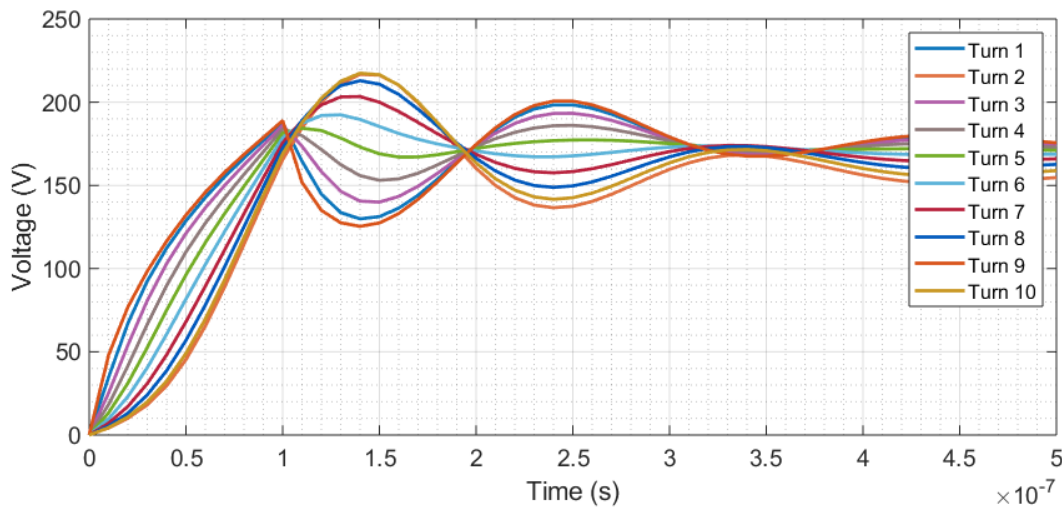


Figure 2–11 TT Voltage stress for 1750 V pulse with 100ns rise time (FE Model)

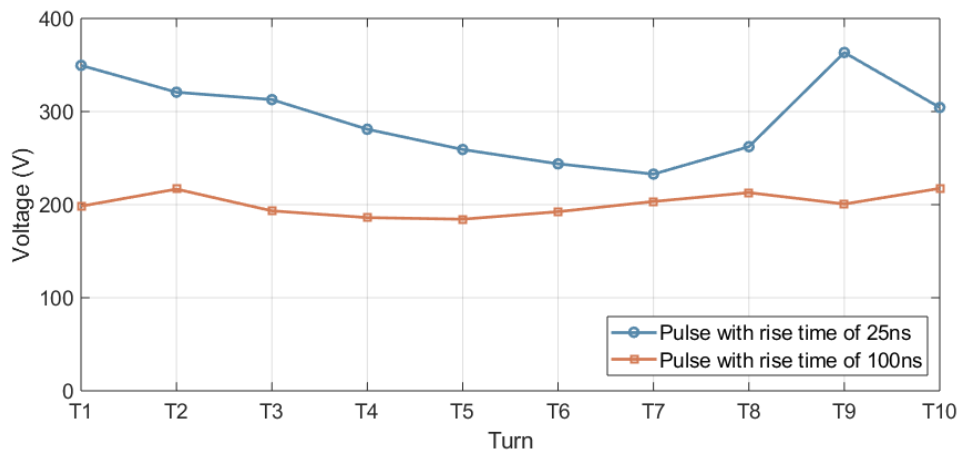


Figure 2–12 Maximum TT stress for 1750 V pulse with different rise time (FE Model)

Fig. 2-12 summarizes maximum stress on each turn for different rise times. Figs. 2-13 and 2-14 show turn to ground (TG) voltage at each turn. Ringing in TG voltages is also very obvious.

However, ringing is not as significant as in TT voltages. Moreover, it can be observed that TG values for each turn is increasing with time if oscillations are not considered. Moreover, the effect of rise time on TG is also clear since oscillations and values of TG voltage are comparatively high for the pulse with shorter rise time.

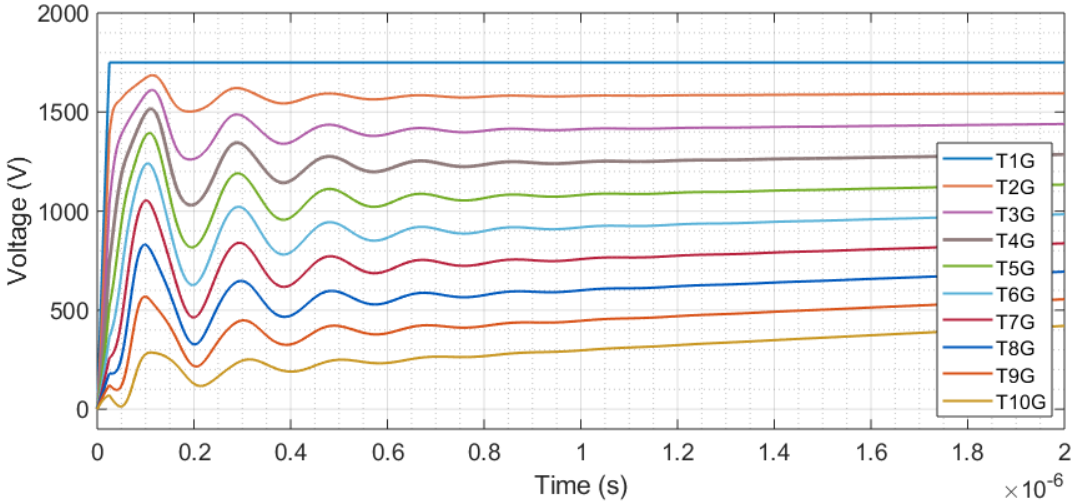


Figure 2–13 TG Voltage stress for 1750 V pulse with 25ns rise time (FE Model)

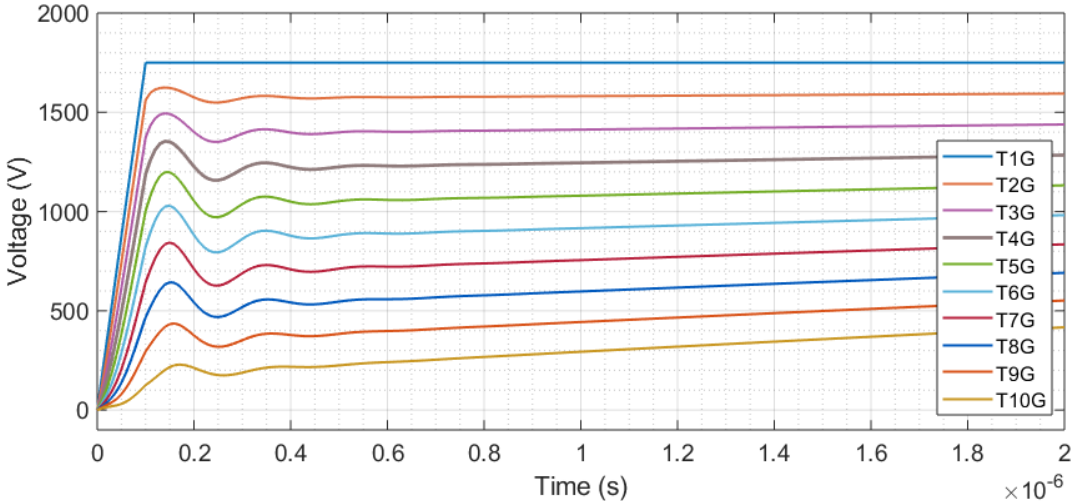


Figure 2–14 TG Voltage stress for 1750 V pulse with 100ns rise time (FE Model)

### RLC Model:

Figs. 2-15 and 2-16 show TT voltage stress or voltage across each turn for a pulse with two different rise times: 25ns and 100ns. Similar conclusions like FE model can be drawn from these results. However, the waveform pattern is different from results obtained from the FE model. It can be observed that voltage across each turn is reducing rapidly over time, which was not the case in the FE model, this is due to difference in inductances. In RLC model, constant value of inductance is used which is calculated for very high frequency. Since the inductance are lower at high frequency, the voltages reach steady state more quickly. Which is not the case in FE model because in FE model, frequency dependent inductances are considered. This is also the reason that RLC model with constant inductances is only reliable to obtain stress for very short time after the pulse is applied. Fig 2-17 summarizes maximum stress on each turn for different rise times obtained from RLC model.

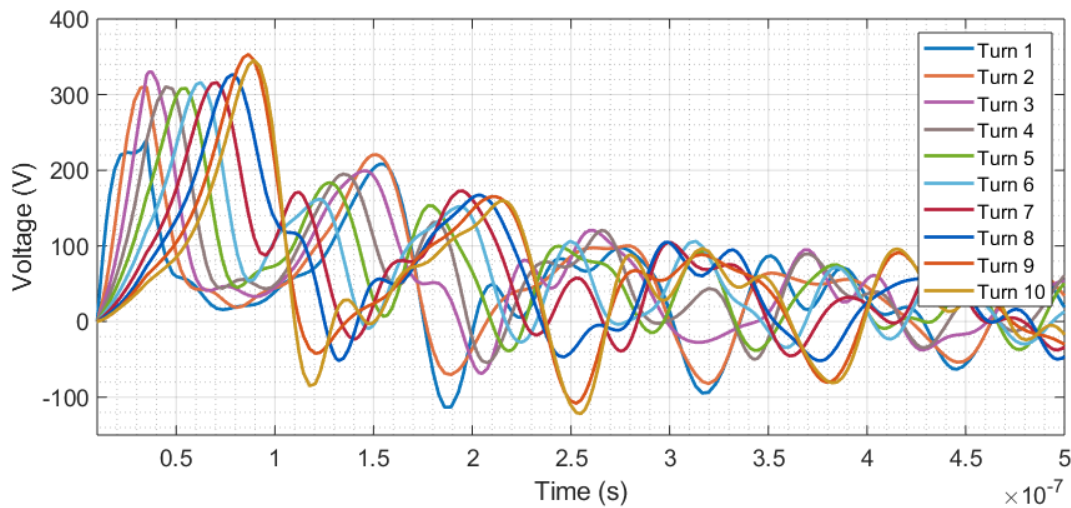


Figure 2–15 TT voltage stress for 1750 V pulse with 25ns rise time (RLC Model)

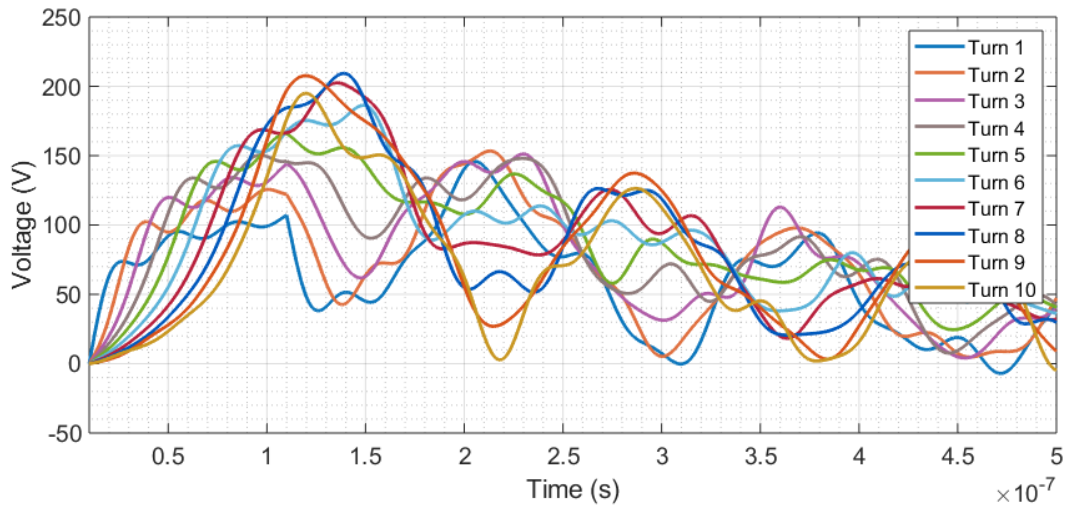


Figure 2–16 TT voltage stress for 1750 V pulse with 100ns rise time (RLC Model)

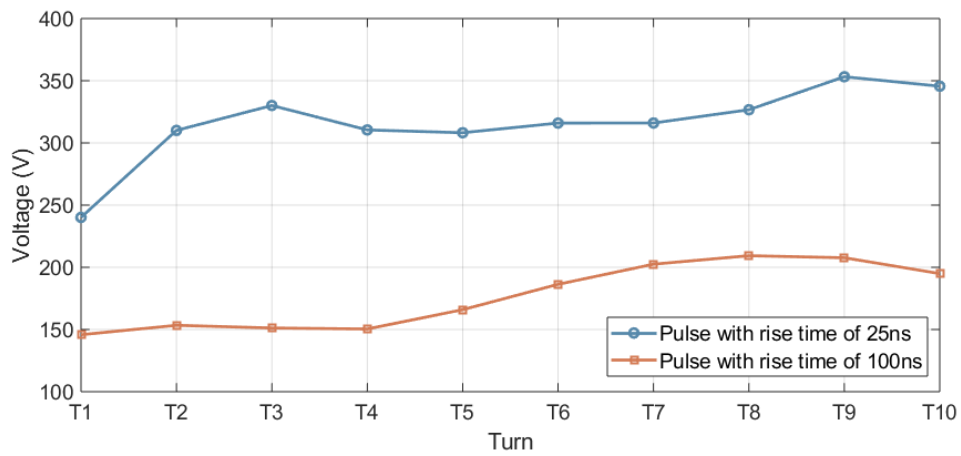


Figure 2–17 Maximum TT stress for 1750 V pulse with different rise time (RLC Model)

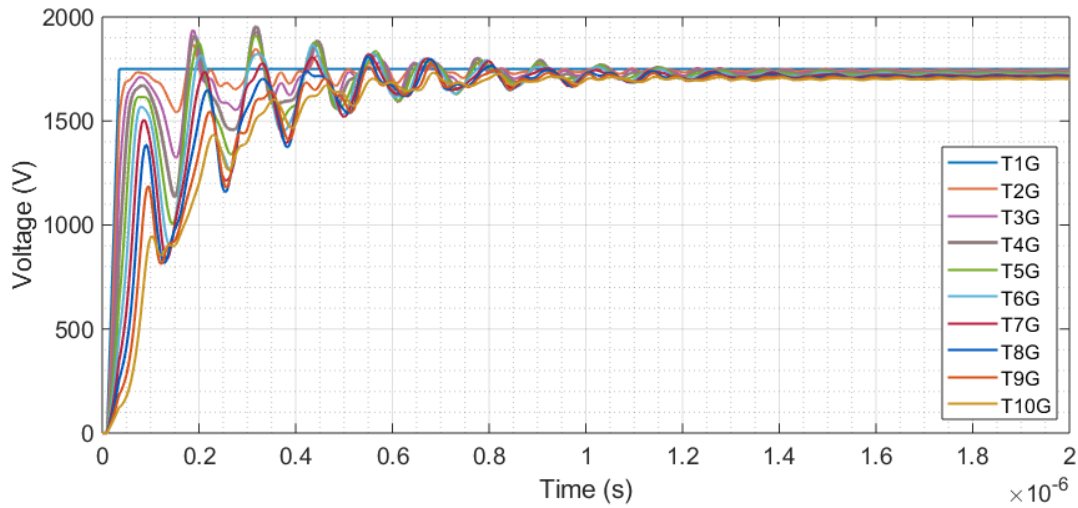


Figure 2–18 TG Voltage stress for 1750 V pulse with 25ns rise time (RLC Model)

Figs. 2-18 and 2-19 show turn to ground (TG) voltage at each turn. Effect of rise time is obvious. Moreover, it can be observed that TG voltages are increasing more rapidly compared to the FE model due to the constant value of inductance. Moreover, it can be observed that TG values for some turns are higher than applied pulse for pulse with 25ns rise time which is not the case in FE model. As expected, it can be observed that TG values are higher for pulse with shorter rise time.

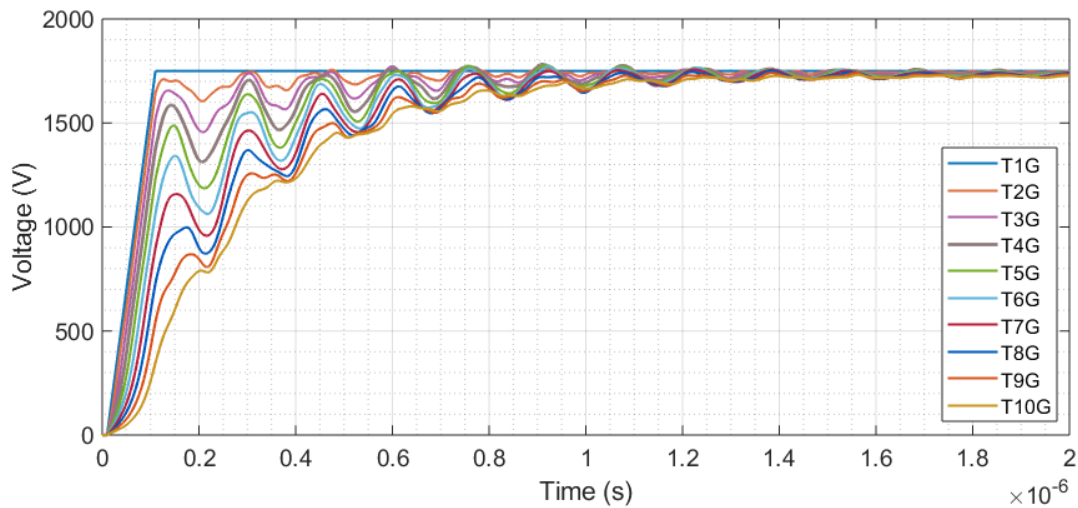


Figure 2–19 TG Voltage stress for 1750 V pulse with 100ns rise time (RLC Model)

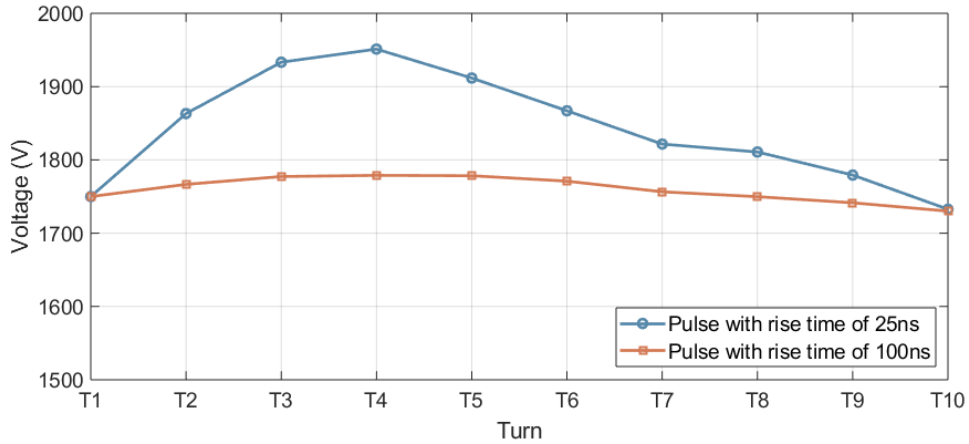


Figure 2–20 Maximum TG stress for 1750 V pulse with different rise time (RLC Model)

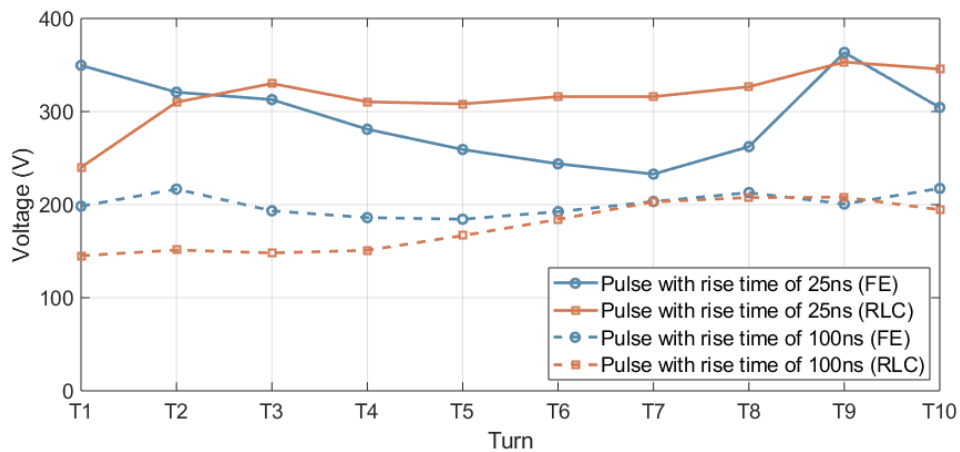


Figure 2–21 Comparison of maximum TT stress obtained from different model

Fig. 2-20 summarizes maximum TG stress obtained from RLC model. Fig. 2-21, compares peak voltages across each turn obtained from FE based modeling and RLC modeling techniques. It can be observed that for a pulse with 25ns rise time, the results are close with each however there is some discrepancy. While, for a pulse with 100ns rise time the results are comparatively closer.

Table 2-3 Comparison of maximum TT voltages

Rise time of applied voltage pulse	Maximum inter-turn (TT) voltage (V)		
	Non-Uniform MTL Model [27]	FE Model	RLC Model
25ns	399	363	354
100ns	225	216	210

Table 2-3 compares maximum voltage stress values obtained from FE and RLC models with reference results obtained using the Non-uniform MTL model in [27]. It can be seen that the values obtained from this study are close to reference results, however they still show some discrepancy. For pulse with 25ns rise time, obtained values show more error when compare to the values for pulse with rise time of 100ns. The results obtained from FE model and RLC model match well with each other. However, for pulse with 25ns, the values obtained show discrepancy in comparison with results obtained from Non-uniform MTL model. For pulse with rise time of 100ns, the results matched well with each other. This discrepancy is due to the disregard of parameter variation in slot and overhang region. Other reason can be the use of different termination technique. Here, it is also very important to note that in RLC model, constant inductance is used in circuit. While in FE model, frequency dependent inductance is internally computed by the solver. So, the computation time taken by FE model is huge compare to RLC model. By including frequency dependent inductances in the RLC model, more accurate results can be achieved. Moreover, resistance is constant in both models, inclusion of frequency dependent resistance would also give more accurate results. Going deeper into frequency dependent parameters, not only inductance for each turn but coupling or mutual inductances among the turns changes with the frequency. In FE model, frequency dependent coupling is taken care of internally by the solver. But including of aforementioned frequency dependent coupling among the conductors in RLC model would give close results to FE model. So, it is possible to make RLC model very accurate, but it requires the inclusion of very complex frequency dependent parameters. In this study, parameter variation over slot and overhang region is not considered.

### **2.3. Summary**

In this chapter, a comprehensive summary of different types of machine winding modeling techniques is presented along with parameter computation. A case study in which form wound winding is modeled using two different approaches is conducted by analyzing the TT and TG voltage stress under pulses with different  $dv/dt$  levels. Maximum stress values obtained from RLC model and FE model matched well with each other. However, the transient behavior of these voltage stresses did not match well with each other. A reason for this discrepancy can be use of constant inductance value in RLC model. Whereas FE model computes frequency dependent parameters internally. Compared to RLC model, the FE model is extremely computationally expensive. By modeling and including frequency dependent parameters in RLC model, the more

accurate winding model can be created. Moreover, slot and overhang regions can be modeled separately along with frequency dependent inductances and resistances to achieve even higher accuracy. Inclusion of these frequency dependent brings many technical challenges.

# Chapter 3: Emulation of Insulation Degradation

This chapter mainly presents the emulation of insulation degradation in random wound machines. Initially, insulation system in stator winding and factor that affects the degradation are presented. Then, the principle behind emulation of insulation degradation is explained. Then emulation of various types and severity of degradation using FE based approach is presented. Then, influence of degradation on input current is presented, which is utilized to investigate insulation degradation detection technique.

## 3.1. Insulation System in Stator Winding

A stator of any machine mainly consists three components: the stator core, conductors, and insulation. The stator core provides a low reluctance path to electromagnetic flux, conductors carry current and produce flux while the insulation prevents short circuit among the conductors or to core. Insulation is passive component in stator, and it does not help in producing or carrying magnetic flux. Insulation also acquires smallest section of the stator; however, it is very important component of the machine which ensures safe, efficient, and reliable operation of a machine.

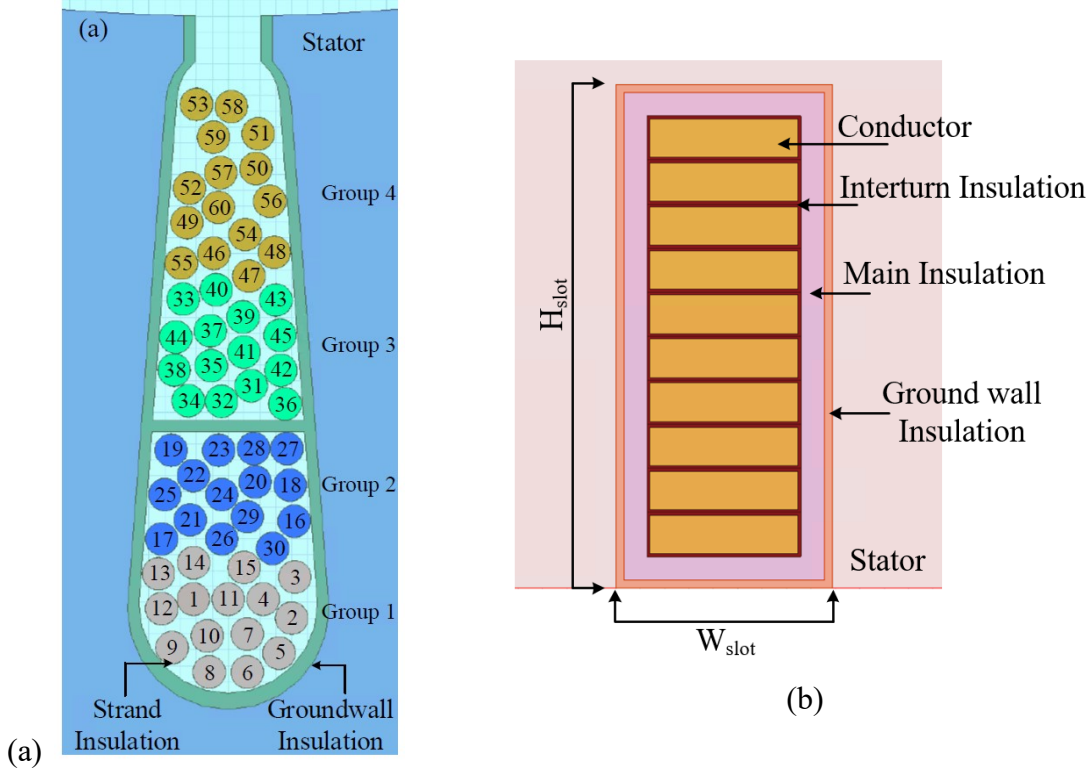


Figure 3-1 Insulations in (a) random (b) form wound coil

The stator mainly consists three types of insulation: strand insulation, turn insulation, and groundwall insulation. Fig. 3-1 shows a cross section of slot for typical form wound and random wound stator windings.

Various materials are being used as insulation. Polyester resins or epoxy, polyester films, mica, and aramid paper are commonly used. Material's ability to withstand electrical stress and mechanical stress varies depending on various factors like their atomic structure, chemical properties, thickness etc. So, it becomes important to choose proper insulation for more reliable and safe operation of the machine.

Typically, low voltage machines consist of random wound stator winding. While medium and high voltage machines use form wound winding. Conductive wires are coated with an insulation layer called strand or turn insulation. Polyamide-imide, polyester-imide, polyurethane, or a combination of polyester-imide and polyamide are very commonly used as strand insulation because they provide better resistance to partial discharge. The copper conductor with an insulation layer on it is readily available from different manufacturers and known as 'magnet wire'. Magnet wire of different sizes, different types of insulations, and with different dielectric strength are available in the market having thermal class of up to 220 °C.

Groundwall insulation separates conductors from the stator wall. This insulation is the most important insulation, and failure in groundwall insulation can result in a severe fault. So, for reliable operation over a long period, groundwall insulation is also made PD resistant. Mica and aramid papers are commonly used as groundwall insulation.

### **3.2. Insulation Degradation**

The insulation is supposed to withstand the electrical and mechanical stress for which it is designed for. However, degradation of insulation is inevitable due to thermal stress, electrical stress, environmental stress, and mechanical stress. There is different insulation design for low voltage, medium voltage, and high voltage machine. In this thesis insulation system in a low voltage machine is kept in focus.

### 3.2.1. Thermal Stress

Thermal stress is considered as one of the dominating factors for insulation degradation. Thermal stress mainly causes two changes in insulation. One is the weakening of chemical bonds of insulation due to chemical degradation reactions, polymerization, and chemical diffusion. The other effect is mechanical changes like expansion or contraction of insulation, which can lead to delamination and cracking of insulation. Based on the temperature, insulation is mainly categorized in class A, B, F, and H and they are suitable for operating of 105 °C, 130 °C, 155 °C and 180 °C, respectively. For temperatures above 180 °C aramid papers are used. Arrhenius model provides an estimation of insulation lifetime and is represented by the following equation [33].

$$k = L_0 e^{\frac{E_a}{RT} \left( \frac{1}{T} - \frac{1}{T_0} \right)} \quad (3-1)$$

Here,  $k$  is lifetime of insulation at temperature  $T$ ,  $L_0$  is lifetime at the reference temperature  $T_0$ ,  $E_a$  is activation energy and  $R$  is gas constant. This estimation is very accurate when a machine is being operated at constant temperature and machine winding is at a constant temperature. However, it is not the case in most applications. Temperature highly affects the lifetime of insulation, study in [34] shows that the lifetime of insulation is higher at lower temperatures. Study also shows that dielectric properties of insulation change differently at different temperature so using proper thermal class of insulation is very crucial. Thermal aging also causes change in the permittivity or dielectric strength of the insulation. Generally, the permittivity of insulation increases with degradation, so that partial discharge inception voltage (PDIV) reduces which can cause more often PD occurrence. Fig. 3-2 shows how the dielectric properties of insulation Nomex® 420 change with temperature [35]. Permittivity of insulation is different at different temperature. Most manufactures provide information on how permittivity changes with temperature.

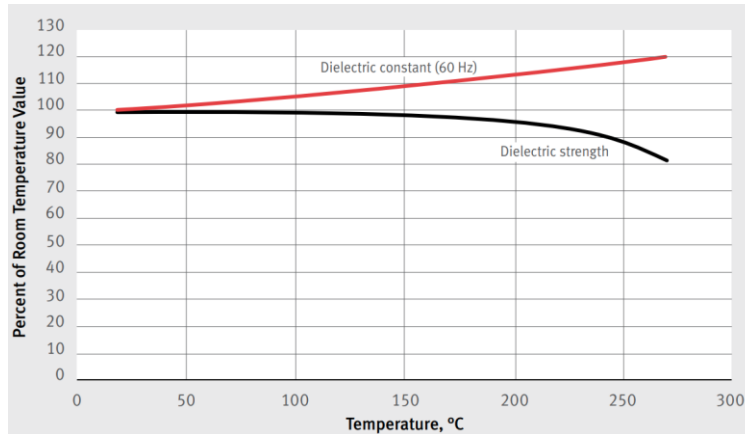


Figure 3–2 Effect of temperature on dielectric strength of insulation [35]

### 3.2.2. Electrical Stress

There are multiple reasons why electrical stress leads to insulation degradation. Factors like construction of insulation material, PD activity, tracking and corona effect and transient voltages affect the insulation degradation caused by electrical stress.

It is common to have air pockets and contamination in insulation materials. PD activity is more likely to happen at these weakened areas due to air pockets or contamination. These PDs can also accelerate degradation due to the reaction of insulation polymers with ozone. Due to contamination of insulation on insulation, leakage current can flow through insulation when enough voltage gradient is applied across. Tracking mainly cause phase to ground faults. Corona effect is not very common in low voltage machines, it is the effect that cause local electrical discharge due to ionization of insulation system.

Inverters driven by PWM pulse also create electrical stress on insulation. With the application of faster switching devices like GaN and SiC, insulation of machine undergoes even higher electrical stress due to high  $dv/dt$  pulse at winding terminals. Research shows that the first few turns from winding terminals are more exposed from these high  $dv/dt$  pulses and better insulation for these turns is recommended [36].

### 3.2.3. Environmental Stress

Environmental stress mainly includes contamination from the surrounding environment like contamination due to foreign material, moisture, chemical contamination, humidity, radiation, etc. In the real world, machines are exposed to surrounding contamination and failure rate higher

compare to machines that run indoors [37]. Moisture, chemicals, oils from bearing, coolant particles, dirt etc. can be considered as environmental contamination. Each of these contamination affects the insulation in different way. Contamination can lead to reduced heat dissipation and hence accelerated degradation due to temperature rise. Conductive contamination can also lead to effects like tracking and PD activity. Fig. 3-3 shows how dielectric properties of polyamide changes with humidity, polyamide is commonly used as insulation on magnet wire [38].

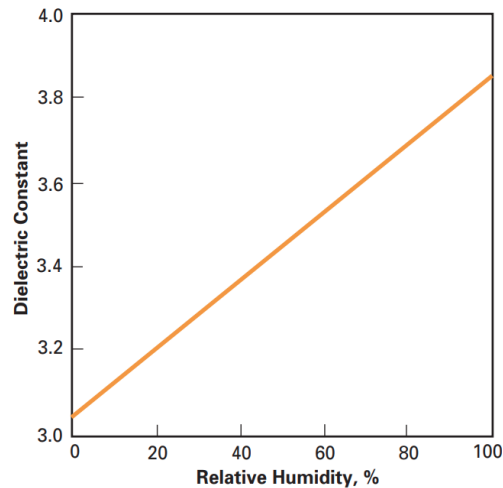


Figure 3–3 Effect of humidity on dielectric properties [38]

External chemicals can degrade the insulation by reacting with it and can make it exposed to voltages and other mechanical stresses. So, keeping electrical machines safe from environmental stress is very important.

#### 3.2.4. Mechanical Stress

There is mechanical stress on machine insulation because of forces on insulation due to vibration, switching of power converters, transient and centrifugal forces. Due to vibration, the insulation material undergoes erosion, which can reduce its strength. In [39], mechanical stress along with electrical stress was applied to evaluate turn to turn insulation, the results show development of crack in insulation. Pulsating current in conductors because of switching of converter causes oscillating magnetic forces on stator conductors and coil. These oscillating magnetic forces cause winding to vibrate which leads to wearing of groundwall insulation. Poor impregnation in winding can also lead to more vibration. The other factor that causes mechanical stress are mechanical wearing in rotor, bearing and shaft of the machine.

### 3.3. Emulation of Insulation Degradation

Degradation of insulation is inevitable, due to insulation degradation mechanical properties and dielectric properties of insulation material changes. Parameters like dielectric strength, PDIV and insulation capacitance changes due to degradation. Various studies investigated how these parameters change over time. In [40], effect of thermal aging on magnet wire is investigated, the insulation on magnet wire with two different insulation material is considered. As insulation, polyester for base material and polyamide-amide for coating on the base layer is used. This insulation combination is commonly used in low voltage machines driven by variable speed drives. Insulation capacitance between the strands and dissipation factor are measured with different levels of degradation caused by stress due to thermal cycle. Results show that capacitance between the strands increases with thermal degradation and increase can up to 30% before the failure. Similar increase in insulation capacitance reported in different studies [41], [42], [34], [8]. So, the capacitance can be used as an indicator to determine the quality of insulation or level of degradation since insulation capacitance increases with insulation degradation. Dielectric losses also change due to degradation. However, change in dielectric loss is very negligible and not considered in this study.

In various studies, change in capacitance is used to emulate insulation degradation [43]–[46]. In this study, capacitances of different values at different location is used to emulate different severity and type of degradation. Principle behind emulation explained using simple form wound winding. Mainly two types of degradation are emulated, one is turn to turn (TT) degradation and other is turn to ground (TG) degradation. When there is degradation in interturn insulation, the capacitance between respective turns changes. As shown in Fig. 3-4, consider capacitance  $C_{12}$  as the capacitance between turn 1 and turn 2 when the insulation is not degraded. Over time this capacitance changes due to degradation. To emulate this TT degradation, additional capacitance  $C_{deg}$  is added in parallel with capacitance  $C_{12}$ . So, the total capacitance between these turns is a sum of  $C_{12}$  and  $C_{deg}$ . By varying the value of  $C_{deg}$ , degradation of different severity can be emulated.

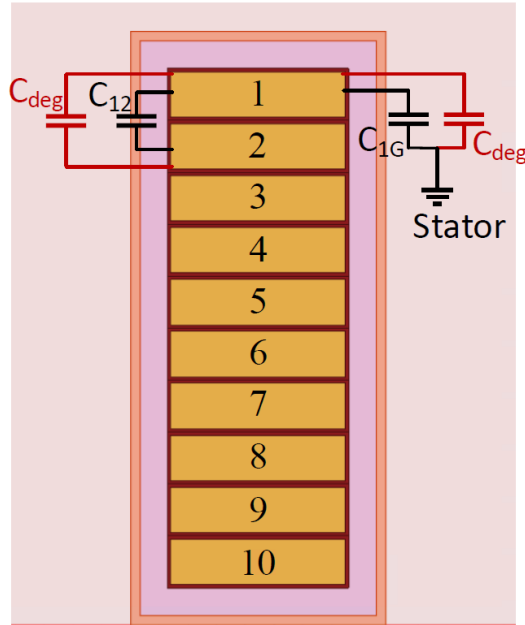


Figure 3–4 Emulation of insulation degradation

Degradation in main insulation and groundwall insulation leads to change in capacitance between turn and ground. Here, the stator is considered as ground. Consider capacitance  $C_{1G}$  as capacitance between turn and ground. To emulate TG degradation, additional capacitance  $C_{deg}$  can be added in parallel with capacitor  $C_{1G}$ , so the resulting capacitance between turn 1 and ground is a sum of both capacitances. Similarly, degradation of insulation over strand insulation or groundwall insulation in random wound machine can be emulated.

### 3.3.1. Emulation of Insulation Degradation Using FE based approach

In this section, FE based modeling approach is presented to model a random wound machine. Firstly, the machine is modeled using a machine design tool to obtain the exact geometry of the stator. Fig. 3-5 shows cross section of a typical machine and Fig. 3-6 shows a stator winding connection diagram. The figure shows the typical model obtained from a machine design tool. These tools are not capable of providing slots filled with individual conductor and insulation layers. So, slots are manually filled with conductors and insulation layers are required to be added. In this study, the effect of the rotor is not considered.

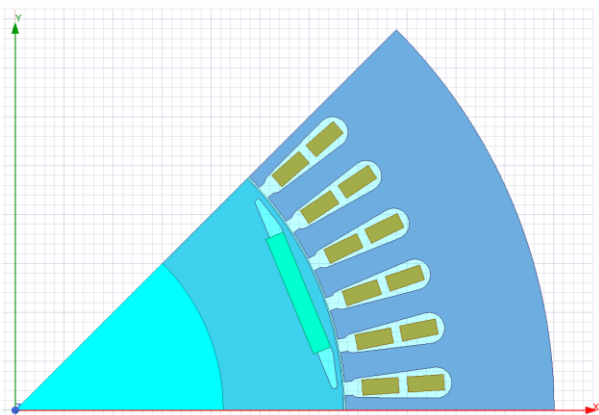


Figure 3-5 Typical machine model

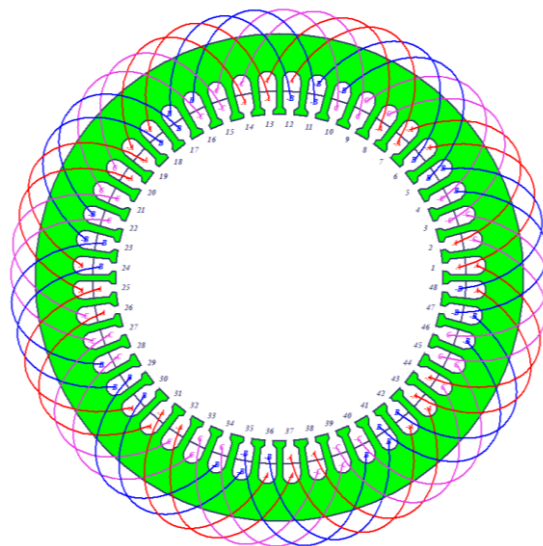


Figure 3-6 Stator connection diagram

Strand level modeling of double layer stator winding with 48 coils and 60 conductors per slot brings an immense amount of complexity and can be computationally expensive. To simplify the study, reduce the complexity and computation load, partial winding is considered.

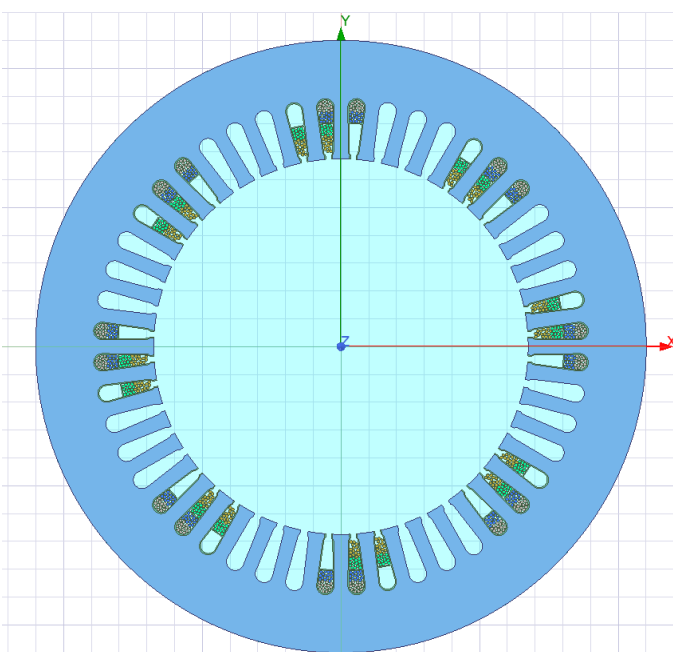


Figure 3-7 Detailed phase A winding

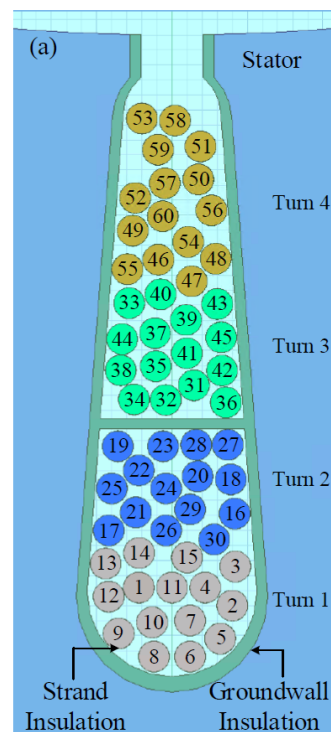


Figure 3-8 Detailed slot model

Fig 3-7 shows complete phase A winding. Figure 3-8 shows detailed slot cross-section, detailed arrangement of conductors and insulations inside the slot is considered.

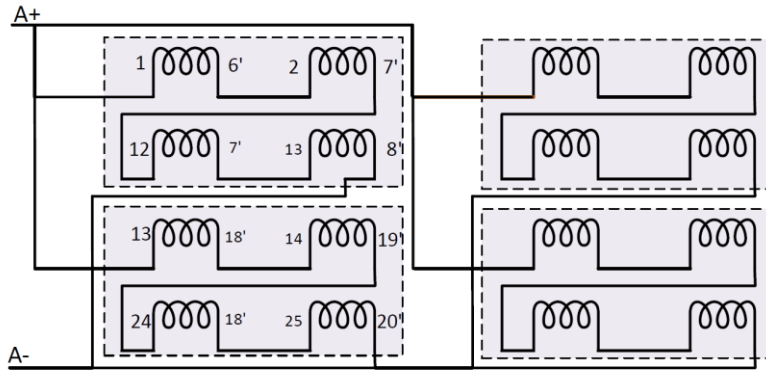


Figure 3-9 Coil connections in phase A

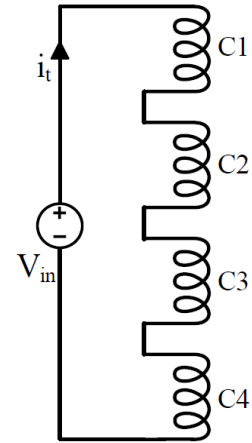


Figure 3-10 Reduced winding

Fig. 3-9 shows the connection of 16 coils in phase A, each section marked by a rectangular box consists 4 coils, each section will undergo same voltage excitation. In this study, reduced winding as shown in Fig 3-10 with 4 coils in series is considered

As shown in Fig. 3-8, in each slot there are 4 turns, and each turn consists 15 parallel conductors each, resulting in 60 conductors in each slot. All four turns are distinguished with different colors. Epoxy Kevlar is used as insulation over the conductors and Nomex® 410 is used as ground wall insulation. Properties of insulation material are summarized in Table 3-1. For simplification, the arrangement of conductors in each slot is considered the same.

Table 3-1 Main parameters of insulations

	<b>Material</b>	<b>Thickness (mm)</b>	<b>Relative permittivity</b>
<b>Groundwall insulation</b>	Nomex® 410	0.36	2.7
<b>Enamel</b>	Epoxy Kevlar	0.004	3.6

### 3.3.2. Parameter Computation

Since FE based approach is used, only resistance and capacitance are required to be calculated. For resistance calculation, analytical method discussed in previous chapter is used. However, more accurate resistance can be calculated by FE analysis. For capacitance calculation, an electrostatics solver in Ansys is used. Since there are 60 conductors in the slot,  $60 \times 60$  Maxwell capacitance matrix obtained is obtained. Numbering of these conductors is shown in Fig 3-8. Maxwell capacitance matrix in form of heatmap is shown in Fig 3-11.

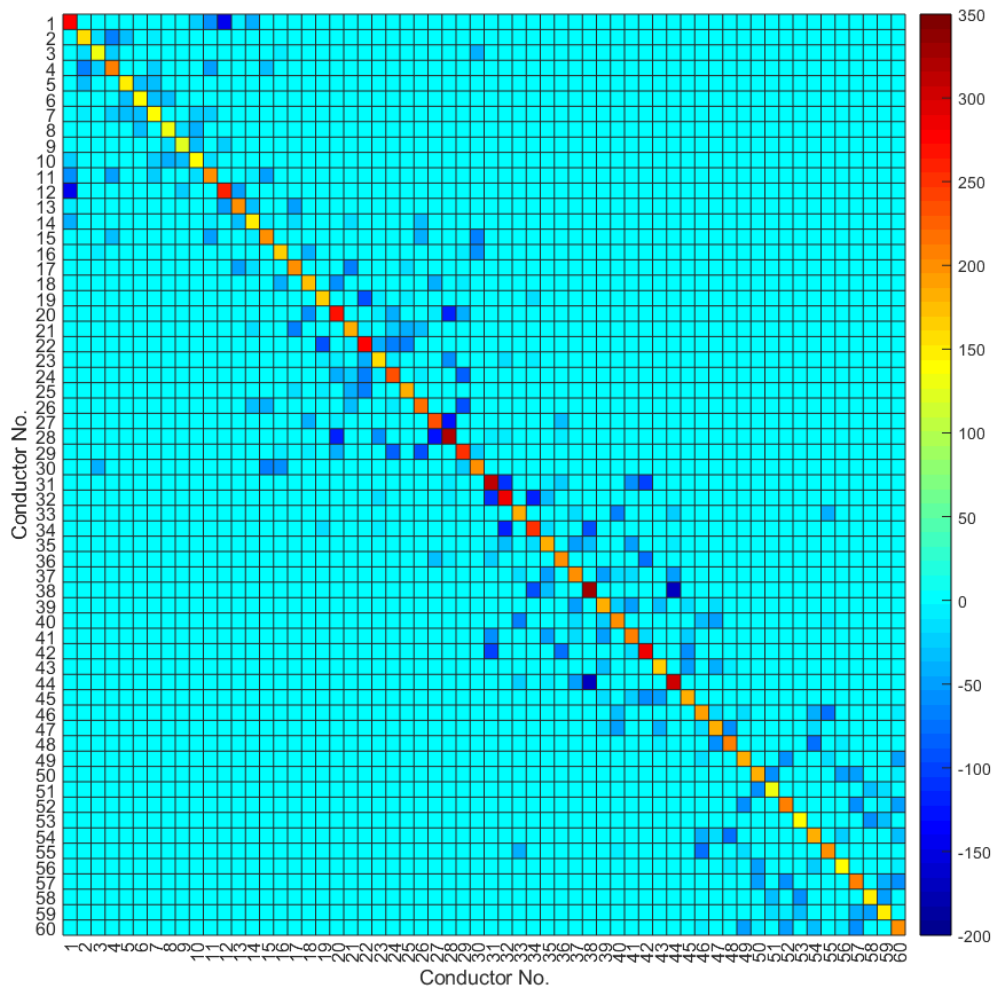


Figure 3–11 Strand level Maxwell capacitance matrix (pF)

To get a better understanding of capacitance, strand level matrix is converted to turn level matrix. Since each turn consists 15 strands,  $4 \times 4$  capacitance matrix is obtained from  $60 \times 60$  strand

level matrix. The diagonal elements represent self capacitances of turns and off diagonal elements represent mutual or interturn capacitances.

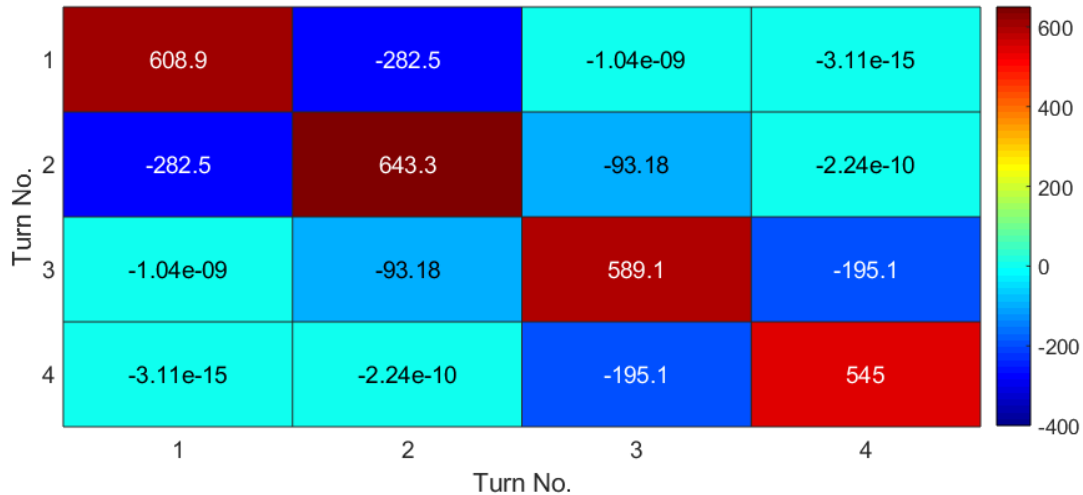


Figure 3–12 Turn level Maxwell capacitance matrix (pF)

From the matrices, it is obvious that conductors away from each other have lower value of mutual capacitance than turns near to each other. Similarly, conductors away from the slot wall have lower value of conductor to ground capacitance, while conductors near the slot wall have comparatively higher conductor to ground capacitance.

### 3.3.3. Integration of External Circuit with Transient Solver

Capacitances and resistances are precalculated. While transient solver internally computes inductances. To integrate all three main parameters, each individual conductor in the model is assigned external excitation, then it will appear as inductance in an external circuit as shown in Fig 3-13. For instance, in each slot there are 60 conductors then are assigned external excitation. Then calculated resistances for corresponding conductors are connected in series. Then mutual and self capacitances are connected in such way that they form  $\pi$  circuit for each conductor. Then all the conductors along with calculated parameters are connected in such manner that they form complete winding. Fig. 3-13 shows how capacitances are connected to form  $\pi$  circuit for each conductor and it also illustrates how other parameters relate to each other. Fig. 3-14 shows a complete circuit for one coil having two turns. Fig. 3-15 shows a complete circuit of the winding used for this study. This strand level modeling is complex and computationally expensive due to enormous network of inductive and capacitive coupling among the conductors.

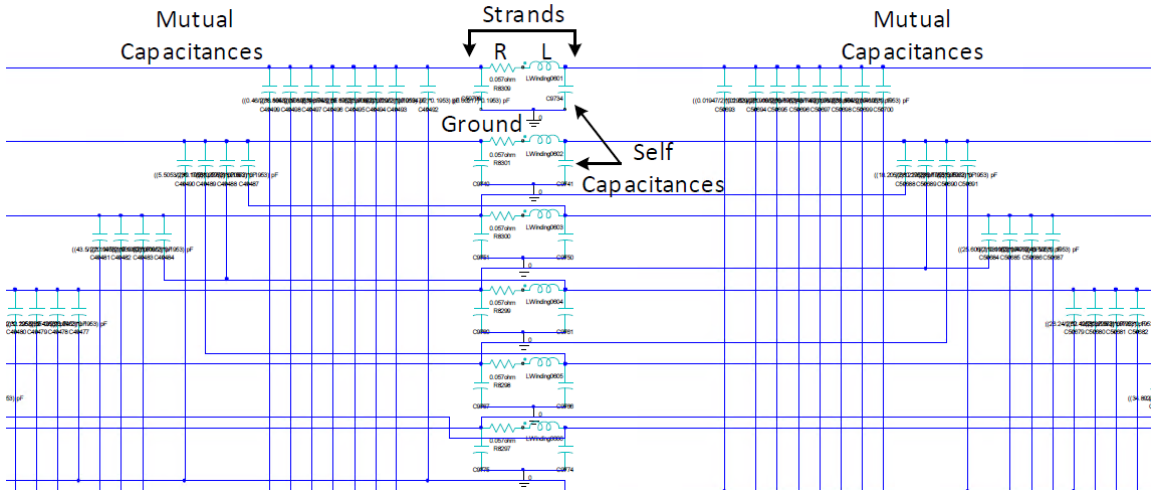


Figure 3–13 Connection of various parameters in external circuit

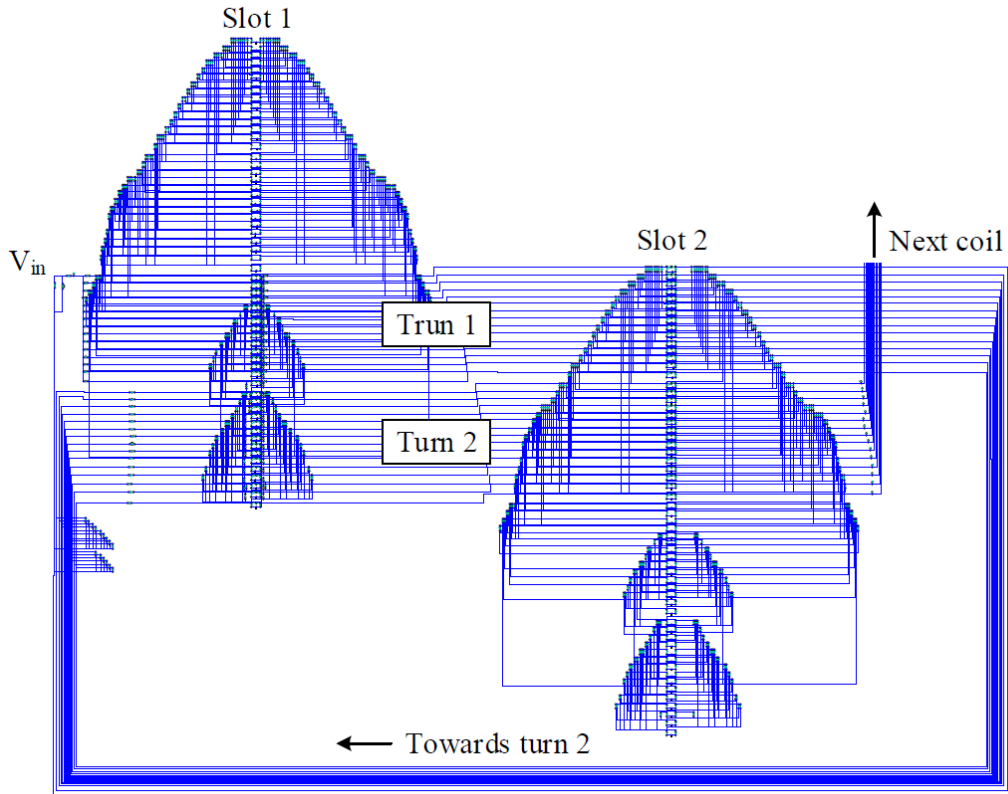


Figure 3–14 Complete circuit for one coil

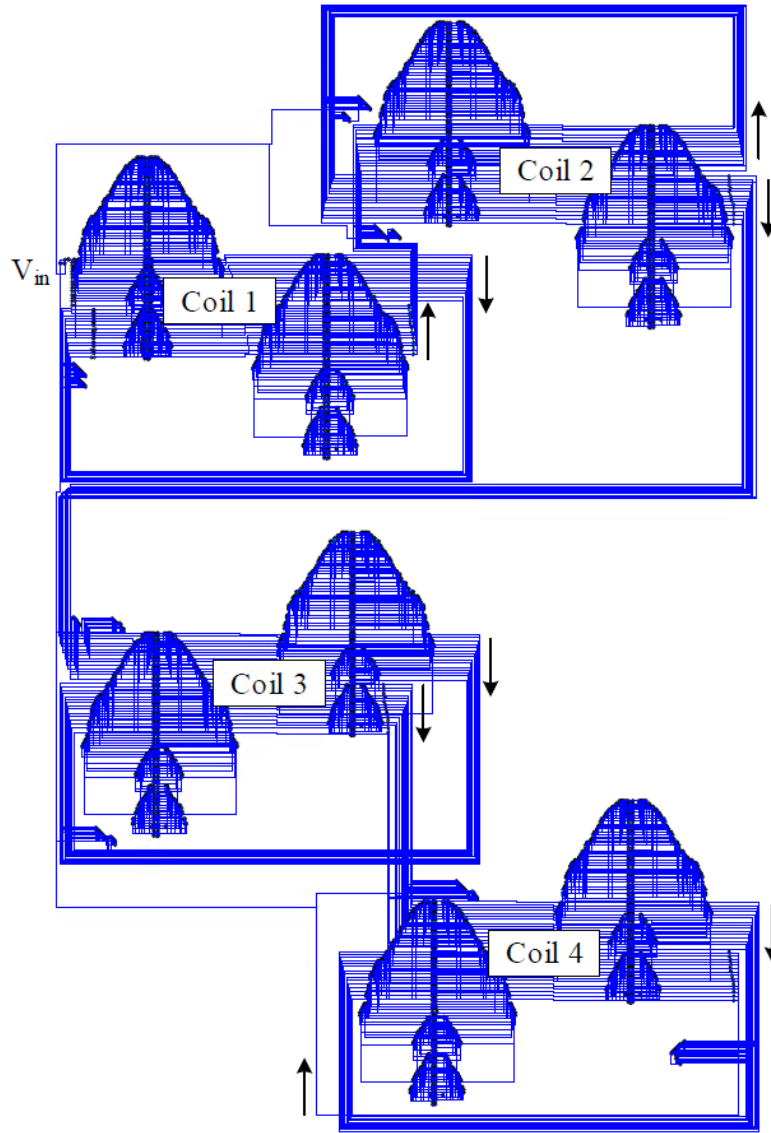


Figure 3–15 Complete circuit for winding

Once an external circuit is created, desired excitation can be applied. Here, PWM like step voltage  $V_{in}$  pulse of 1750V with 80ns rise time is applied to the winding which corresponds to  $dv/dt$  of 21.9 kV/ $\mu$ s. Electrical stress and currents can be obtained at various points in the winding.

### 3.3.4. Emulation of Insulation Degradation

As explained earlier, two types of degradation are emulated using FE based approach, one is TT degradation and the other is TG degradation. In the random wound machine when there is degradation between strands from different turns due to degradation in insulation material over wire, it is considered as TT degradation. Moreover, when there is degradation between strand from any turn and stator, it is TG degradation. TG degradation is caused due to degradation in groundwall insulation. In the random wound machine, there are multiple strands per turn so there are multiple ways to emulate TT or TG degradation.

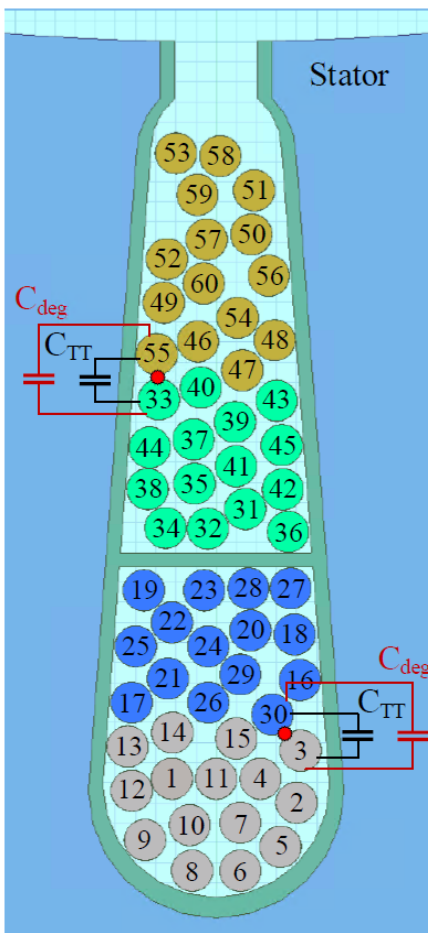


Figure 3-16 TT degradation emulation

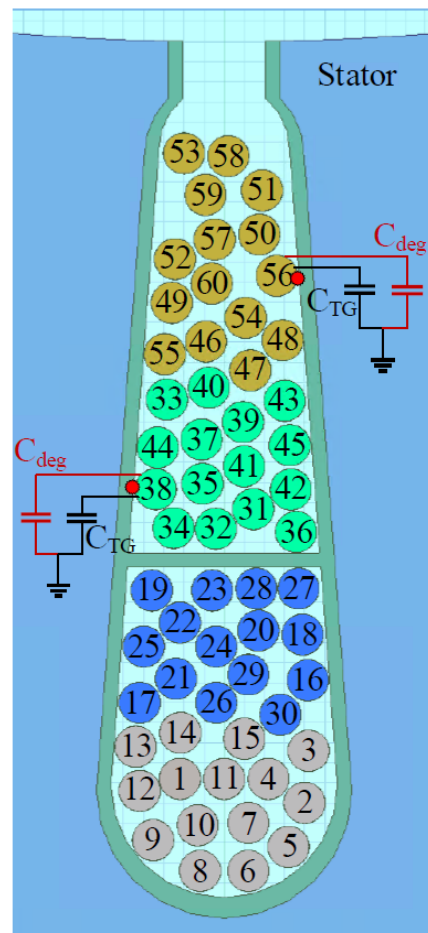


Figure 3-17 TG degradation emulation

For example, to emulate TT degradation between turn 1 and turn 2, capacitance between strand 33 from turn 1 and strand 55 from turn 2 is changed in circuit. Similarly, to emulate the degradation between turn 5 and turn 6, capacitance between strand 3 from turn 5 and strand 30 from turn 6 is changed. Using the same methodology, TG degradations are emulated by varying the capacitance

value between strand form desired turn and ground. For example, to emulate TG degradation at strand 38 corresponding to turn 1, the capacitance between strand 38 and ground is changed. Fig. 3-16 illustrates TT degradation emulation and Fig. 3-17 illustrates TG degradation emulation.

### 3.4. Influence of Insulation Degradation on Current Response

One of the purposes of this study is to investigate the insulation condition monitoring technique which will be discussed in the next chapter. Keeping insulation condition monitoring in focus, how transient current changes with different types and severity of degradation is presented in this section. Voltage pulse  $V_{in}$  of 1750V with 80ns rise time is applied to the winding and current flowing  $i_t$  through the winding or current response is obtained. Degradation of various severity are emulated, it is assumed that the change of capacitance is 200 pF, 500 pF and 1000pF. In other words, each type of degradation at different for different severity is emulated at different locations inside the winding. Fig. 3-18 shows part of applied voltage pulse and current response when the insulation is good or when there is no degradation in insulation. The current rises at a steady rate due to winding's inductance. Moreover, the transient part in current can be observed which reflects winding's high frequency behavior.

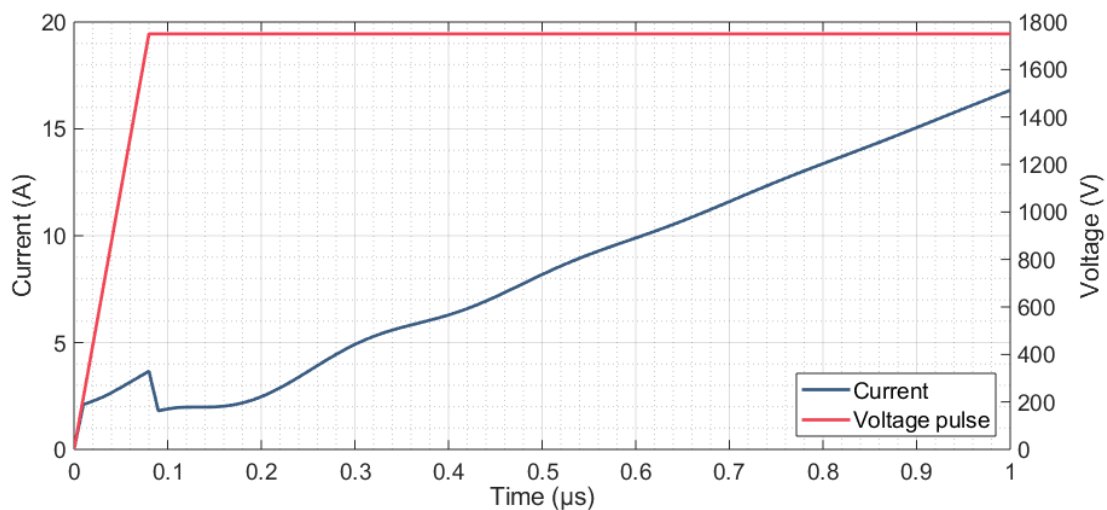


Figure 3–18 Current response to applied voltage pulse

In this section, current responses  $i_t$ , when pulse  $V_{in}$  is applied to the winding is presented for different emulations of TT and TG degradation.

### 3.4.1.1. Turn to Ground (TG) Degradations

Fig 3-19 to 3-26 shows, current response for TG degradation of different severity at different turns. It can be observed, that for each case of degradation, the value of current during the first 80ns is increasing with the severity of degradation. Similar behavior can be observed for ringing or oscillations.

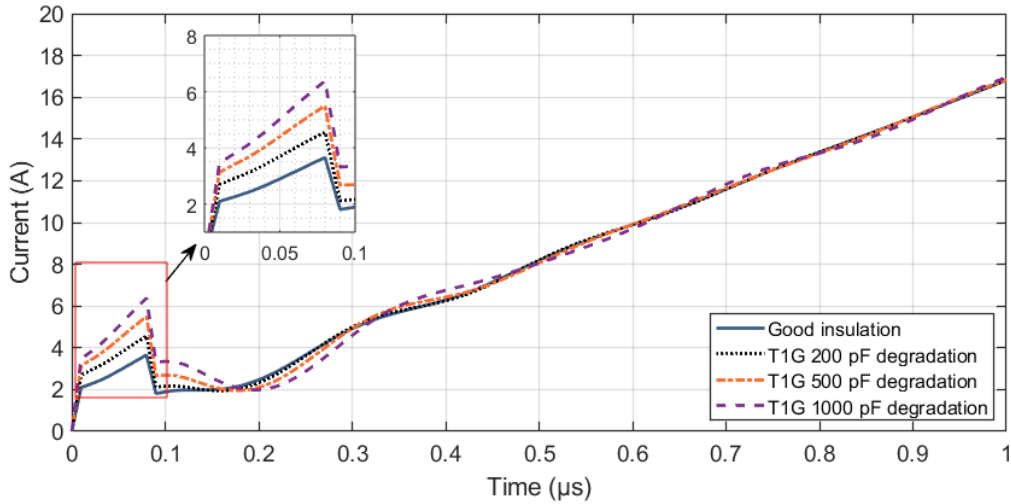


Figure 3–19 Current for T1G degradation

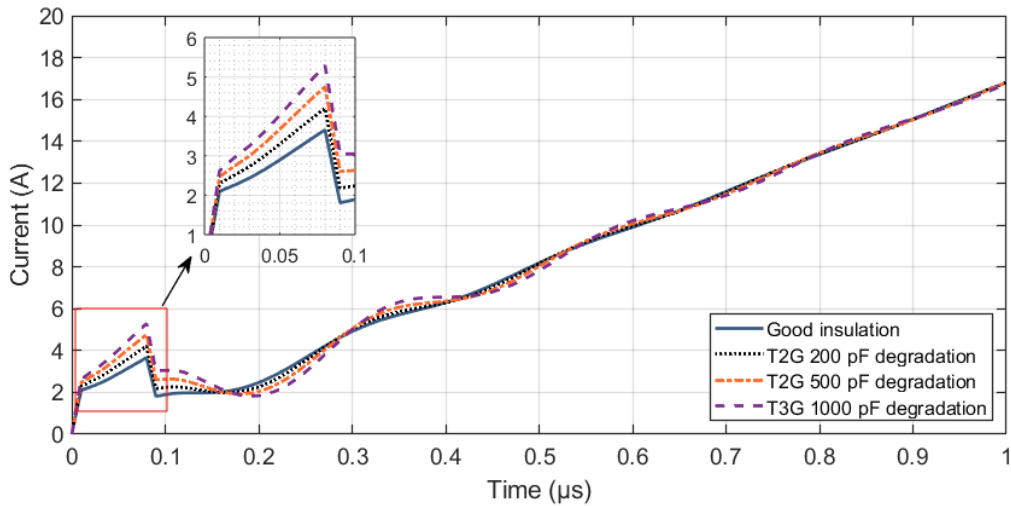


Figure 3–20 Current for T2G degradation

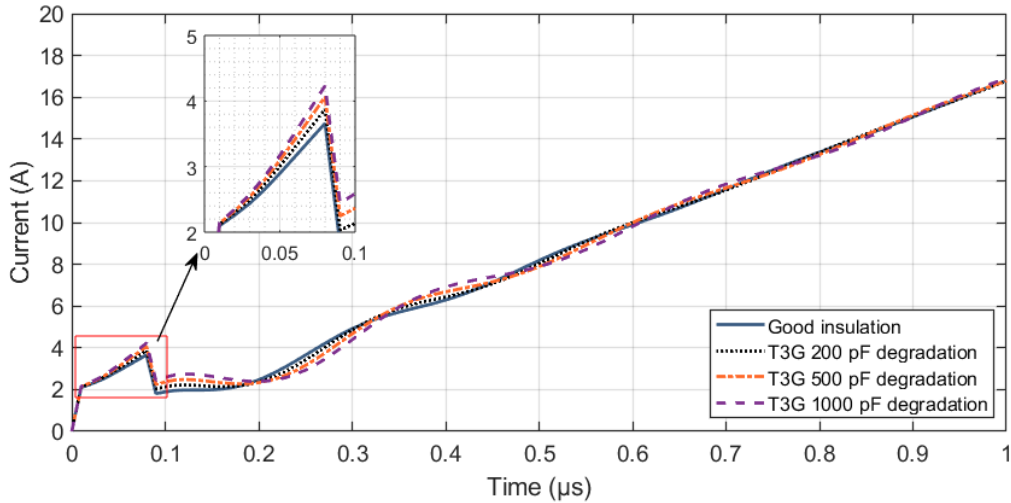


Figure 3–21 Current for T3G degradation

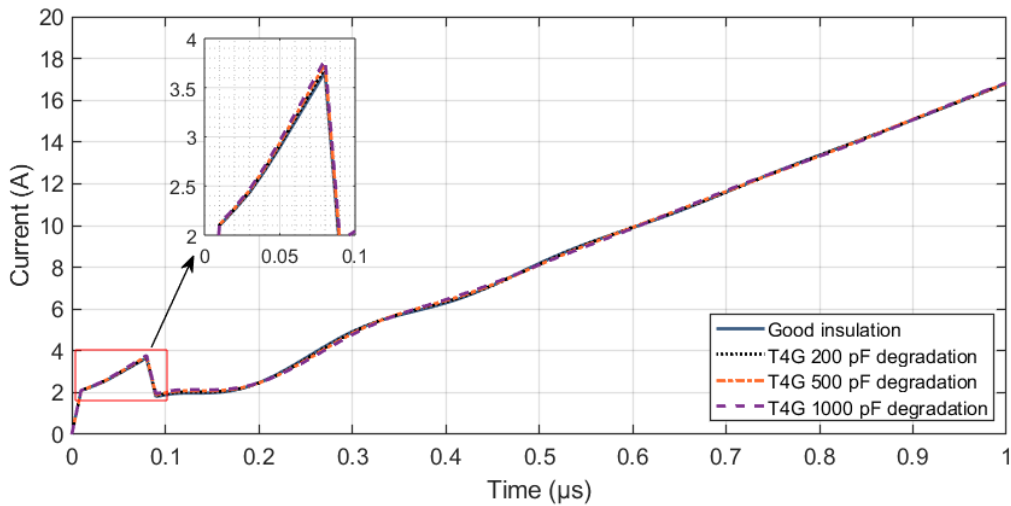


Figure 3–22 Current for T4G degradation

As degradation location moved from turn 1 to turn 2, the value of current during first 80ns is decreased. Moreover, similar decrease in current can be seen up to degradation at turn 5. Moreover, decrease in ringing is also obvious. As degradation moved from turn 1 to turn 5, there is a monolithic decrease in current during first 80ns as well as there is decrease in ringing. It is interesting to observe that, for degradation at turn 5, current barely changed when compared with current at no degradation condition. So, it is obvious that, even though the severity of degradation is the same, their effect on current response is not same since the degradations are taking place at different locations of the winding.

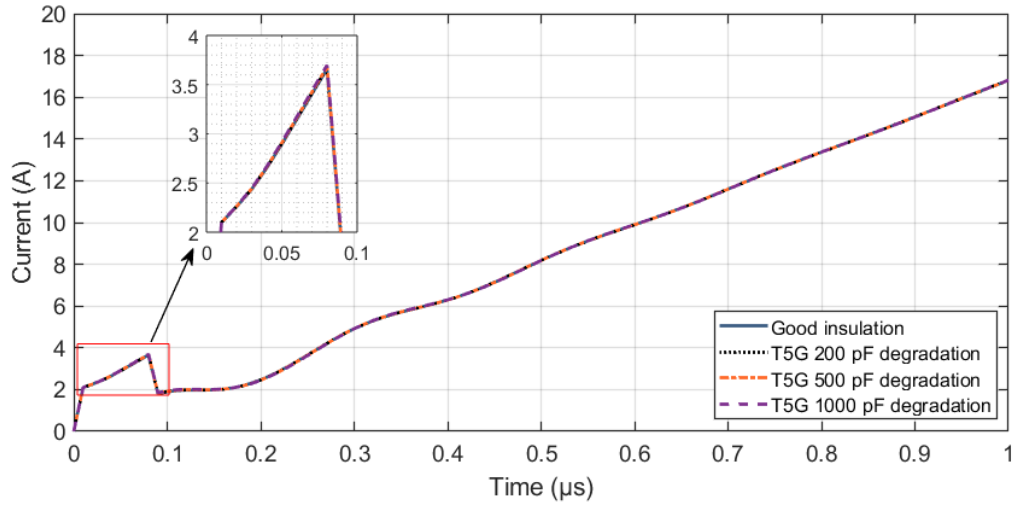


Figure 3-23 Current for T5G degradation

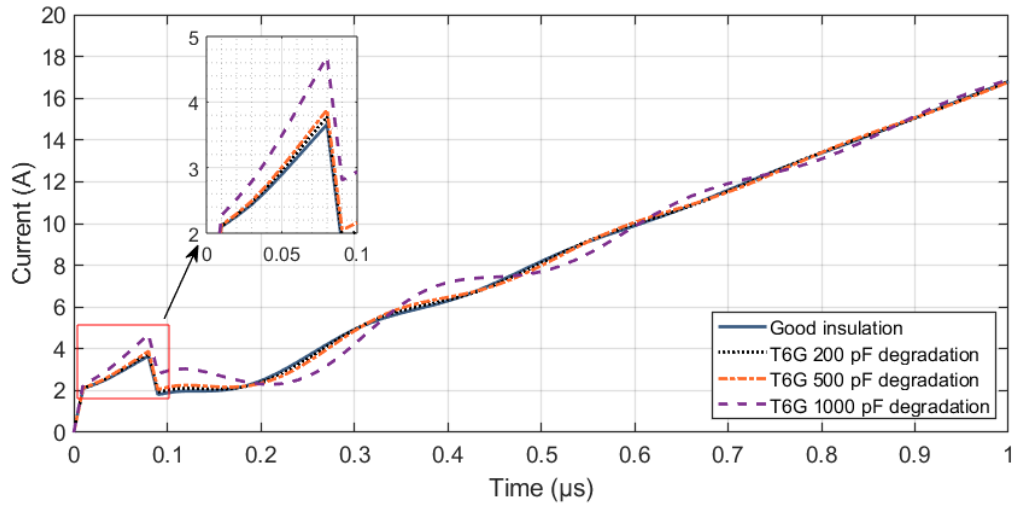


Figure 3-24 Current for T6G degradation

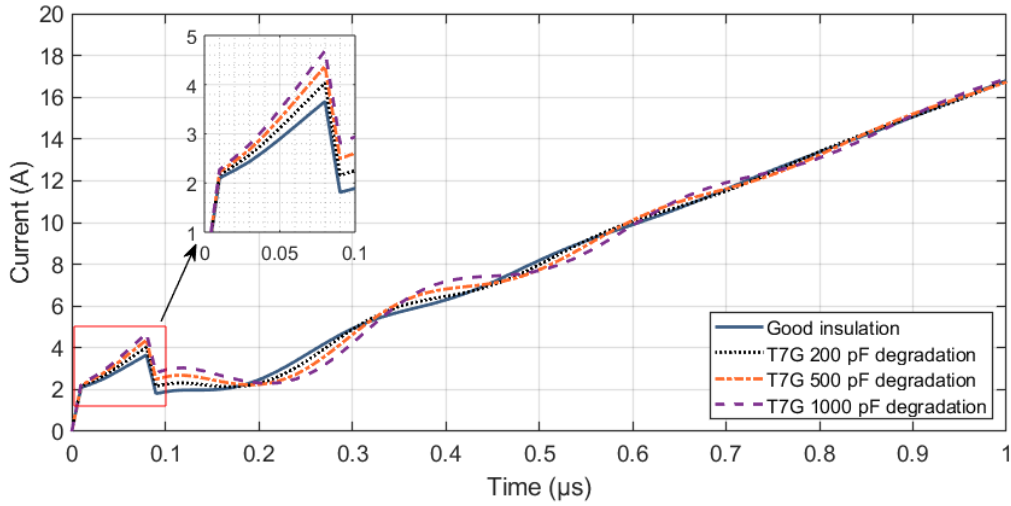


Figure 3–25 Current for T7G degradation

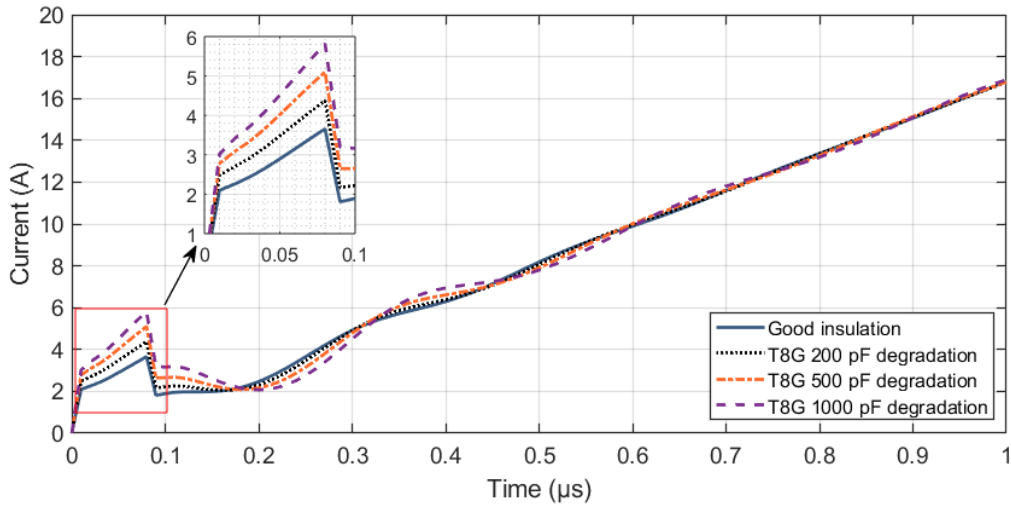


Figure 3–26 Current for T8G degradation

By observing current responses for degradations at turn 6 to 8, there is again a monolithic increase in current values and ringing as degradation further moved away from turn 5. In other words, it is fair to conclude that, degradation further away from winding terminals has comparatively less influence on the current response.

### 3.4.1.2. Turn to Turn (TT) Degradations

Fig 3-27 to 3-30 shows current response for TT degradation of different severity between various turns. Similar to TG degradation cases, a monolithic increase in current values during first the 80ns with increasing degradation severity can be observed.

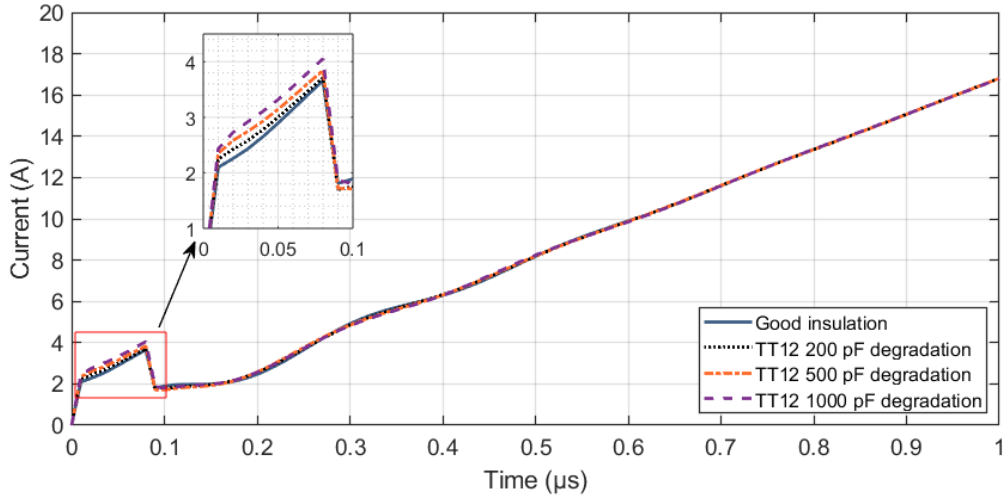


Figure 3-27 Current for TT12 degradation

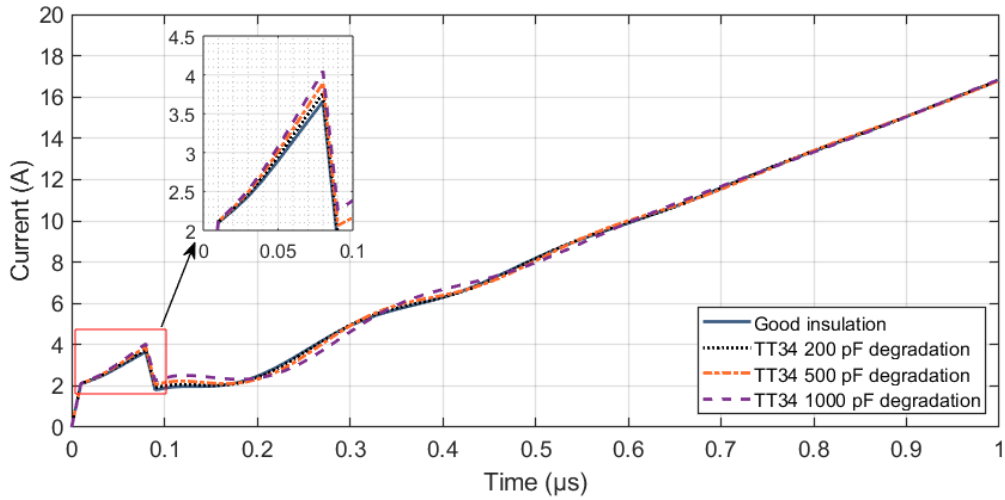


Figure 3-28 Current for TT34 degradation

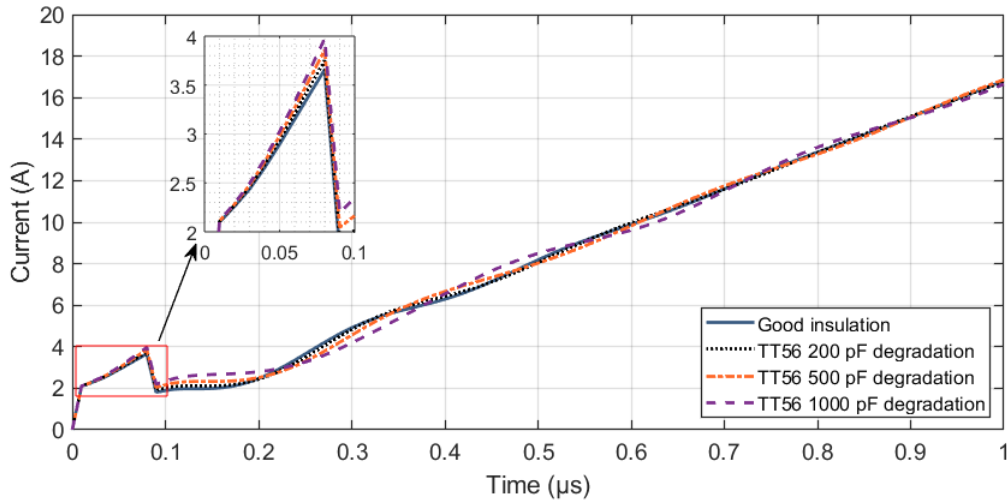


Figure 3–29 Current for TT56 degradation

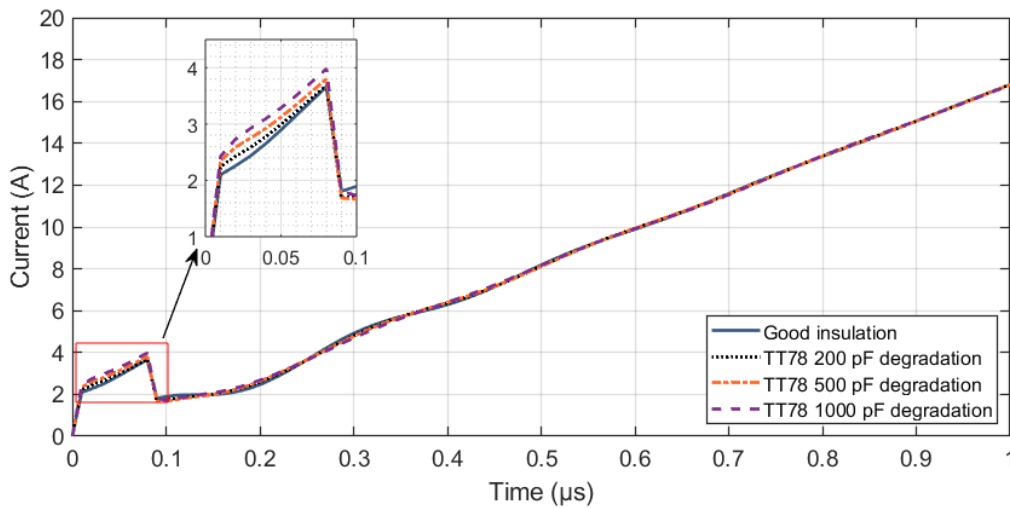


Figure 3–30 Current for TT78 degradation

Considering case TT12 and TT34, an increase in current values during first 80ns is comparatively high for TT12 degradation. While more increase in ringing is observed for TT34 degradation. Moving further to degradation TT56, current values during first 80ns reduced slightly. While an increase in ringing can be observed. For TT78, current during first 80ns is increased while ringing is reduced significantly. Current responses for TT12 and TT78 are close to each other. While responses for TT34 and TT56 are close to each other.

### **3.5. Summary**

In this chapter, the methodology and procedure for emulation of insulation degradation is presented. Initially, various types of insulation in stator winding and factors that affect insulation degradation are discussed. Then theory and procedure for emulation of insulation degradation is presented. Two types of degradation with different levels of severity are emulated on random wound machines using FE based approach. Then the influence of degradation on transient current is investigated. With an increase in severity of degradation, a monolithic increase in current amplitude and oscillations is observed for each case. Moreover, it can be concluded that the location of degradation or turns at which degradation is emulated influences transient current differently. It is found that degradations closer to the winding terminals have more influence on transient current.

## **Chapter 4: Detection and Classification of Insulation Degradation**

In this chapter, various insulation condition monitoring techniques have been summarized. Then the new insulation condition detection technique based on current response and wavelet packet decomposition (WPD) is proposed, which can determine overall state of health (SOH) of insulation and type of degradation.

### **4.1. Condition Monitoring Techniques**

Condition monitoring techniques are divided into online monitoring and offline monitoring techniques. In offline monitoring machine is taken out of the service to perform tests. While in online monitoring, a machine is kept on service to perform tests. Online monitoring is the most desired method to avoid downtime and extra cost associated with offline monitoring

#### **4.1.1. Offline Monitoring Techniques**

Most offline methods require direct contact with insulation or winding and they are considered to be accurate. Some of the offline monitoring techniques are insulation resistance (IR) test, polarization index (PI) test, DC high potential (HiPot) test, AC high potential (HiPot) test, capacitance test, dissipation factor test, off-line partial discharge (PD) test, blackout test and power factor (PF) tip-up test. These methods mainly rely on measurement of resistance, partial discharge activity, insulation capacitance, polarization index and dissipation factor of insulation. Ease to perform these tests, effectiveness and expense of these tests can be explored. Sometimes the direct connection with some parts of the winding is not possible. Moreover, to perform these kinds of tests, machine is required to be disconnected from the service, which is one of the main disadvantages of offline monitoring techniques. In this section, insulation resistance test, capacitance and dissipation factor test, and surge-based techniques are discussed.

##### **4.1.1.1. Insulation Resistance Test**

This method is the most widely used test and has been in utilization for more than five decades. In this method, leakage current from winding to stator is measured. This leakage current flows through the ground-wall insulation of the machine, which can be used to determine the state of insulation since degradation in capacitance leads to more leakage current. In industry, this technique is known by various names like ‘Megger™ Test’, ‘HiPot Test’ and ‘IR Test’. However, they work on the same principle of measuring leakage current and estimating resistance between

winding and stator. Theoretically, this resistance should be infinite, and no current should flow through the insulation. However, in practice, the value of resistance is not infinitely high. Value of resistance is associated with the quality of insulation. Lower the value of resistance, it is more likely to have degradation in insulation. Detailed procedure for IR test and recommendations are described in IEEE standard 43 [47]. For IR test following model is considered.

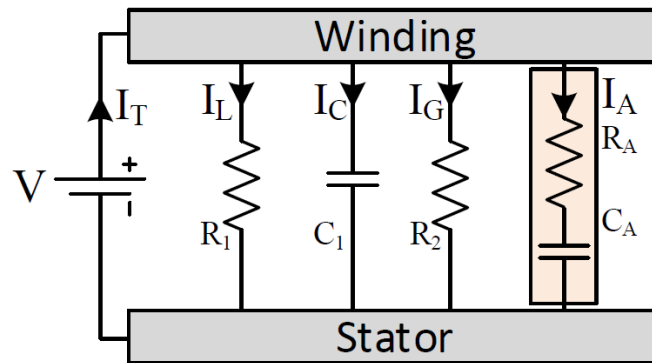


Figure 4-1 IR insulation test model

When voltage is applied, there is an instantaneous capacitive current flowing through the insulation due to interaction between different dielectrics having different permittivity. This current is represented as  $I_C$ . This current appears for a short duration when voltage is applied so it does not affect IR measured at one minute and ten minutes. While  $I_L$  represents steady state surface leakage current which is generally present on end-turn surface, this current highly depends on amount of contamination like amount of conductive material over the surface, moisture, and temperature. Current  $I_G$  is conduction current that flows through the insulation, which is constant over time. Current  $I_A$  is the absorption current, which represents the polarization and electric drift phenomenon, which decays over time. At about ten minutes measurement, the value of  $I_A$  is very small. So, total current  $I_T$  is the summation of conduction current  $I_G$  and surface leakage current  $I_L$ . In this test, high voltage is applied between winding and stator. Then leakage current is measured after 1 minute and 10 minutes and values of IR are obtained which can be given by the following equation of Ohm's law.

$$R_t = \frac{V}{I_t} \quad (4-1)$$

Here,  $V$  is applied voltage while  $I_t$  and  $R_t$  are leakage current and IR respectively at given time  $t$ . Polarization Index (PI) is a ratio of IR measured at 10 minutes and 1 minute.

$$PI = \frac{R_{10}}{R_1} \quad (4-2)$$

$R_1$  is resistance at 1 min and  $R_{10}$  is resistance measured at 10 min. The recommended values of IR and PI for safe operation are provided in the standard. This method is capable of detecting contamination and severe degradation in groundwall insulation.

Another test is HiPot test, which is a little different than IR test since winding may pass or fail the test. In this test DC or AC voltage higher than the voltage that the machine experiences during normal operation is applied to the machine winding and insulation state determined. If the winding withstands the applied high potential and if the insulation does not fail, the winding insulation is considered in good condition and the machine can be returned to the service. If the winding insulation fails, then the machine is required to rewind. This test is destructive in nature since it applied additional stress on the insulation of the machine winding. HiPot test is generally performed on medium and high voltage machines. In IEEE standard 95, a guideline to perform DC HiPot test is provided [48]. In this test, DC voltage which is about 1.7 times the rated RMS voltage of the machine is applied for about 1 minute and if the winding withstands the applied voltage or not is checked. It is recommended to measure IR during the experiment to confirm the quality of insulation. Similar test in which DC voltage at very low frequency is applied and described in IEEE standard 433 [49]. In IEEE standard 56, guidelines to perform AC HiPot test are provided [50]. In this test, high AC voltage which can be up to 1.5 times rated voltage of the machine at machine frequency is applied. Since these tests solely depend on insulation's capacity to withstand applied voltage, they do not provide any information on condition of the insulation. HiPot tests are only capable of detecting severe faults in insulation.

#### **4.1.1.2. Capacitance and Dissipation Factor (DF) Test**

Offline methods based on the measurement of capacitance and dissipation factor are also very common. Capacitance measurement based techniques are considered accurate to detect insulation degradation due to thermal stress and the presence of moisture, this method works on the fact that the capacitance of the insulation material changes due to degradation or contamination due to

foreign particles. However, it is considered that measurement of dissipation factor along with capacitance provides additional surety. DF provides information on dielectric loss in the insulation. Insulation can be considered as series of equivalent series resistance (ESR) and capacitance ( $C_{ideal}$ ) as shown in Fig.4-2. Loss in the dielectric is represented by its resistance, while ideal capacitance is due to the dielectric properties of insulation.

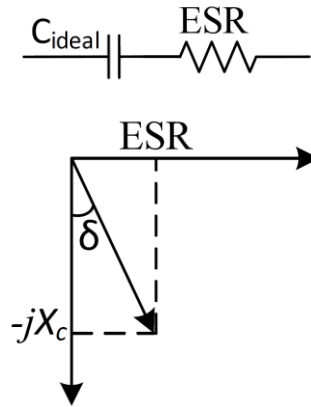


Figure 4–2 Insulation model with equivalent resistance and ideal capacitance

In most tests DF ( $\tan\delta$ ) is measured which can be expressed as the following equation and shows its relationship between ESR and capacitance ( $C_{ideal}$ ).

$$\tan\delta = \frac{ESR}{\omega C_{ideal}} \quad (4-3)$$

DF is measured and compared for assessment of insulation condition.

Capacitance tip-up test is another test based on capacitance measurement and provides information on partial discharge. Due to degradation of insulation, there might be an increase in the numbers of voids in the material which results in the reduction of overall thickness of insulation and hence an increase in capacitance. Due to more voids in insulation, PD activity increases significantly. So, by measuring the capacitance, void in the insulation can be estimated and hence PD activity can be estimated. The capacitance tip-up ( $\Delta C$ ) can be described by the following equation.

$$\Delta C = \frac{C_{HV} - C_{LV}}{C_{LV}} \quad (4-4)$$

Here,  $C_{HV}$  is capacitance measured at high voltage and  $C_{LV}$  is capacitance measured at low voltage. PDs are more likely to happen at high voltages, by obtaining the difference between capacitance at low voltage and high voltage, PD activity can be estimated. Higher value of  $\Delta C$  shows more PD activity. Guideline and recommended practices for capacitance and DF measurement based tests are described in IEEE standard 286 [51].

#### **4.1.1.3. Offline Partial Discharge test**

Capacitance tip-up test is an indirect method for PD estimation. In offline partial discharge test, pulse current resulting from PD is measured. When PD occurs, there is a short burst of electrons that flows through the insulation, this discharge of electrons can be detected from current. To detect this short burst of current, a high voltage capacitor is connected between the terminals and resistive load is connected in series with the capacitor. When PD happens, the current pulse passes through the capacitor and creates voltage drop across the resistor which can be analyzed using an oscilloscope or other similar devices. Detailed guidelines and procedure to measure PD are described in IEEE standard 1434 [52]. In this test, AC voltage of about rated value of phase to ground voltage is applied at machine frequency. However, this method cannot be used for the assessment of inverter fed machines, where insulation undergoes additional electrical stress due to high  $dv/dt$  pulses. IEC standard 61934 describes the procedure and guideline to perform PD test for inverter fed machines [53]. Offline PD tests are comparatively difficult and similar to other offline tests, this test cannot provide detailed information on condition of the insulation. Moreover, this test is recommended only for form wound machines and it is not feasible for low voltage machines.

Another PD based test is blackout test. Similar to the offline PD test, AC voltage of about rated value of phase to ground voltage is applied to the winding and using UV light camera or imaging equipment PD activity is observed since PD activity creates optical output. In IEEE standard 1799, guidelines and procedure are described [54]. This method can be used only for degradation in end winding and not preferred for low voltage machines.

#### **4.1.1.4. Surge Test**

Degradation in interturn insulation may lead to a short circuit. So, assessing the condition of interturn insulation is as important as groundwall insulation. Surge test can be used to assess the condition of interturn insulation. This test can be considered as the HiPot test for interturn

insulation since voltage surge is applied between different turns of the winding and insulation may or may not withstand it. The voltage surge is applied between the turns being assessed and based on the voltage impulse response, the short circuit in the insulation is identified. Resonance frequency and amplitude of voltage response changes due to short circuit. In IEEE standard 522, detailed guideline to perform surge test on form wound machine is provided [55]. This method is also a survival based method and does not provide any information on the condition of the insulation. This method is not practical for random machines and no standard to perform this test on random wound machines is established.

To summarize, most offline monitoring techniques can detect either fault in groundwall insulation or in interturn insulation. Moreover, only a few methods are not designed particularly for low voltage machines. These methods are also capable of providing condition of the insulation. The main disadvantage of using the offline monitoring technique is that the machine is required to be disconnected from the service.

#### **4.1.2. Online Monitoring Techniques**

Online monitoring techniques are highly desired technique as machine can be in service. The online monitoring technique is suitable for EVs. There are various insulation monitoring techniques that have been proposed over the years. They work on measurement or estimation of different quantities like PD, capacitance, high frequency impedance, temperature, magnetic flux, stator current, leakage current etc. Some of the techniques can detect a fault in insulation while only a few techniques can detect degradation in the insulation. In this section literature review is presented.

Offline methods based on partial discharge measurement are discussed in the previous section. There are various online methods that detect partial discharge that have been proposed over the years for grid-fed as well as inverter-fed machines [56]–[65]. PDs can be detected from inrush current flow or voltage as PD causes a burst of electrons through insulation which appears in voltage and current. However, to detect PDs, high frequency and high bandwidth sensors are required [58]. Most of these methods require sensors such as high frequency transformer, coupling capacitor, high frequency antenna, photomultiplier, high bandwidth current sensor, voltage sensor etc. Moreover, a measured signal is required to be processed to extract useful information. Procedure and testing for monitoring of PD are explained in [66]. Measurement of PD in inverter

fed machine is different from grid fed machine, which are discussed in [59]–[61], [67]. Various methods also use ultra-high frequency antennas to detect PD [58] [59]. PD based methods are capable of providing an overall insulation state however no technique can classify the type of degradation in the machine. PD based techniques are not discussed in this thesis as they require additional sensors, computation and comparatively more expensive.

There are various online monitoring techniques that can detect short circuit or turn to turn faults in stator winding [64]–[71]. Most of these techniques do not require any additional sensors; the current sensor available in most drive systems is enough. These methods can accurately predict no. of wire shorted and some of these methods can also identify location of fault. However, these methods are also not capable of detecting degradation in insulation. One of the tests that is capable of detecting degradation in insulation is the online surge test. Similar to the offline surge test, this method also works on the response of the machine for applied surge [76]–[78]. However, the online surge test cannot classify the type of degradation and required additional components to perform a test.

Currently, there are two state of the art techniques which can detect degradation with great accuracy and minimal addition cost are discussed. One is common mode voltage/current response measurement based technique. The other is current's transient response based technique.

The common mode current (CMC) based monitoring technique was introduced in [79]. In this technique, voltage is applied between stator and ground, depending on the degradation in insulation, part of the current flows through the insulation. This is CMC measured and from the value of current, indicators like capacitance, dissipation factor and insulation resistance are calculated. In [80], a complete analysis is presented which compares CMC based techniques with other online and offline monitoring techniques. Similar techniques are presented in [81]–[86]. Detection of degradation in groundwall insulation and phase insulation is presented. Challenges associated with these techniques are discussed in [87].

Current response measurement based techniques are proposed in [43]–[46], this can be considered as a state of the art method for insulation monitoring which does not require any additional sensors or equipment. In this method, the current response is measured and processed to determine insulation condition. The principle behind this method is the fact that degradation in insulation leads to a change in current response. However, the method cannot classify type on degradation.

## 4.2. A Novel approach for Detection and Classification of Insulation Degradation

As discussed, there is no technique that can detect as well as classify types of degradation in the stator winding. In this section, a new insulation degradation detection technique that can determine the state of health (SOH) of insulation and classify the type of degradation is proposed. This method can be further implemented for online monitoring. However, in this thesis, this technique is investigated by emulating insulation degradation utilizing FEA based tools. Firstly, the methodology is explained. Then investigation on how insulation degradation influences current response is presented. Then results on how this technique performs for different severity and types of insulation degradation is presented.

### 4.2.1. Methodology

As discussed earlier, the current response changes due to insulation degradation. Change in transient current is used to detect and classify this degradation. Firstly, PWM like step voltage excitation pulse  $V_{PWM}$  is applied and current  $i_t$  is obtained.

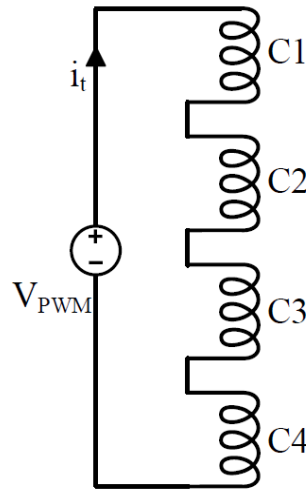


Figure 4-3 Winding with four coils

The obtained current  $i_t$  can be considered as a superposition of transient current and linear current rise and can be represented by following equation.

$$i_t(t) = i_{trans}(t) + \frac{1}{L_M} \int_{-\infty}^t V_{PWM}(t) dt \quad (4-5)$$

The current rises at a steady rate due to winding's inductance  $L_M$ , and  $i_{trans}$  is high frequency current which provides information related to the high frequency behavior of winding. Current

$i_{trans}$  provides information related to high frequency. As degradation in insulation affects high frequency behavior if the winding and hence  $i_{trans}$  changes based on the level of degradation. To obtain information related to insulation condition, the measured current  $i_t$  needed to be processed to obtain  $i_{trans}$ . Then  $i_{trans}$  is further processed using WPD to establish indicators. These indicators can be obtained for different conditions and SOH and type of degradation can be determined.

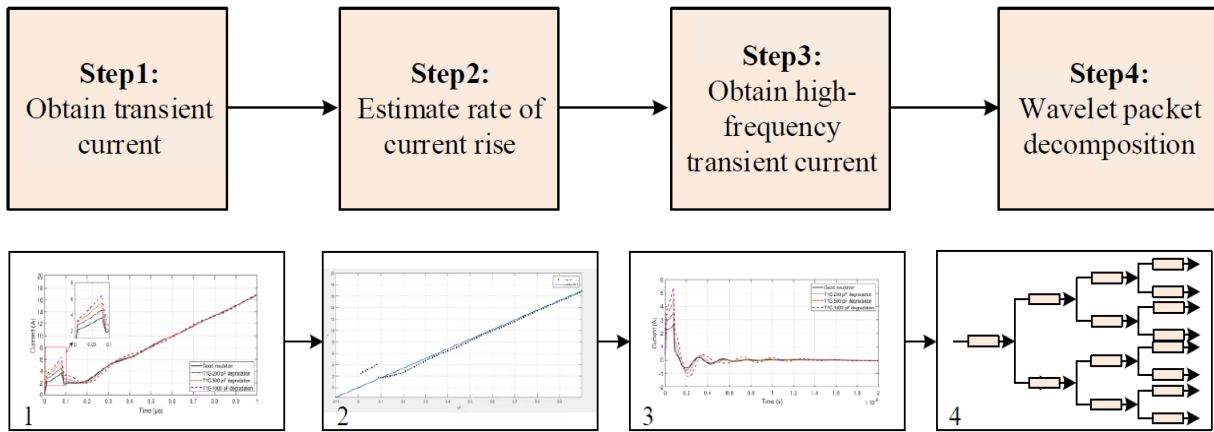


Figure 4-4 Steps for signal processing

Basically, the proposed method consists of four fundamental steps. In the first step, a transient current  $i_t$  is obtained when step voltage excitation is applied. In the second step, the rate of current rise is estimated using polynomial curve fitting and this steady rise current is due to the inductance of winding. In step three, transient current  $i_{trans}$  is obtained by eliminating a steady rise in the current. In the last step, current  $i_{trans}$  is further processed using WPD for insulation monitoring.

#### 4.2.1.1. Wavelet Packet Decomposition (WPD)

Wavelet packet decomposition is a form of wavelet transform where a signal is processed through multiple filters. WPD is also known as ‘wavelet packet decomposition’ and ‘optimal sub-band tree structuring’. WPD decomposes the signal to provide great resolution, at each level signal is passed through high pass and low pass filters and signal is further decomposed into smaller frequency. Fig. 4-5 shows three level WPD. The number of packets or nodes after  $n$  level of decomposition is  $2^n$ . However, based on the requirement of frequency resolution, the level of decomposition can be determined. For instance, if level of decomposition is 3 then no. of packets received are 8. So, if the maximum frequency of input signal is  $f$ , then at level three each packet contains information of bandwidth of  $f/8$ . Notation of each node is given as  $(l,i)$ , where  $l$  is level of decomposition and  $i$  is the number of the node.

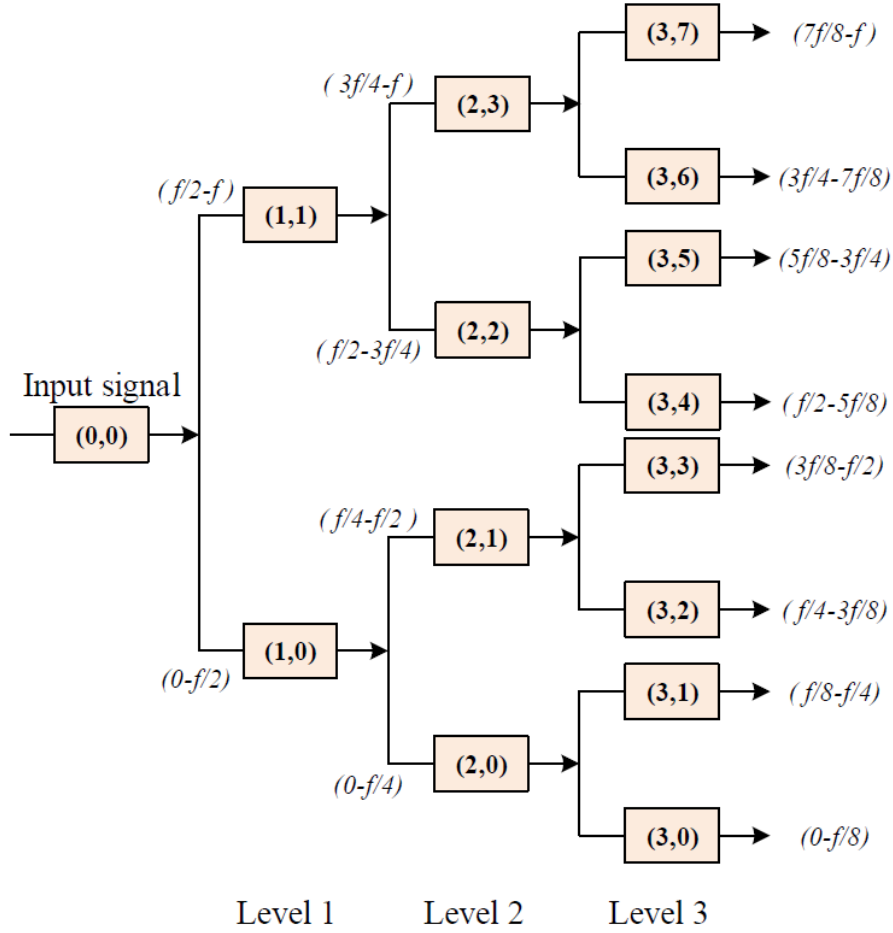


Figure 4–5 Three level WPD

Wavelet coefficients at level  $l$  and node  $i$  can be given by the following equations.

$$d_k^{j+1,2n} = \sum_k h_{0(2l-k)} d_l^{j,n} \quad (4-6)$$

$$d_k^{j+1,2n+1} = \sum_k h_{1(2l-k)} d_l^{j,n} \quad (4-7)$$

Here,  $d_l^{j,n}$ ,  $d_k^{j+1,2n}$ , and  $d_k^{j+1,2n+1}$  are wavelet packet coefficients,  $h_{0(2l-k)}$  is low pass filter coefficient, and  $h_{1(2l-k)}$  is high pass filter coefficient. In this method, the norm of packet coefficient is used as an indicator.

### 4.3. Investigation of the Influence of Degradation on Transient Current Response

To establish a method which can detect and classify insulation degradation, it is crucial to understand how a current response is influenced by different types and severity of insulation degradation. In particular, this section focuses on how high frequency behavior of transient current  $i_{trans}$  changes with degradation.

#### 4.3.1. Turn to Ground (TG) degradation

##### 4.3.1.1. Transient Current Response

Figs. 4-6 to 4-13 show transient current  $i_{trans}$  for various TG degradation cases. It can be observed that for each case, during first the 80ns, there is a monolithic increase in current with an increase in degradation severity. Moreover, for a higher level of degradation more oscillation can be observed. It is also very important to note that even though the level of degradation is the same, the current gets less influenced as degradation moved further away from winding terminals. In other words, the influence of degradation on the current is reduced as degradation location further moved from terminals, so moving from turn 1 to turn 4, the current becomes closer to the case when insulation is good. Moreover, for degradation cases for turn 5, minor variation in current is observed. Moving further and closer to the end of the winding, the current gets more influenced. More and more influence on current can be observed as degradation moves from turn 6 to turn 8.

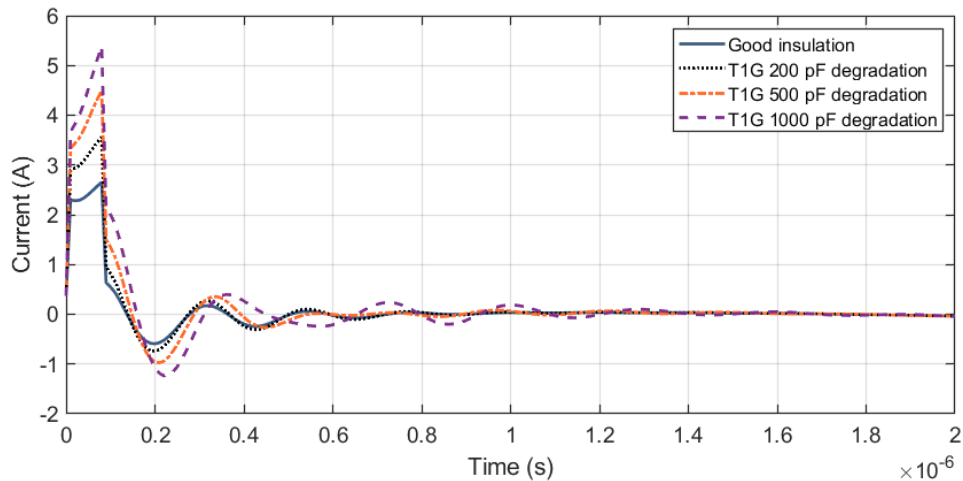


Figure 4–6 Transient current for T1G degradation

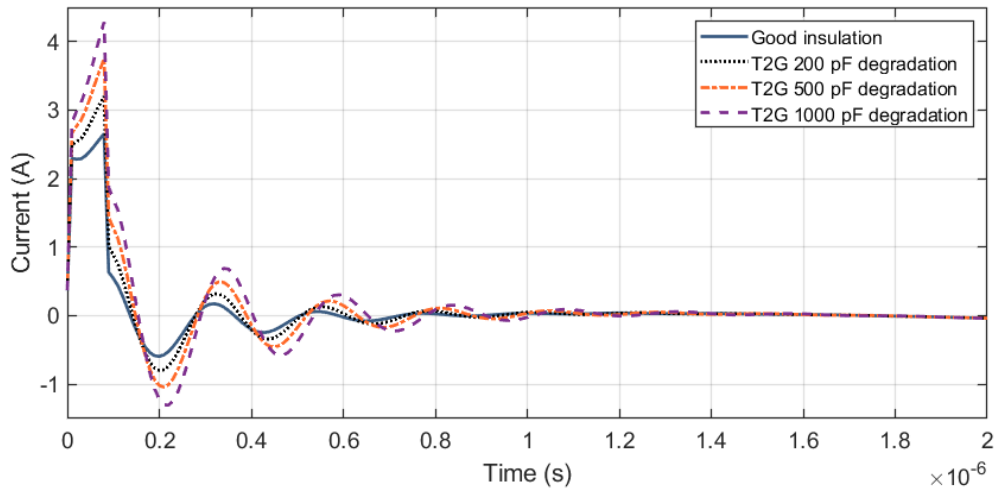


Figure 4-7 Transient current for T2G degradation

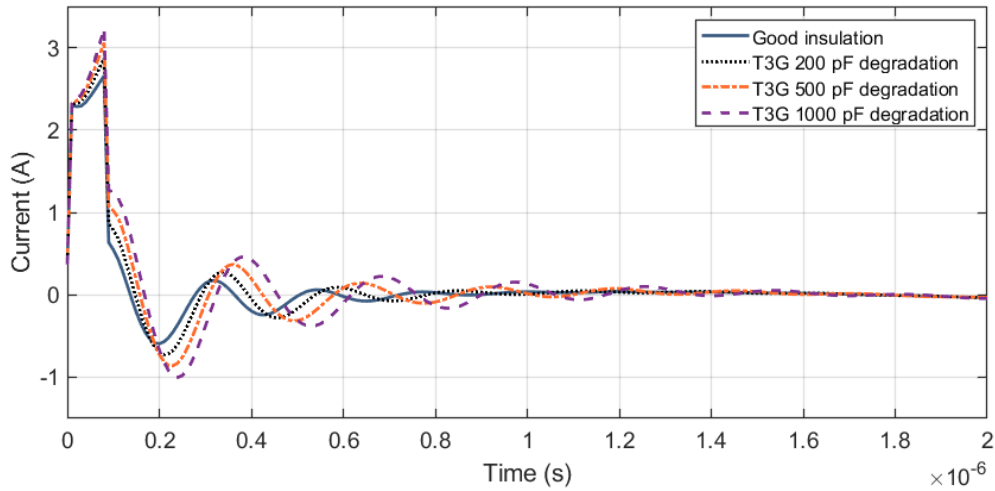


Figure 4-8 Transient current for T3G degradation

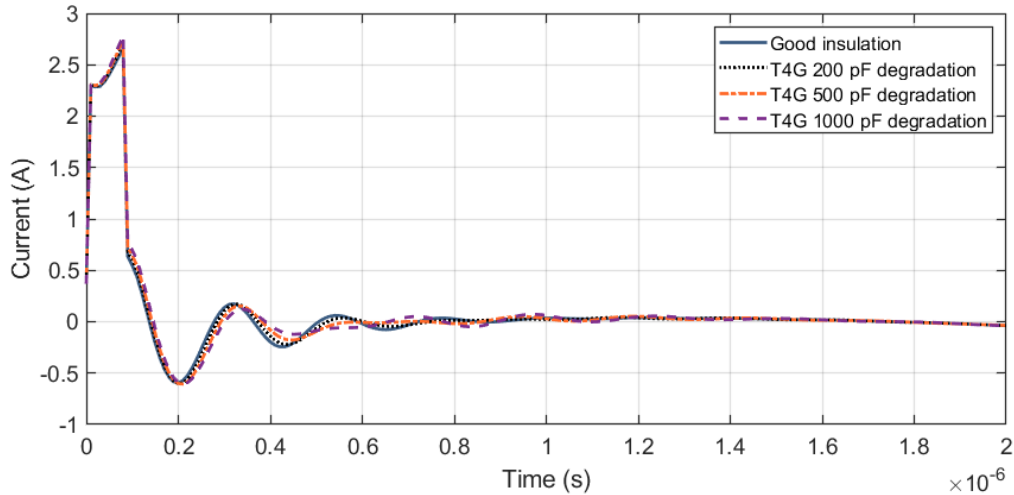


Figure 4-9 Transient current for T4G degradation

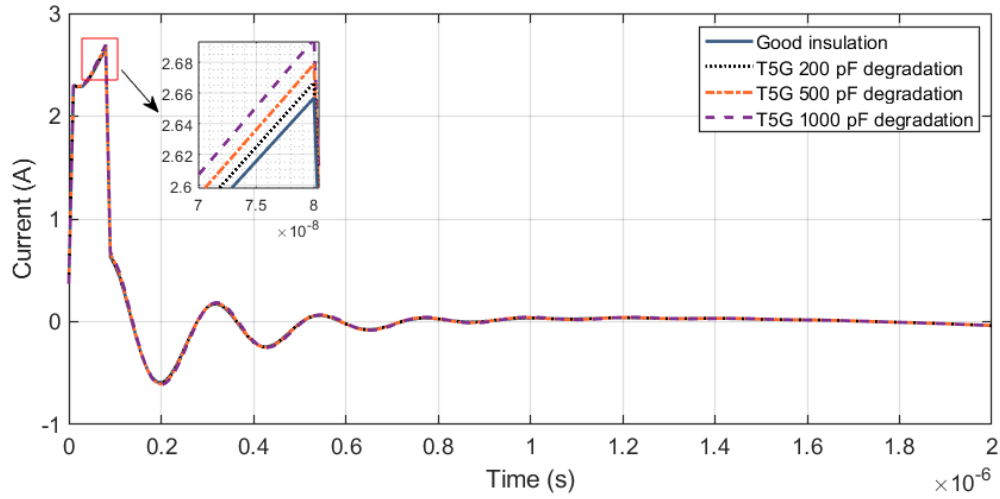


Figure 4–10 Transient current for T5G degradation

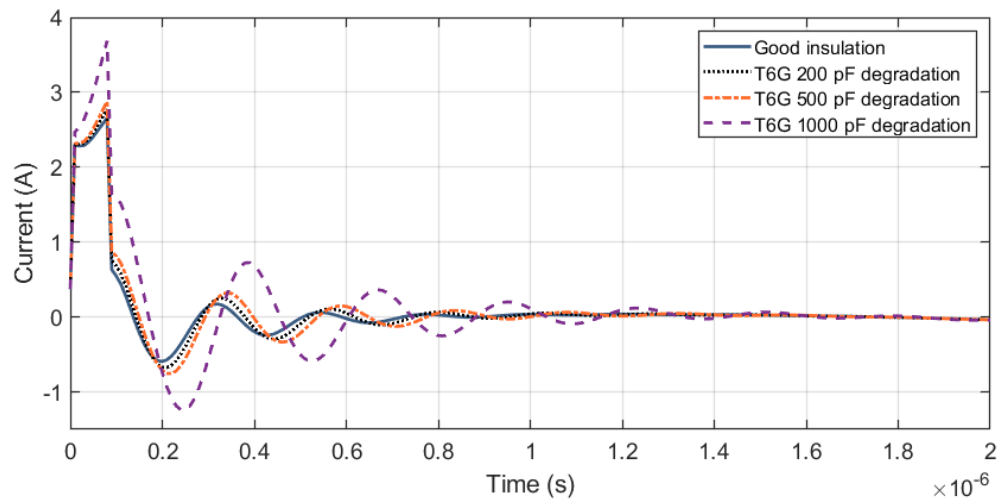


Figure 4–11 Transient current for T6G degradation

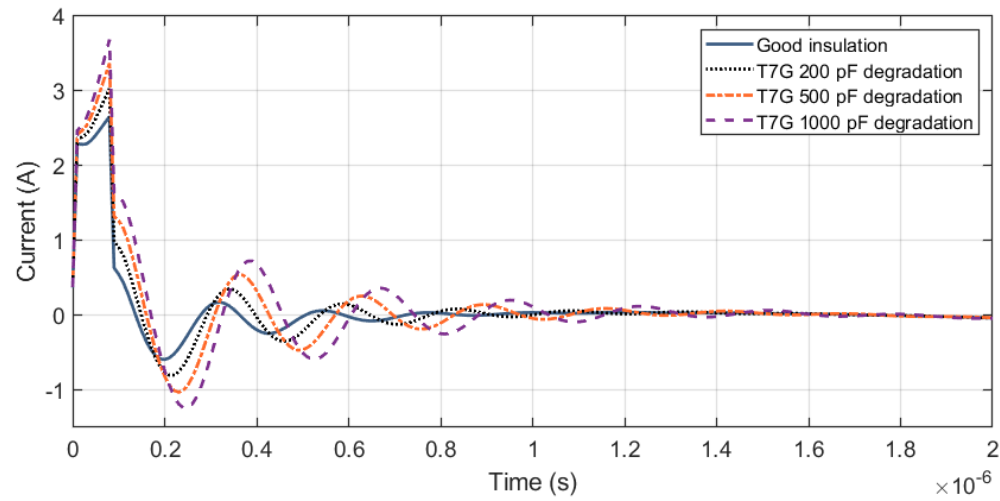


Figure 4–12 Transient current for T7G degradation

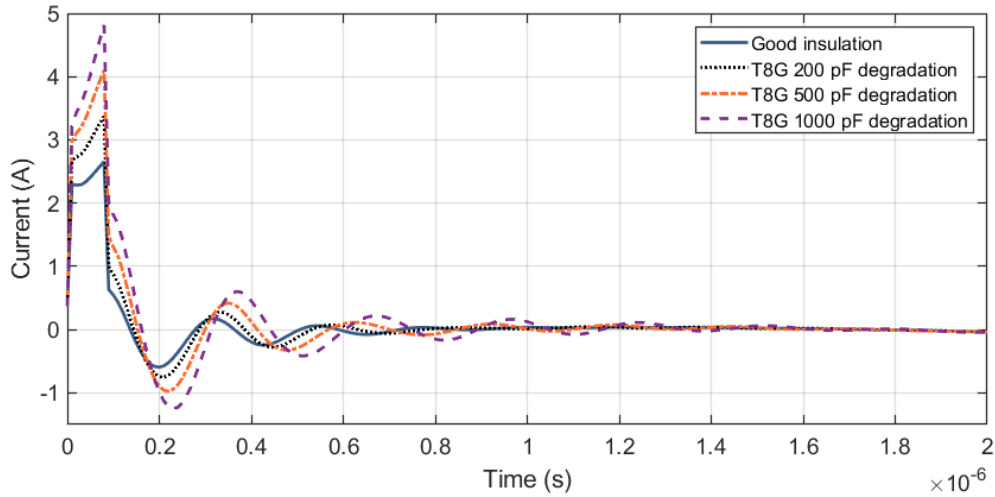


Figure 4–13 Transient current for T8G degradation

#### 4.3.1.2. Amplitude spectrum

To investigate, how high frequency behavior of current response changes with different levels of insulation degradation, amplitude spectrums are obtained. Figs. 4-14 to 4-21 show spectrum obtained from  $i_{trans}$  for different TG degradation, how amplitude change over frequency up to 50MHz is presented. Amplitude spectrums show a similar pattern as transient current. For most cases of degradation, change in amplitude from 1Hz to 5MHz is obvious, however there is a small change over the whole spectrum. Monolithic increase with more severe degradation for each can be observed. Moreover, the influence of degradations away from the terminal of winding is less.

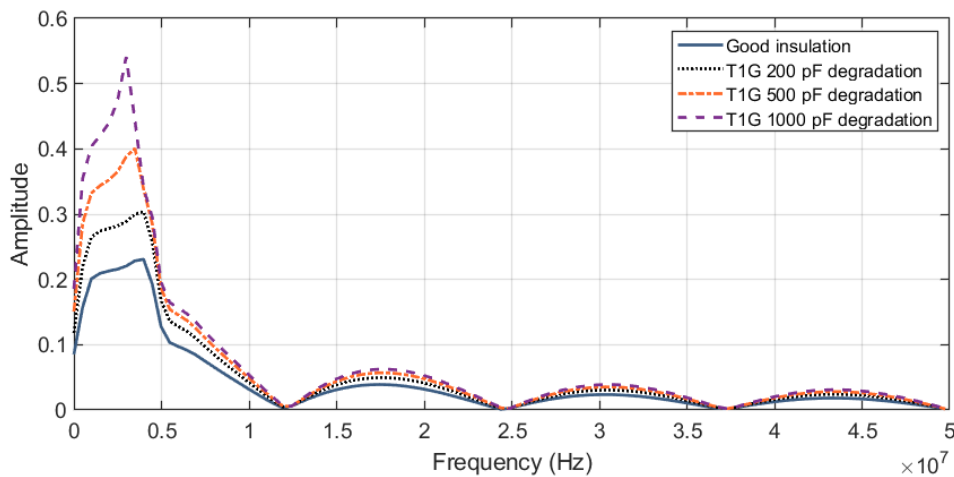


Figure 4–14 Amplitude spectrum of transient current for T1G degradation

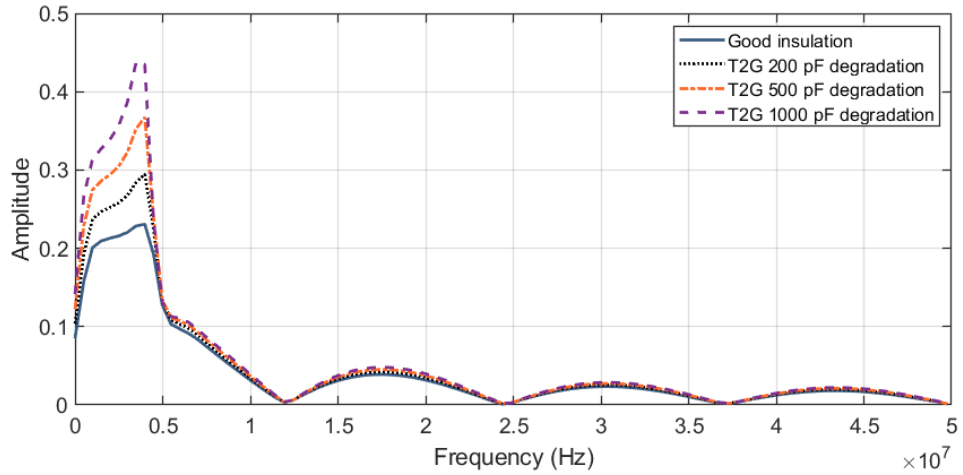


Figure 4-15 Amplitude spectrum of transient current for T2G degradation

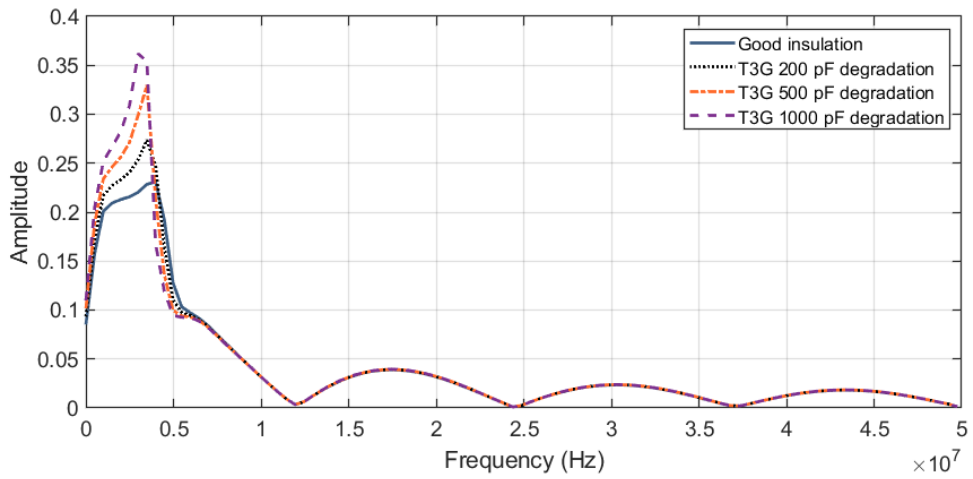


Figure 4-16 Amplitude spectrum of transient current for T3G degradation

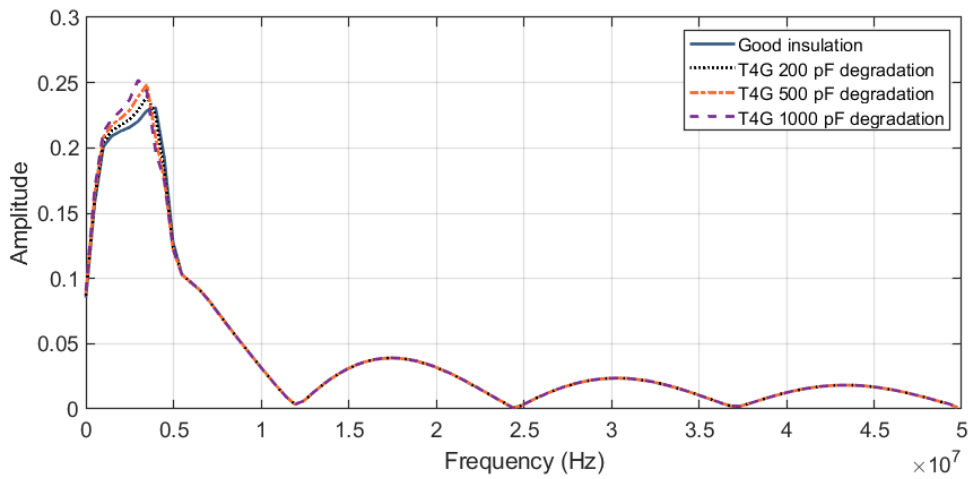


Figure 4-17 Amplitude spectrum of transient current for T4G degradation

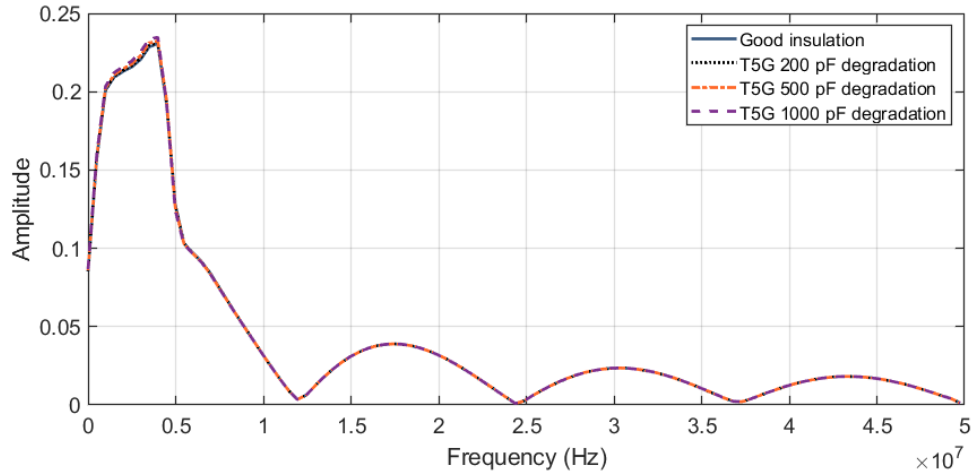


Figure 4-18 Amplitude spectrum of transient current for T5G degradation

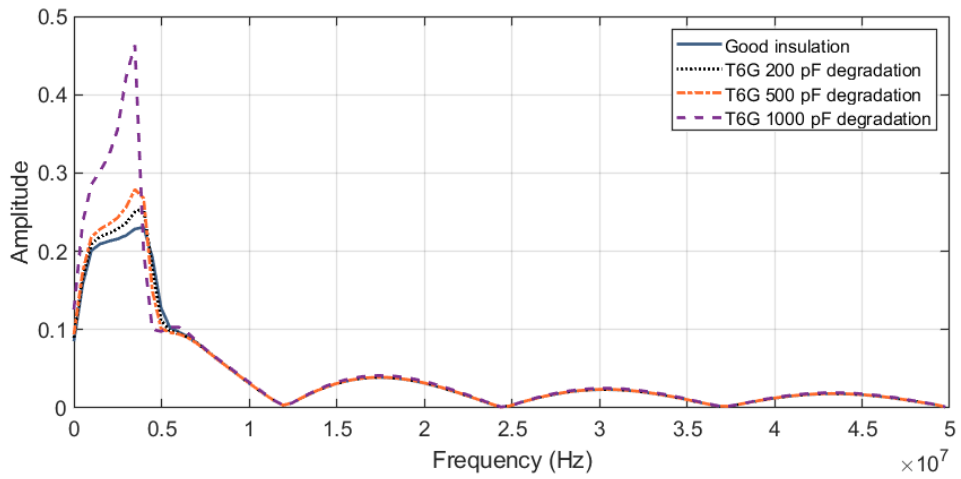


Figure 4-19 Amplitude spectrum of transient current for T6G degradation

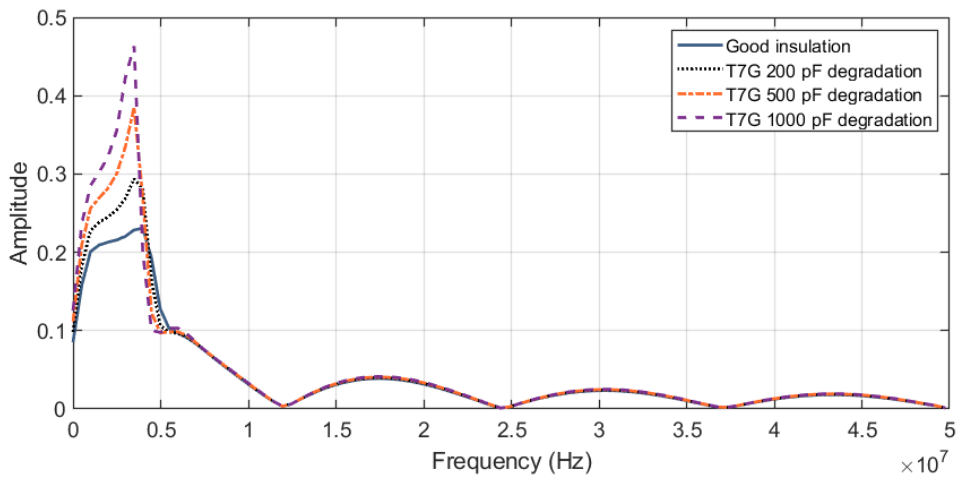


Figure 4-20 Amplitude spectrum of transient current for T7G degradation

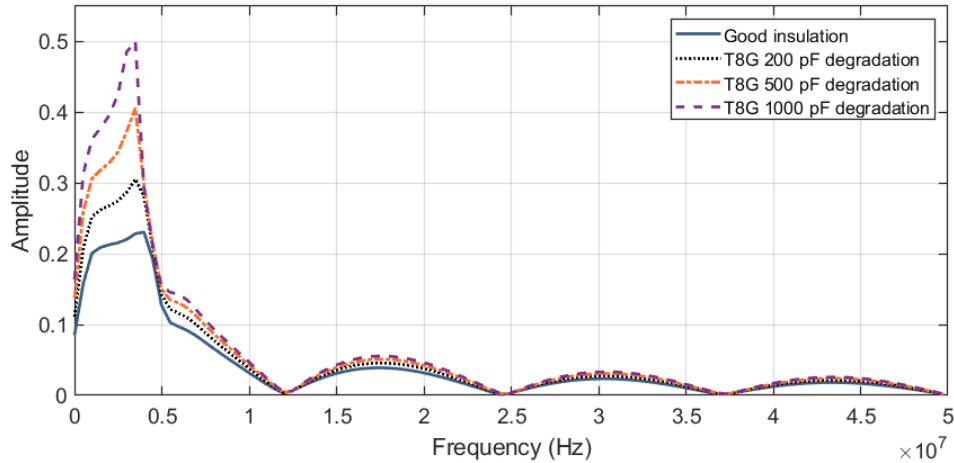


Figure 4–21 Amplitude spectrum of transient current for T8G degradation

## 4.3.2. Turn to Turn Degradation

### 4.3.2.1. Transient Current Response

Figs. 4-22 to 4-25 shows transient current response  $i_{trans}$  for various TT degradation. For each case, monolithic increase in current amplitude for first 80ns with an increase in severity of degradation is obvious. However, this increase is comparatively less with respect to TG degradation cases. This is because TG degradation allows a small amount of current to flow through the insulation directly to the stator, while it is not possible in TT degradation. Similar to TG degradation, the influence of degradations further away from winding terminals is less on transient current. For first 80ns, the increase in amplitude for TT12 degradations is very obvious. As degradation moved between turn 3 and turn 4, an increase in amplitude is very less. Similar amplitude increase can be observed for degradation between turn 5 and turn 6. While, for degradation between the last two turns, the amplitude increase is again very obvious. This concludes that the influence of degradations near the winding terminals is more than degradations further away from terminals.

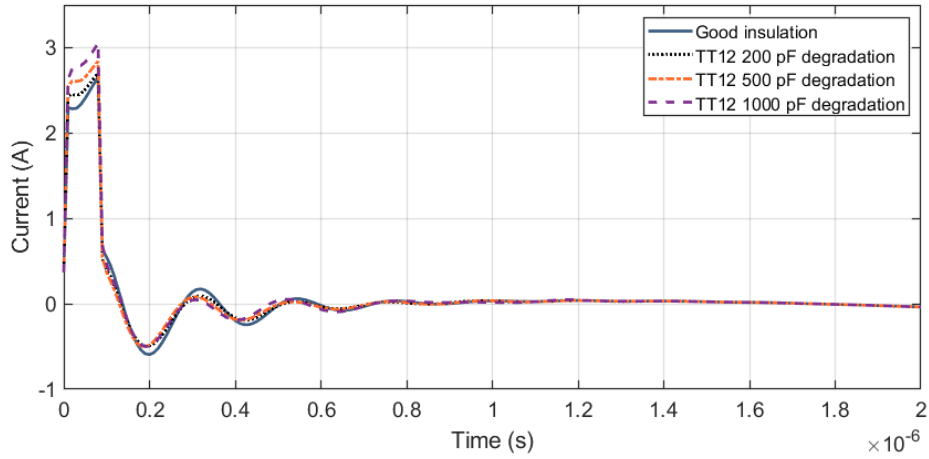


Figure 4-22 Transient current for TT12 degradation

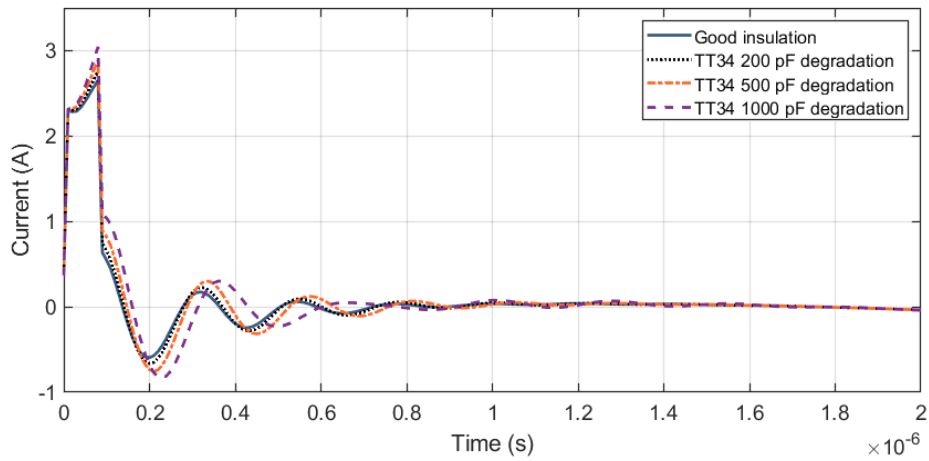


Figure 4-23 Transient current for TT34 degradation

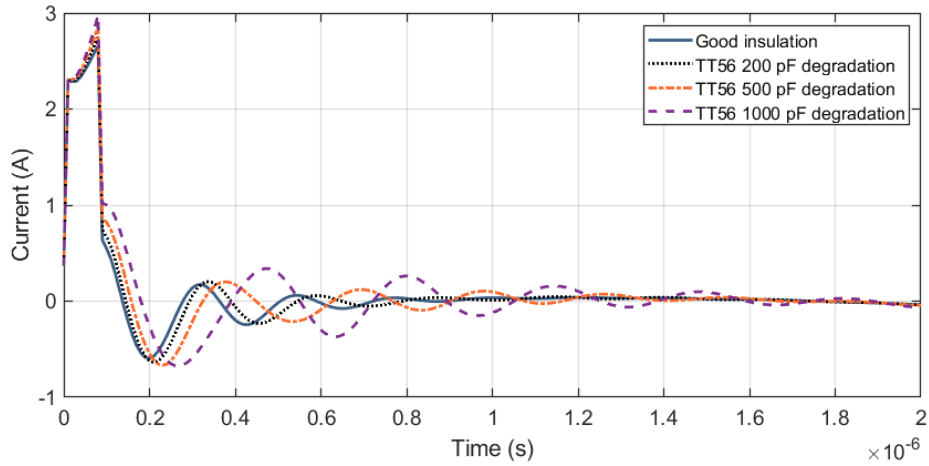


Figure 4-24 Transient current for TT56 degradation

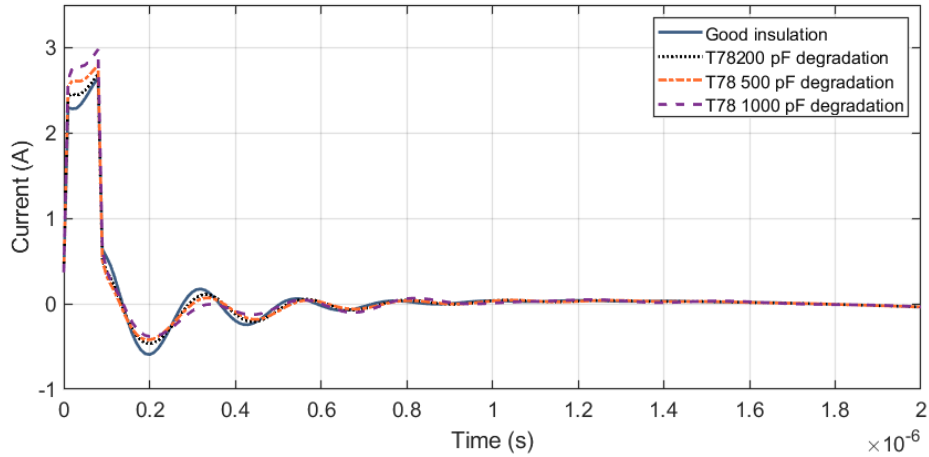


Figure 4–25 Transient current for TT78 degradation

Figs. 4-26 to 4-29 shows a spectrum obtained from  $i_{trans}$  for different TT degradation. Similar monolithic increase in amplitude with the severity of degradation can be observed. For cases TT12 and TT78, the amplitude changes over the whole spectrum similar to the TG cases. While for cases TT34 and TT56, amplitude changes only up to about 7.5MHz. Moreover, the change amplitude is comparatively more than other cases when degradation is near to the winding terminals.

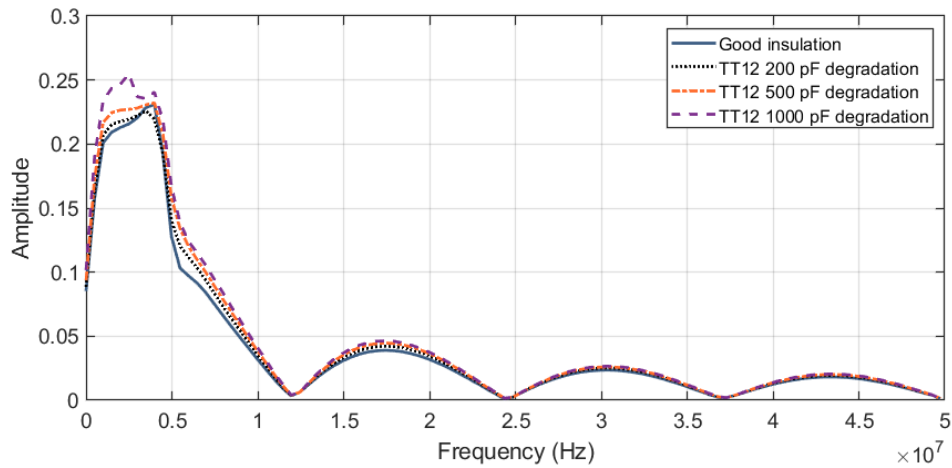


Figure 4–26 Amplitude spectrum of transient current for TT12 degradation

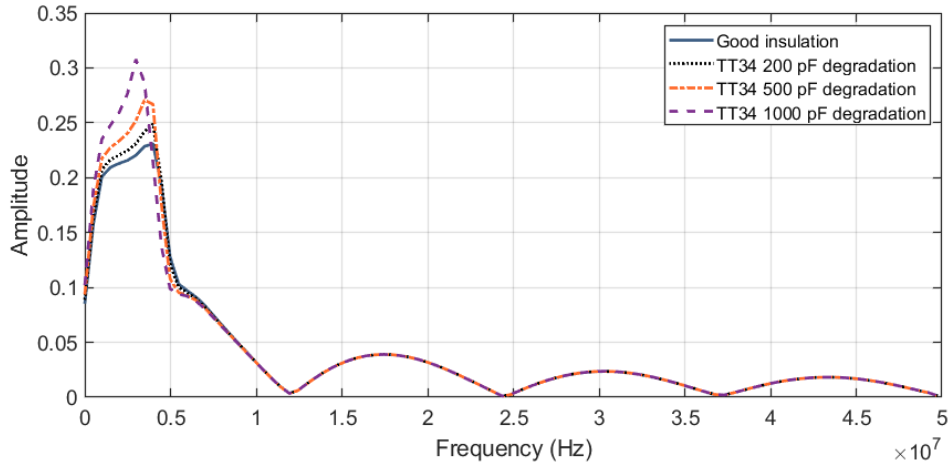


Figure 4–27 Amplitude spectrum of transient current for TT34 degradation

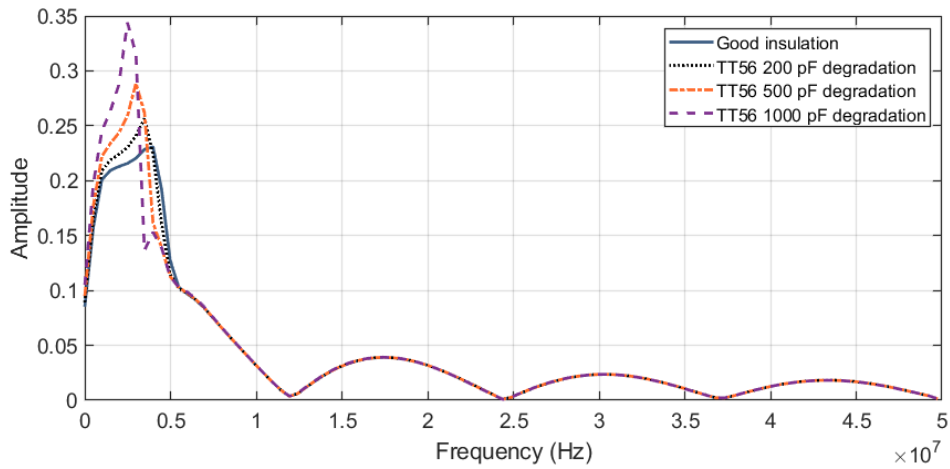


Figure 4–28 Amplitude spectrum of transient current for TT56 degradation

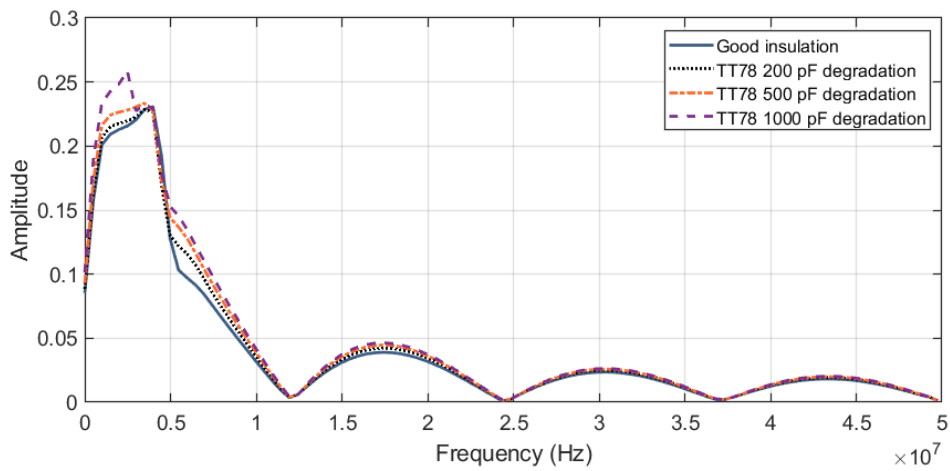


Figure 4–29 Amplitude spectrum of transient current for TT78 degradation

From frequency response analysis, it is clear that for most TG degradation, amplitude over frequency range 15MHz to 20MHz changes. While for a couple of cases when transient current response is too close to the current response for good insulation, this change is not obvious. Since current does not get affected by degradation, these kinds of degradations are difficult to be detected. Moreover, they are not serious since it does not have any effect on transient current. However, if the degradation is severe enough to influence the transient current, it can be observed from the amplitude spectrum. For TT degradations, amplitude change over the frequency range 15MHz to 20MHz is negligible. However, for cases TT12 and TT78, amplitude change over this region is significant. However, this can be due to higher influence of degradations near the winding terminals on transient current. As simple winding with only 8 turns is used, more TT degradation cases cannot be investigated. So, frequency response over the range 15MHz to 20MHz can be used to classify the type of degradation, since TG degradation leads to change in response over mentioned range while TT degradation has no influence over this frequency range.

On the other hand, regardless of the type of degradation, amplitude changes over frequency up to about 7.5MHz. For TG degradation cases, this change is significant over the aforementioned frequency range. While for TT degradations, this change is comparatively less. This is because TG degradations are more severe and have a higher influence on the current response while TT degradations are comparatively less severe. So, it fair to conclude that, the amplitude of spectrum up to about 7.5MHz is a good indicator to determine the overall SOH of insulation. Higher the deviation from reference case or when the good case, it is more severe degradation.

#### **4.4. Indicators for Determination of SOH and Classification from WPD.**

From spectrum analysis, it is clear that amplitude change over a frequency range up to 7.5MHz can be used to determine overall SOH, while amplitude change over 15MHz to 20MHz can be indicative of the type of degradation. Here, WPD with five level of decomposition is used, hence 32 packets obtained. Higher order wavelet 'db14' is used for decomposition. Fig. 4-30 shows, five level of decomposition and packets along with frequency bandwidth. For convenience, packets are named from p0-p31 going from node (5,0) to (5,31).

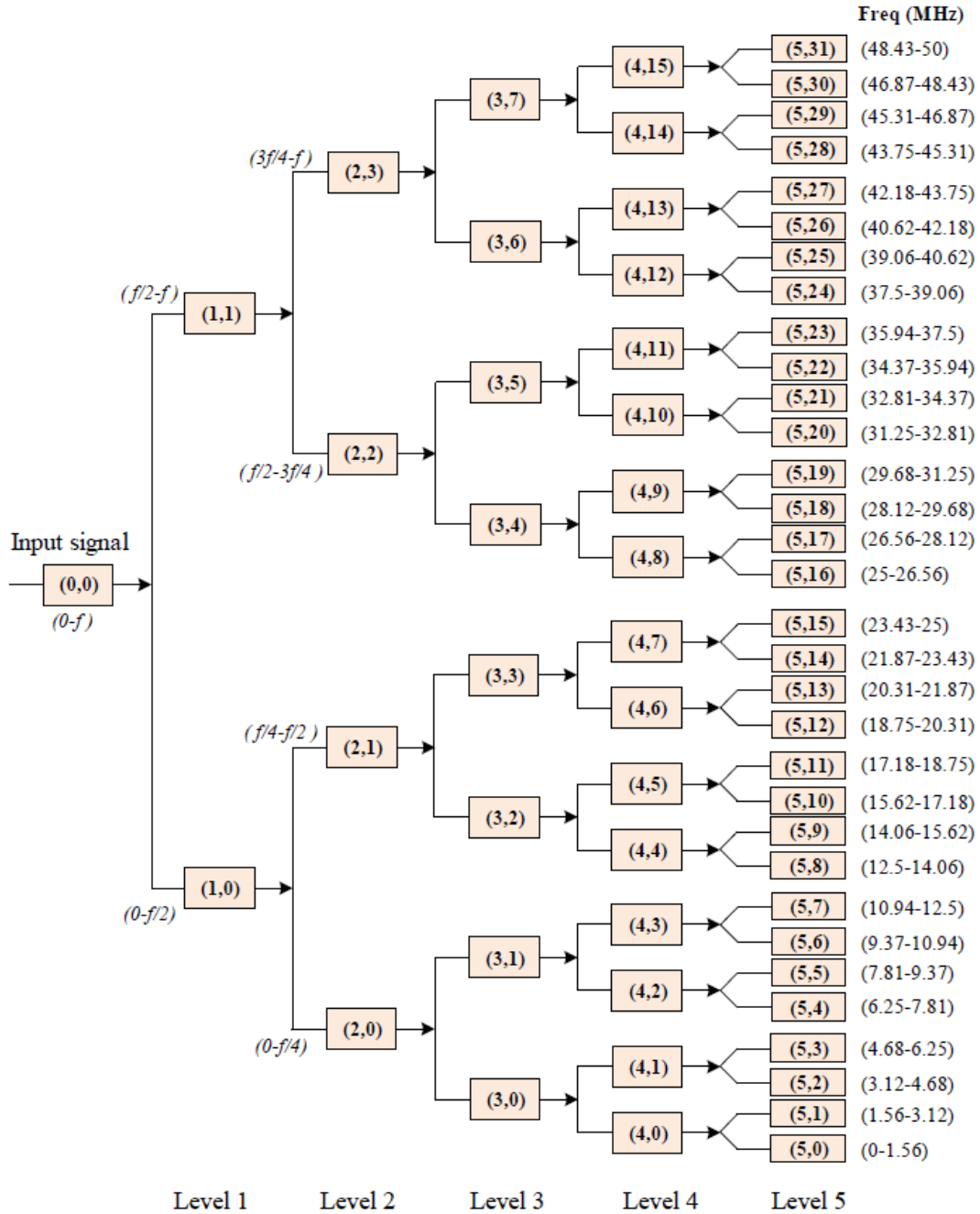


Figure 4–30 Five level WPD for degradation detection and classification

To determine SOH, information over 7.5MHz is required, which can be obtained from packets p0, p1, p2, p3, p4, and p5. While for degradation classification, information over a frequency range of 15MHz to 20MHz is required, which can be obtained from packets p9, p10, p11, and p12. From analysis, it was concluded that the norm of packet p0 can be used to determine the overall SOH of a stator. While norm of packet p10 can be used to classify the type of degradation.

## Overall SOH Determination

Fig. 4-31 shows the norm of packet p0 for different types and severity of degradation. Higher the value of norm compares to the norm when insulation is good, severe the degradation. Thresholds can be established with this kind of analysis and SOH can be tracked. It can be observed that for each type of degradation, the value of the norm increases with severity of degradation. In fact, the pattern in norms is similar to the pattern observed in the amplitude spectrum. This method can detect the smallest influence on current due to degradation. For instance, for TG degradation for turn 5, a very small variation in transient current is observed which is also reflected as a small variation in norm values for same case. Moreover, since TT degradation is less severe than TG degradation, norms for TT degradations is less compare to TG degradations. It is important to note that this method is very accurate when it comes to detecting degradation which has influence on transient current. However, not all types and severity of degradations have influence on transient current, so it is fair to say that this method is very accurate since the smallest variation can be detected.

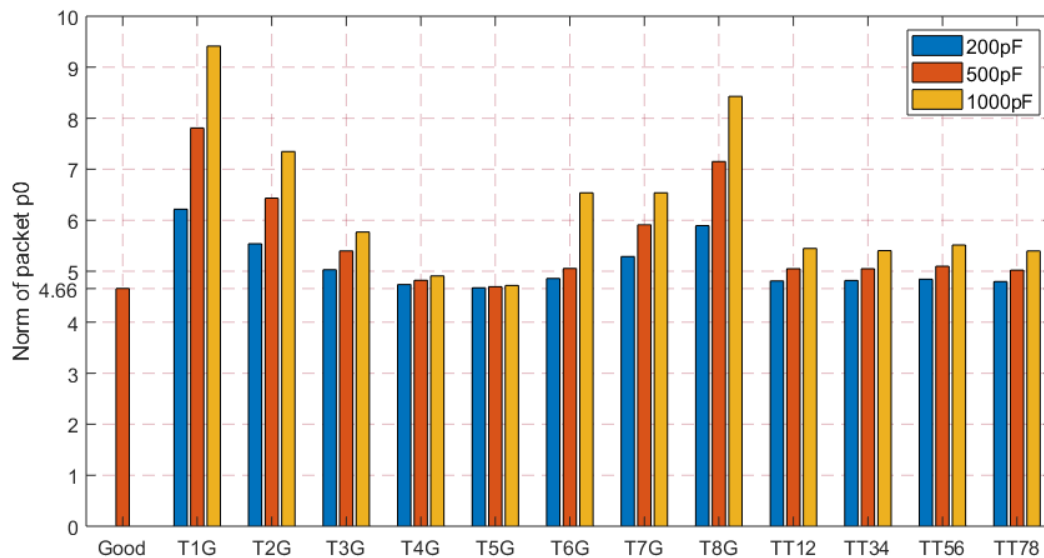


Figure 4-31 Norm form packet p0 for different degradations

## Degradation Classification

Fig. 4-32 shows the norm of packet p10 for different types and severity of degradation. Based on the value of norm from packet p10, the type of degradation can be determined. This method solely depends on the assumption that TG degradation cause change amplitude of spectrum over frequency from 15.62MHz to 17.18MHz, while TT degradation does not cause any change over

this range. Packet p10 provides information on frequency range from 15.62MHz to 17.18MHz. As mentioned earlier, TG degradation causes variation over this frequency range and the norm of p10 varies depending on the change over this frequency range. So, if the value of norm is higher than the value in a case when insulation is good, then its TG degradation else it is TT degradation. The value of norm of p10 is 0.6864 for good insulation.

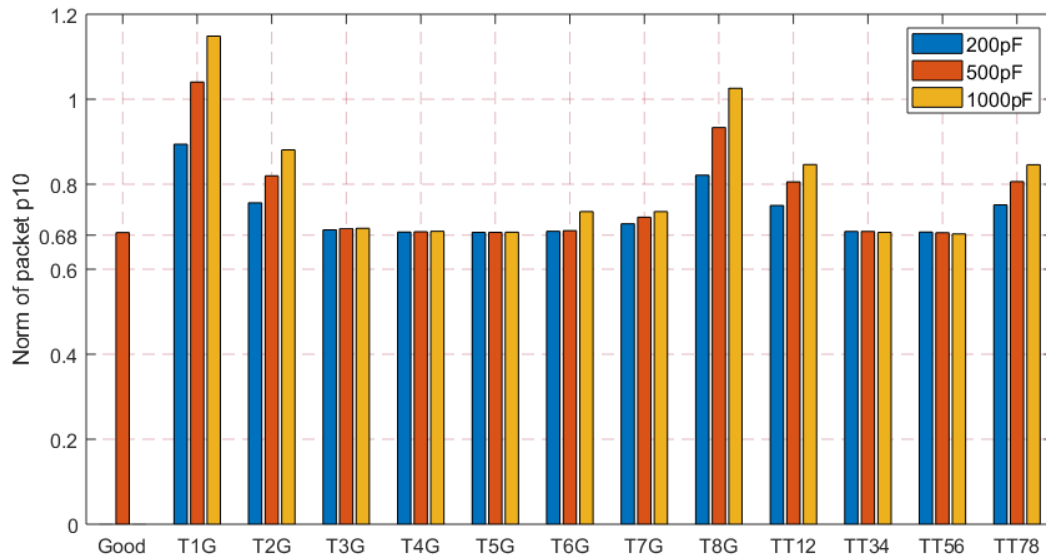


Figure 4-32 Norm form packet p10 for different degradations

Table 4-1 Norms from p10 for TG degradations

Severity	Norm of packet 10							
	T1G	T2G	T3G	T4G	T5G	T6G	T7G	T8G
<b>200pF</b>	0.8941	0.7562	0.6925	0.6874	0.6866	0.6892	0.7068	0.8215
<b>500pF</b>	1.0404	0.8199	0.6954	0.6882	0.6869	0.69091	0.72233	0.9335
<b>1000pF</b>	1.1485	0.881	0.6962	0.6891	0.6872	0.7315	0.7357	1.0257

Table 4-2 Norms from p10 for TT degradations

Severity	Norm of packet 10			
	TT12	TT34	TT56	TT78
<b>200pF</b>	0.7498	0.6887	0.6875	0.7515
<b>500pF</b>	0.8053	0.6889	0.6861	0.8064
<b>1000pF</b>	0.8464	0.6866	0.6831	0.8457

Table 4-1 and 4-2 provide information on the norm of p10 for various degradations. From norm values of cases T1G, T2G, T6G, T7G, T8G, TT34, and TT56, it is obvious that they can be classified correctly based on this method. However, for other cases, this method is not working as expected. In fact, it is more accurate to conclude that this method is capable of detecting the smallest change in insulation that causes a change in frequency behavior over frequency range from 15.62MHz to 17.18MHz. However, not all degradation causes significant effect over this region. For instance, for T5G case, the transient current barely changed compare to reference case. Which resulted in no change in amplitude spectrum over the frequency range from 15.62MHz to 17.18MHz. Similar effects can be observed for T3G, T4G and T5G. So, it is fair to say that the severity of degradation for these cases is very low that it does not affect the amplitude spectrum over aforementioned frequency range. More, analysis can be done on this with more severe degradation. However, it is excellent to see that that this method can detect even smallest change in the degradation. Moreover, monolithic increase in norm value with the severity of degradation can be observed. Similarly, for cases TT12 and TT78, no change in amplitude was expected over frequency range from 15.62MHz to 17.18MHz. However, the change in amplitude spectrum is clear. This can be due to fact that these degradations are emulated near the winding terminals, which causes a similar current response as TG degradation. In chapter 3, it was made clear that degradations location or how far degradations are from winding terminals does affect the transient current. This method has already proved its credibility when it comes to detecting and classifying degradation of higher severity which has significant effect on transient current. For most real world applications, thresholds can be established to get intuition on type and severity of degradation.

#### **4.5. Summary**

In this chapter, initially various insulation condition monitoring techniques along with their advantages and disadvantages is discussed. Then a new insulation condition detection technique is proposed. This technique has a capability to determine SOH and type of degradation. Influence of degradation on transient current response is investigated by analyzing amplitude spectrums for different degradation. This method proved extremely well in determining overall SOH of winding. However, more investigations are required for classifying degradation. For most applications, thresholds can be established to get intuition on the type and severity of degradation. To conclude, this method seems very promising. However, due to limitations associated with the reduced winding, more emulations and analysis cannot be performed.

## **Chapter 5: Conclusions and Future Work**

### **5.1. Conclusions**

This thesis mainly presented: 1) comparative analysis on winding modeling techniques utilized for electrical stress analysis; 2) Emulation of insulation degradation in random wound machine winding using FE based method; and 3) Insulation degradation detection technique which provides overall SOH of insulation and classify types of insulation degradation.

### **Chapter 2**

In this chapter, FE based modeling technique and RLC based modeling technique are compared. For which, a form wound machine winding is modeled. Electrical stress between various turns and stress at each turn with respect to ground is analyzed against  $dv/dt$  pulse are considered. Maximum electrical stress values obtained from the RLC model and FE model matched well with each other. However, the transient behavior of these voltage stresses did not match well with each other which can be due to the use of constant inductance value in RLC model. While FE model computes frequency dependent inductances internally. By modeling and including frequency dependent parameters in RLC model, more accurate winding model can be created. Moreover, to achieve even higher accuracy, slot and overhang regions can be modeled separately along with frequency dependent inductances and resistances. Compared to RLC model, the FE model proved extremely computationally expensive.

### **Chapter 3**

In this chapter, the emulation of insulation degradation using FE based approach is presented. A random wound machine winding is modeled, and steps for emulating degradation is presented. At different locations inside the winding, turn to turn degradation and turn to ground degradations of different severity are emulated. Moreover, the influence of these degradations on current response under the same given voltage pulse is investigated. For each case, it is found that an increase in severity of degradation causes a monolithic increase in current amplitude and oscillations. Which assures that transient current is good indicative of insulation degradation. Moreover, it is observed that location of degradation strongly influences the transient current. It is found that degradations closer to the winding terminals have more influence on transient current.

## Chapter 4

This chapter mainly proposes a new insulation degradation detection technique which can determine the overall SOH of insulation and types of degradation. To do so, WPD on transient current is performed and norm from some of the packets is used as an indicator for SOH and degradation type determination. This method is excellent when it comes to determining SOH, monolithic increase in indicator values with the severity of degradation can be observed. Moreover, this method can detect even a very small change in insulation state, even when there is no visible change in the transient current like T5G degradation. However, this method is not perfect, when it comes to classifying the degradation. For TT12 and TT78 degradation, no change in amplitude was expected over frequency range from 15.62MHz to 17.18MHz, just like TT34 and TT56 degradation. This can be due to fact that degradation near to winding terminal affects transient current in a different way. This method seems promising. However, to completely verify the credibility of this method for this method, more analysis for more degradation cases is required. But, due to limitations associated with the reduced winding, more emulations and analysis cannot be performed at this stage.

### 5.2. Future Work

The proposed research in this thesis can be further extended and they are discussed as follows:

1. The winding modeling technique can be improved by incorporating the frequency dependent parameters and variation of parameters in slot and overhang region to achieve better accuracy.
2. This study emulated faults on a strand level model, however this procedure is very complex and computationally expensive. A turn level model that can provide results with similar accuracy can be investigated to achieve higher computation efficiency.
3. The insulation degradation detection and classification method proposed in this study can be applied to analyze more degradation cases and machines with other winding configurations. Moreover, the reliability of this method for different  $dv/dt$  levels should be investigated through experiments.
4. The insulation indicator developed in this study can be employed in online insulation monitoring for VSI-fed electric machines.

## References

- [1] “Global EV Outlook 2020 – Analysis,” *IEA*. <https://www.iea.org/reports/global-ev-outlook-2020> (accessed Dec. 01, 2020).
- [2] “Zero-emission vehicles,” *AECAA 15208055*. <https://tc.canada.ca/en/road-transportation/innovative-technologies/zero-emission-vehicles> (accessed Dec. 01, 2020).
- [3] “Electric Vehicle Incentives – Plug’n Drive.” <https://www.plugndrive.ca/electric-vehicle-incentives/> (accessed Dec. 01, 2020).
- [4] C. Gan, J. Wu, Q. Sun, W. Kong, H. Li, and Y. Hu, “A Review on Machine Topologies and Control Techniques for Low-Noise Switched Reluctance Motors in Electric Vehicle Applications,” *IEEE Access*, vol. 6, pp. 31430–31443, 2018, doi: 10.1109/ACCESS.2018.2837111.
- [5] P. Nussbaumer, A. Mitteregger, and Th. M. Wolbank, “Online detection of insulation degradation in inverter fed drive systems based on high frequency current sampling,” in *IECON 2011 - 37th Annual Conference of the IEEE Industrial Electronics Society*, Melbourne, Vic, Australia, Nov. 2011, pp. 1954–1959, doi: 10.1109/IECON.2011.6119605.
- [6] R. E. Adjaye and K. J. Cornick, “Distribution of switching surges in the line-end coils of cable-connected motors,” *IEE Journal on Electric Power Applications*, vol. 2, no. 1, pp. 11–21, Feb. 1979, doi: 10.1049/ij-epa.1979.0002.
- [7] V. Mihaila, S. Duchesne, D. Roger, and P. Y. Liegeois, “Prediction of the turn-to-turn voltages in parallel connected wires configuration for motor coils fed by steep fronted pulses,” in *2011 Electrical Insulation Conference (EIC)*., Annapolis, MD, USA, Jun. 2011, pp. 407–412, doi: 10.1109/EIC.2011.5996188.
- [8] F. Perisse, P. Werynski and D. Roger, "A New Method for AC Machine Turn Insulation Diagnostic Based on High Frequency Resonances," in *IEEE Transactions on Dielectrics and Electrical Insulation*, vol. 14, no. 5, pp. 1308-1315, October 2007, doi: 10.1109/TDEI.2007.4339494.
- [9] M. Toudji, G. Parent, S. Duchesne, and P. Dular, “Determination of Winding Lumped Parameter Equivalent Circuit by Means of Finite Element Method,” *IEEE Transactions on Magnetics*, vol. 53, no. 6, pp. 1–4, Jun. 2017, doi: 10.1109/TMAG.2017.2671423.
- [10] V. Mihaila, S. Duchesne and D. Roger, "A simulation method to predict the turn-to-turn voltage spikes in a PWM fed motor winding," in *IEEE Transactions on Dielectrics and Electrical Insulation*, vol. 18, no. 5, pp. 1609-1615, October 2011, doi: 10.1109/TDEI.2011.6032831.
- [11] A. Krings, G. Paulsson, F. Sahlen, and B. Holmgren, “Experimental investigation of the voltage distribution in form wound windings of large AC machines due to fast transients,” in *2016 XXII International Conference on Electrical Machines (ICEM)*, Lausanne, Switzerland, Sep. 2016, pp. 1700–1706, doi: 10.1109/ICELMACH.2016.7732753.
- [12] J. Smajic *et al.*, “Simulation and Measurement of Lightning-Impulse Voltage Distributions Over Transformer Windings,” *IEEE Transactions on Magnetics*, vol. 50, no. 2, pp. 553–556, Feb. 2014, doi: 10.1109/TMAG.2013.2283061.
- [13] T. Zupan, B. Trkulja, R. Obrist, T. Franz, B. Cranganu-Cretu, and J. Smajic, “Transformer Windings’ Parameters Calculation and Lightning Impulse Voltage Distribution Simulation,” *IEEE Transactions on Magnetics*, vol. 52, no. 3, pp. 1–4, Mar. 2016, doi: 10.1109/TMAG.2015.2481004.

- [14] L. Gubbala, A. von Jouanne, P. Enjeti, C. Singh, and H. Toliyat, "Voltage distribution in the windings of an AC motor subjected to high dV/dt PWM voltages," in *Proceedings of PESC '95 - Power Electronics Specialist Conference*, Atlanta, GA, USA, 1995, vol. 1, pp. 579–585, doi: 10.1109/PESC.1995.474867.
- [15] Yifan Tang, "Analysis of steep-fronted voltage distribution and turn insulation failure in inverter-fed form-wound AC motor," *IEEE Transactions on Industrial Applications*, vol. 34, no. 5, pp. 1088–1096, Oct. 1998, doi: 10.1109/28.720449.
- [16] G. Suresh, H. A. Toliyat, D. A. Rendusara, and P. N. Enjeti, "Predicting the transient effects of PWM voltage waveform on the stator windings of random wound induction motors," *IEEE Transactions on Power Electronics*, vol. 14, no. 1, pp. 23–30, Jan. 1999, doi: 10.1109/63.737589.
- [17] P. Bidan, T. Lebey, G. Montseny, and J. Saint-Michel, "Transient voltage distribution in inverter fed motor windings: experimental study and modeling," *IEEE Transactions on Power Electronics*, vol. 16, no. 1, pp. 92–100, Jan. 2001, doi: 10.1109/63.903993.
- [18] R. S. Ferreira and A. C. Ferreira, "Transient Voltage Distribution in Induction Motor Stator Windings Using Finite Elements Method," in *IECON 2018 - 44th Annual Conference of the IEEE Industrial Electronics Society*, Washington, DC, Oct. 2018, pp. 737–742, doi: 10.1109/IECON.2018.8595148.
- [19] R. S. Ferreira and A. C. Ferreira, "End-Windings Influence in the Transient Voltage Distribution in Electrical Machine Windings Using Finite Elements Method," in *2019 IEEE International Electric Machines & Drives Conference (IEMDC)*, San Diego, CA, USA, May 2019, pp. 468–475, doi: 10.1109/IEMDC.2019.8785294.
- [20] O. Magdun, S. Blatt, and A. Binder, "Calculation of stator winding parameters to predict the voltage distributions in inverter fed AC machines," in *2013 9th IEEE International Symposium on Diagnostics for Electric Machines, Power Electronics and Drives (SDEMPED)*, VALENCIA, Spain, Aug. 2013, pp. 447–453, doi: 10.1109/DEMPED.2013.6645754.
- [21] O. Magdun, A. Binder, A. Rocks, and O. Henze, "Prediction of common mode ground current in motors of inverter-based drive systems," in *2007 International Aegean Conference on Electrical Machines and Power Electronics*, Bodrum, Turkey, Sep. 2007, pp. 806–811, doi: 10.1109/ACEMP.2007.4510552.
- [22] M. T. Wright, S. J. Yang, and K. McLeay, "General theory of fast-fronted interturn voltage distribution in electrical machine windings," *IEE Proc. B Electr. Power Appl. UK*, vol. 130, no. 4, p. 245, 1983, doi: 10.1049/ip-b.1983.0040.
- [23] C. Petrarca, A. Maffucci, V. Tucci, and M. Vitelli, "Analysis of the Voltage Distribution in a Motor Stator Winding Subjected to Steep-Fronted Surge Voltages by Means of a Multiconductor Lossy Transmission Line Model," *IEEE Transactions On Energy Conversion*, vol. 19, no. 1, pp. 7–17, Mar. 2004, doi: 10.1109/TEC.2003.821834.
- [24] G. Lupo, C. Petrarca, M. Vitelli, and V. Tucci, "Multiconductor transmission line analysis of steep-front surges in machine windings," *IEEE Transactions on Dielectrics and Electrical Insulation*, vol. 9, no. 3, pp. 467–478, Jun. 2002, doi: 10.1109/TDEI.2002.1007711.
- [25] Peng Ying and Ruan Jiangjun, "Investigation of very fast transient overvoltage distribution in taper winding of tesla transformer," *IEEE Transactions on Magnetics*, vol. 42, no. 3, pp. 434–441, Mar. 2006, doi: 10.1109/TMAG.2005.862759.

- [26] M. K. Hussain and P. Gomez, "Modeling of machine coils under fast front excitation using a non-uniform multiconductor transmission line approach," *2016 North American Power Symposium (NAPS)*, Denver, CO, USA, 2016, pp. 1-6, doi: 10.1109/NAPS.2016.7747877.
- [27] M. K. Hussain and P. Gomez, "Optimized dielectric design of stator windings from medium voltage induction machines fed by fast front pulses," *IEEE Transactions on Dielectrics and Electrical Insulation*, vol. 24, no. 2, pp. 837-846, Apr. 2017, doi: 10.1109/TDEI.2017.006249.
- [28] Y. Xie, J. Zhang, F. Leonardi, A. R. Munoz, M. W. Degner and F. Liang, "Modeling and Verification of Electrical Stress in Inverter-Driven Electric Machine Windings," in *IEEE Transactions on Industry Applications*, vol. 55, no. 6, pp. 5818-5829, Nov.-Dec. 2019, doi: 10.1109/TIA.2019.2937068.
- [29] Y. Xie, J. Zhang, F. Leonardi, A. R. Munoz, M. W. Degner and F. Liang, "Voltage Stress Modeling and Measurement for Random-Wound Windings Driven by Inverters," *2019 IEEE International Electric Machines & Drives Conference (IEMDC)*, San Diego, CA, USA, 2019, pp. 1917-1924, doi: 10.1109/IEMDC.2019.8785133.
- [30] Y. Xie, J. Zhang, F. Leonardi, A. R. Munoz, M. W. Degner and F. Liang, "Voltage Stress Modeling and Measurement for Random-Wound Machine Windings Driven by Inverters," in *IEEE Transactions on Industry Applications*, vol. 56, no. 4, pp. 3536-3548, July-Aug. 2020, doi: 10.1109/TIA.2020.2986184.
- [31] R. G. Rhudy, E. L. Owen and D. K. Sharma, "Voltage Distribution Among the Coils and Turns of a Form Wound AC Rotating Machine Exposed to Impulse Voltage," in *IEEE Power Engineering Review*, vol. PER-6, no. 6, pp. 40-41, June 1986, doi: 10.1109/MPER.1986.5528005.
- [32] J. Kim and Y. Park, "Approximate Closed-Form Formula for Calculating Ohmic Resistance in Coils of Parallel Round Wires With Unequal Pitches," in *IEEE Transactions on Industrial Electronics*, vol. 62, no. 6, pp. 3482-3489, June 2015, doi: 10.1109/TIE.2014.2370943.
- [33] A. Griffio, I. Tsyokhla, and J. Wang, "Lifetime of Machines Undergoing Thermal Cycling Stress," in *2019 IEEE Energy Conversion Congress and Exposition (ECCE)*, Baltimore, MD, USA, Sep. 2019, pp. 3831-3836, doi: 10.1109/ECCE.2019.8913216.
- [34] K. N. Gyftakis, M. Sumislawska, D. F. Kavanagh, D. A. Howey and M. D. McCulloch, "Dielectric Characteristics of Electric Vehicle Traction Motor Winding Insulation Under Thermal Aging," in *IEEE Transactions on Industry Applications*, vol. 52, no. 2, pp. 1398-1404, March-April 2016, doi: 10.1109/TIA.2015.2495296.
- [35] "Nomex® 410 - Technical Data Sheet," p. 8. <https://www.dupont.com/products/nomex-400-series.html> (accessed Dec. 01, 2020)
- [36] M. K. W. Stranges, G. C. Stone, and D. L. Bogh, "IEC 60034-18-41: A New Draft Technical Specification for Qualification and Acceptance Tests of Inverter Duty Motor Insulation," in *Record of Conference Papers Industry Applications Society 52nd Annual Petroleum and Chemical Industry Conference*, Denver, CO, USA, 2005, pp. 297-302, doi: 10.1109/PCICON.2005.1524566.
- [37] O. V. Thorsen and M. Dalva, "A survey of faults on induction motors in offshore oil industry, petrochemical industry, gas terminals, and oil refineries," in *IEEE Transactions on Industry Applications*, vol. 31, no. 5, pp. 1186-1196, Sept.-Oct. 1995, doi: 10.1109/28.464536.
- [38] "Kapton® Summary of Properties," p. 20. <https://www.dupont.com/electronic-materials/kapton-polyimide-film.html> (accessed Dec. 01, 2020).

- [39] A. Cavallini, "Reliability of low voltage inverter-fed motors: What have we learned, perspectives, open points," *2017 International Symposium on Electrical Insulating Materials (ISEIM)*, Toyohashi, 2017, pp. 13-22, doi: 10.23919/ISEIM.2017.8088680.
- [40] V. Madonna, P. Giangrande, and M. Galea, "Evaluation of strand-to-strand capacitance and dissipation factor in thermally aged enamelled coils for low-voltage electrical machines," *IET Science, Measurement & Technology*, vol. 13, no. 8, pp. 1170–1177, Oct. 2019, doi: 10.1049/iet-smt.2019.0071.
- [41] V. Madonna, P. Giangrande, G. Migliazza, G. Buticchi and M. Galea, "A Time-Saving Approach for the Thermal Lifetime Evaluation of Low-Voltage Electrical Machines," in *IEEE Transactions on Industrial Electronics*, vol. 67, no. 11, pp. 9195-9205, Nov. 2020, doi: 10.1109/TIE.2019.2956378.
- [42] P. Werynski, D. Roger, R. Corton and J. F. Brudny, "Proposition of a new method for in-service monitoring of the aging of stator winding insulation in AC motors," in *IEEE Transactions on Energy Conversion*, vol. 21, no. 3, pp. 673-681, Sept. 2006, doi: 10.1109/TEC.2006.875465.
- [43] C. Zoeller, T. M. Wolbank and M. A. Vogelsberger, "Insulation condition monitoring of traction drives based on transient current signal resulting from differential and common mode excitation," *2015 IEEE International Electric Machines & Drives Conference (IEMDC)*, Coeur d'Alene, ID, USA, 2015, pp. 1426-1432, doi: 10.1109/IEMDC.2015.7409249.
- [44] P. Nussbaumer, M. A. Vogelsberger and T. M. Wolbank, "Induction Machine Insulation Health State Monitoring Based on Online Switching Transient Exploitation," in *IEEE Transactions on Industrial Electronics*, vol. 62, no. 3, pp. 1835-1845, March 2015, doi: 10.1109/TIE.2014.2361114.
- [45] C. Zoeller, M. A. Vogelsberger, T. M. Wolbank, and H. Ertl, "Impact of SiC semiconductors switching transition speed on insulation health state monitoring of traction machines," *IET Power Electronics*, vol. 9, no. 15, pp. 2769–2775, Dec. 2016, doi: 10.1049/iet-pel.2015.0988.
- [46] C. Zoeller, M. A. Vogelsberger, R. Fasching, W. Grubelnik, and T. M. Wolbank, "Evaluation and Current-Response-Based Identification of Insulation Degradation for High Utilized Electrical Machines in Railway Application," *IEEE Transactions on Industrial Electronics*, vol. 53, no. 3, pp. 2679–2689, May 2017, doi: 10.1109/TIA.2017.2661718.
- [47] "IEEE Recommended Practice for Testing Insulation Resistance of Electric Machinery," in *IEEE Std 43-2013 (Revision of IEEE Std 43-2000)*, vol., no., pp.1-37, 6 March 2014, doi: 10.1109/IEEESTD.2014.6754111.
- [48] "IEEE Recommended Practice for Insulation Testing of Large AC Rotating Machinery with High Direct Voltage," in *ANSI/IEEE Std 95-1977*, vol., no., pp.1-27, 29 April 1977, doi: 10.1109/IEEESTD.1977.82914.
- [49] "IEEE Recommended Practice for Insulation Testing of AC Electric Machinery with High Voltage at Very Low Frequency," in *IEEE Std 433-2009 (Revision of IEEE Std 433-1974)*, vol., no., pp.1-30, 24 Feb. 2010, doi: 10.1109/IEEESTD.2009.5423694
- [50] "IEEE Guide for Insulation Maintenance of Electric Machines," in *IEEE Std 56-2016*, pp.1-86, 11 Nov. 2016, doi: 10.1109/IEEESTD.2016.7740867.
- [51] "IEEE Recommended Practice for Measurement of Power Factor Tip-Up of Electric Machinery Stator Coil Insulation," in *IEEE Std 286-2000*, vol., no., pp.1-29, 1 March 2000, doi: 10.1109/IEEESTD.2000.8685849.

- [52] "IEEE Guide for the Measurement of Partial Discharges in AC Electric Machinery," in *IEEE Std 1434-2014 (Revision of IEEE Std 1434-2000)*, pp.1-89, 4 Dec. 2014, doi: 10.1109/IEEESTD.2014.6973042.
- [53] International Electrotechnical Commission, International Electrotechnical Commission, and Technical Committee 112, *Electrical insulating materials and systems--electrical measurement of partial discharges (PD) under short rise time and repetitive voltage impulses*. Geneva: International Electrotechnical Commission, 2011.
- [54] "IEEE Recommended Practice for Quality Control Testing of External Discharges on Stator Coils, Bars, and Windings," in *IEEE Std 1799-2012*, vol., no., pp.1-48, 30 Nov. 2012, doi: 10.1109/IEEESTD.2012.6365722.
- [55] "IEEE Guide for Testing Turn Insulation of Form-Wound Stator Coils for Alternating-Current Electric Machines," in *IEEE Std 522-2004 (Revision of IEEE Std 522-1992)*, vol., no., pp.1-28, 9 Aug. 2004, doi: 10.1109/IEEESTD.2004.94591.
- [56] I. J. Kemp, "Developments in partial discharge plant-monitoring technology," *1993 International Conference on Partial Discharge*, Canterbury, UK, 1993, pp. 52-55.
- [57] G. C. Stone and H. G. Sedding, "In-service evaluation of motor and generator stator windings using partial discharge tests," in *IEEE Transactions on Industry Applications*, vol. 31, no. 2, pp. 299-303, March-April 1995, doi: 10.1109/28.370277.
- [58] G. C. Stone, "Condition monitoring and diagnostics of motor and stator windings – A review," in *IEEE Transactions on Dielectrics and Electrical Insulation*, vol. 20, no. 6, pp. 2073-2080, December 2013, doi: 10.1109/TDEI.2013.6678855.
- [59] G. C. Stone, H. G. Sedding and C. Chan, "Experience With Online Partial-Discharge Measurement in High-Voltage Inverter-Fed Motors," in *IEEE Transactions on Industry Applications*, vol. 54, no. 1, pp. 866-872, Jan.-Feb. 2018, doi: 10.1109/TIA.2017.2740280.
- [60] A. Cavallini, D. Fabiani and G. C. Montanari, "A novel method to diagnose PWM-fed induction motors," in *IEEE Transactions on Dielectrics and Electrical Insulation*, vol. 15, no. 5, pp. 1313-1321, October 2008, doi: 10.1109/TDEI.2008.4656239.
- [61] G. C. Montanari, R. Hebner, P. Seri and R. Ghosh, "Noise rejection and partial discharge identification in PDIV tests of insulated wires under repetitive impulse supply voltage," *2019 IEEE Electrical Insulation Conference (EIC)*, Calgary, AB, Canada, 2019, pp. 505-508, doi: 10.1109/EIC43217.2019.9046587.
- [62] D. Choi, T. Kang, S. B. Lee, J. Kim and J. Kim, "Stator insulation quality assurance testing for appliance motors with aluminum windings," *2016 IEEE Energy Conversion Congress and Exposition (ECCE)*, Milwaukee, WI, 2016, pp. 1-8, doi: 10.1109/ECCE.2016.7855465.
- [63] J. Yang et al., "Experimental evaluation of using the surge PD test as a predictive maintenance tool for monitoring turn insulation quality in random wound AC motor stator windings," in *IEEE Transactions on Dielectrics and Electrical Insulation*, vol. 19, no. 1, pp. 53-60, February 2012, doi: 10.1109/TDEI.2012.6148502.
- [64] P. Wang, A. Cavallini and G. C. Montanari, "The influence of repetitive square wave voltage parameters on enameled wire endurance," in *IEEE Transactions on Dielectrics and Electrical Insulation*, vol. 21, no. 3, pp. 1276-1284, June 2014, doi: 10.1109/TDEI.2014.6832275.
- [65] P. Wang, S. Ma, S. Akram, K. Zhou, Y. Chen and M. T. Nazir, "Design of Archimedes Spiral Antenna to Optimize for Partial Discharge Detection of Inverter Fed Motor Insulation," in *IEEE Access*, vol. 8, pp. 193202-193213, 2020, doi: 10.1109/ACCESS.2020.3033300.

- [66] M. Tozzi, A. Cavallini and G. C. Montanari, "Monitoring off-line and on-line PD under impulsive voltage on induction motors - part 1: standard procedure," in *IEEE Electrical Insulation Magazine*, vol. 26, no. 4, pp. 16-26, July-Aug. 2010, doi: 10.1109/MEI.2010.5511185.
- [67] S. B. Lee, A. Naeini, S. Jayaram, G. C. Stone and M. Šašić, "Impulse Voltage-based Test Method for Identifying the Stator Insulation Component with PD Activity for Low Voltage AC Motors," *2019 IEEE Electrical Insulation Conference (EIC)*, Calgary, AB, Canada, 2019, pp. 392-395, doi: 10.1109/EIC43217.2019.9046584.
- [68] H. H. Eldeeb, A. Berzoy, A. A. Saad, H. Zhao and O. A. Mohammed, "Differential Mathematical Morphological-Based Online Diagnosis of Stator Interturn Failures in Direct Torque Control Drive Systems," in *IEEE Transactions on Industry Applications*, vol. 56, no. 6, pp. 6272-6285, Nov.-Dec. 2020, doi: 10.1109/TIA.2020.3019779.
- [69] M. Wolkiewicz, G. Tarchała, T. Orłowska-Kowalska and C. T. Kowalski, "Online Stator Interturn Short Circuits Monitoring in the DFOC Induction-Motor Drive," in *IEEE Transactions on Industrial Electronics*, vol. 63, no. 4, pp. 2517-2528, April 2016, doi: 10.1109/TIE.2016.2520902.
- [70] S. He, X. Shen and Z. Jiang, "Detection and Location of Stator Winding Interturn Fault at Different Slots of DFIG," in *IEEE Access*, vol. 7, pp. 89342-89353, 2019, doi: 10.1109/ACCESS.2019.2926538.
- [71] S. E. Pandarakone, Y. Mizuno and H. Nakamura, "Frequency spectrum investigation and analytical diagnosis method for turn-to-turn short-circuit insulation failure in stator winding of low voltage induction motor," in *IEEE Transactions on Dielectrics and Electrical Insulation*, vol. 23, no. 6, pp. 3249-3255, Dec. 2016, doi: 10.1109/TDEI.2016.006095.
- [72] M. Malekpour, B. T. Phung and E. Ambikairajah, "Online technique for insulation assessment of induction motor stator windings under different load conditions," in *IEEE Transactions on Dielectrics and Electrical Insulation*, vol. 24, no. 1, pp. 349-358, Feb. 2017, doi: 10.1109/TDEI.2016.006139.
- [73] Y. Qi, M. Zafarani, V. Gurusamy and B. Akin, "Advanced Severity Monitoring of Interturn Short Circuit Faults in PMSMs," in *IEEE Transactions on Transportation Electrification*, vol. 5, no. 2, pp. 395-404, June 2019, doi: 10.1109/TTE.2019.2913357..
- [74] B. Aubert, J. Régnier, S. Caux and D. Alejo, "Kalman-Filter-Based Indicator for Online Interturn Short Circuits Detection in Permanent-Magnet Synchronous Generators," in *IEEE Transactions on Industrial Electronics*, vol. 62, no. 3, pp. 1921-1930, March 2015, doi: 10.1109/TIE.2014.2348934.
- [75] C. Lai, A. Balamurali, V. Bousaba, K. L. V. Iyer and N. C. Kar, "Analysis of stator winding inter-turn short-circuit fault in interior and surface mounted permanent magnet traction machines," *2014 IEEE Transportation Electrification Conference and Expo (ITEC)*, Dearborn, MI, USA, 2014, pp. 1-6, doi: 10.1109/ITEC.2014.6861775.
- [76] S. Grubic, J. Restrepo and T. G. Habetler, "Online Surge Testing Applied to an Induction Machine With Emulated Insulation Breakdown," in *IEEE Transactions on Industry Appli.*, vol. 49, no. 3, pp. 1358-1366, May-June 2013, doi: 10.1109/TIA.2013.2253535.
- [77] S. Grubic, J. Restrepo, J. M. Aller, B. Lu, and T. G. Habetler, "A New Concept for Online Surge Testing for the Detection of Winding Insulation Deterioration in Low-Voltage Induction Machines," *IEEE Transactions on Industrial Applications*, vol. 47, no. 5, pp. 2051-2058, Sep. 2011, doi: 10.1109/TIA.2011.2161972.

- [78] D. A. Asfani, D. C. Riawan, I. M. Y. Negara, D. Fahmi, M. F. Anshori and M. Wahyudi, "Evaluation of rotor position effect on stator diagnostic based on surge voltage test," *2017 International Seminar on Application for Technology of Information and Communication (iSemantic)*, Semarang, 2017, pp. 164-168, doi: 10.1109/ISEMANTIC.2017.8251863.
- [79] Sang Bin Lee, Jinkyu Yang, K. Younsi, and R. Bharadwaj, "An on-line groundwall and phase to phase insulation quality assessment technique for ac machine stator windings," in *Fourtieth IAS Annual Meeting. Conference Record of the 2005 Industry Applications Conference, 2005.*, Hong Kong, China, 2005, vol. 1, pp. 10–19, doi: 10.1109/IAS.2005.1518285.
- [80] J. Yang, S. B. Lee, J. Yoo, S. Lee, Y. Oh and C. Choi, "A Stator Winding Insulation Condition Monitoring Technique for Inverter-Fed Machines," in *IEEE Trans. on Power Electronics*, vol. 22, no. 5, pp. 2026-2033, Sept. 2007, doi: 10.1109/TPEL.2007.904236.
- [81] P. Zhang, K. Younsi and P. Neti, "A Novel Online Stator Ground-Wall Insulation Monitoring Scheme for Inverter-Fed AC Motors," in *IEEE Trans. on Industry Applications*, vol. 51, no. 3, pp. 2201-2207, May-June 2015, doi: 10.1109/TIA.2014.2385937.
- [82] P. Neti and S. Grubic, "Online Broadband Insulation Spectroscopy of Induction Machines Using Signal Injection," in *IEEE Transactions on Industry Applications*, vol. 53, no. 2, pp. 1054-1062, March-April 2017, doi: 10.1109/TIA.2016.2639014.
- [83] I. Tsyokhla, A. Griffio and J. Wang, "On-Line Motor Insulation Capacitance Monitoring Using Low-Cost Sensors," *2019 IEEE Energy Conversion Congress and Exposition (ECCE)*, Baltimore, MD, USA, 2019, pp. 6996-7003, doi: 10.1109/ECCE.2019.8912241.
- [84] I. Tsyokhla, A. Griffio, and J. Wang, "Detection of humidity ingress using online common-mode insulation impedance-monitoring system," *The Journal of Engineering*, vol. 2019, no. 17, pp. 4411–4414, Jun. 2019, doi: 10.1049/joe.2018.8256.
- [85] I. Tsyokhla, A. Griffio and J. Wang, "Online Condition Monitoring for Diagnosis and Prognosis of Insulation Degradation of Inverter-Fed Machines," in *IEEE Transactions on Industrial Electronics*, vol. 66, no. 10, pp. 8126-8135, Oct. 2019, doi: 10.1109/TIE.2018.2885740.
- [86] G. Lu, Y. Wu and P. Zhang, "Analytical Analysis and Design of an Advanced Differential-Mode Current Sensor for Insulation Monitoring for Industrial Electrical Assets," in *IEEE Access*, vol. 8, pp. 151360-151370, 2020, doi: 10.1109/ACCESS.2020.3015763.
- [87] F. Alvarez-Gonzalez, D. Hewitt, A. Griffio and J. Wang, "Challenges of Common Mode Current and Voltage Acquisition for Stator Winding Insulation Health Monitoring," *2020 IEEE Energy Conversion Congress and Exposition (ECCE)*, Detroit, MI, USA, 2020, pp. 4452-4459, doi: 10.1109/ECCE44975.2020.9235717.